The Pennsylvania State University

The Graduate School

Department of Chemistry

ULTRAFAST CHARGE TRANSFER IN CONVENTIONAL SOLVENTS AND IONIC LIQUIDS

A Thesis in

Chemistry

by

Xiang Li

Submitted in Partial Fulfillment
of the Requirements
for the Degree of

Doctor of Philosophy

January 2011

The thesis of Xiang Li was reviewed and approved* by the following:

Mark Maroncelli
Professor of Chemistry
Dissertation Advisor
Chair of Committee

Tom Mallouk
DuPont Professor of Materials Chemistry and Physics

John Golbeck
Professor of Biochemistry and Biophysics and Professor of Chemistry

John Asbury
Assistant Professor of Chemistry

Barbara J. Garrison
Shapiro Professor of Chemistry
Head of the Department of Chemistry

*Signatures are on file in the Graduate School

ABSTRACT

This thesis work is aimed at understanding ultrafast intermolecular electron transfer and solvation processes in conventional solvents and ionic liquids. Following a brief introduction in Chapter 1, Chapter 2 explains the main experimental techniques and data analysis methods used in this thesis. Chapter 3 and Chapter 4 are focused on charge transfer reactions in representative ionic liquids in comparison to conventional solvents. Chapter 5 carefully examines a selected system for studying dynamic heterogeneity studies in ionic liquids.

Charge transfer is an important step in many types of chemical and biochemical reactions. The energetics and rates of charge transfer are greatly affected by the polarity and dynamics of the surrounding medium and extensive research has explored the effect of polar solvents on charge transfer. In contrast, despite the large amount of attention on ionic liquids for many applications, few studies have focused on fundamental aspects of charge transfer ionic liquids. I have surveyed the behavior of several solvent-controlled intramolecular charge transfer reactions in representative ionic liquids and compared it to what is found for these same reactions in conventional dipolar solvents using time-resolved fluorescence spectroscopy.

In chapter 3, crystal violet lactone (CVL), which exhibits distinct dual emission in fluid solution as a result of a rapid excited-state charge transfer reaction, was measured in series of conventional solvents as background for ionic liquids studies. Solvatochromic analysis using a dielectric continuum model suggests dipole moments of 9-12 D for the initially excited (LE) state and ~24 D for the charge-transfer (CT) state. Intensities of

steady-state emission as well as kinetic data provide free energies for the LE → CT reaction that range from +12 kJ/mol in nonpolar solvents to -10 kJ/mol in highly polar solvents at 25 °C. Reaction rates constants, which lie in the range of 10-100 ns^{-1} in most solvents, depend on both solvent polarity and solvent friction. In highly polar solvents, this charge transfer reaction was confirmed to follow two-state kinetics as used in typical dual fluorescence probes like aminobenzonitriles. Reaction rates are correlated to solvation times in a manner that indicates the reaction is a solvent-controlled electron transfer on an adiabatic potential surface having a modest barrier.

In Chapter 4, the charge transfer reaction of CVL was studied in ionic liquids. Compared with conventional solvents, the reaction is much more complicated. Equilibrium is not reached in any ionic liquid due to the much slower reaction. Furthermore, in two other well-studied charge transfer probes in several classes of ionic liquids, we also found the reaction kinetics are typically more complicated. Multi-exponential decays are observed when reaction times are comparable to solvation times, which are on the nanosecond scale in most ionic liquids at room temperature. Time-resolved spectra were dissected into LE and CT states using non-polar solvents as reference. Reaction times in ionic liquids calculated from LE/CT decays are slower than in conventional solvents approximately in proportion to the larger viscosities and longer solvation times of ionic liquids

In Chapter 5, C102 in the ionic liquid $[N_{4441}][Tf_2N]$ was chosen as a promising system to confirm the red edge excitation dependence observed in previous studies using C153 in $[Nip_{311}][Tf_2N]$. We were not able to approach the far red edge of the ionic liquid

in the previous study. This study is also aimed to support the other dynamic heterogeneity observations in ionic liquids. An experimental temperature was first determined to get the complete solvation response function. Decay data was collected at perpendicular angle for better defined time-resolved spectra. Normalized time-resolved spectra show no difference with the ones collected at magic angle, which is evidence for using perpendicular angle for future experimental condition. The asymmetry factor was also fixed when fitting the spectra with log-normal function. Solvation response function was fitted with stretched exponential function and the frequency at time infinity was found to be important in solvation time calculation. No significant trend of solvation time dependence on excitation wavelength was observed considering the uncertainty of TCSPC instrumentations. Other systems or detection system with higher resolution is needed for future studies.

Chapter 6 describes the initial result of an on-going project in our group about the "up-relaxation" behavior of solvation dynamics in slow solvents using nanosecond dye laser. Only one set of up-relaxtion behavior is observed for now using 4-AP in propanol at -90 °C. Spectra exciting at far-edge are still too noisy and need to be improved with other instrumentation skill. Probes with longer lifetime and ionic liquids will be studied in the future in a similar way.

TABLE OF CONTENTS

LIST OF FIGURES

LIST OF TABLES

ACKNOWLEDGEMENTS

Graduate school is such a valuable experience and it has taught me more than just planning and executing experiments. It also taught me how to think critically, to trouble shoot and cooperate inside and outside of my research work. I would like to take this opportunity to express my deepest appreciation to the people who have helped me through this process.

First, I would like to thank my advisor, Dr. Mark Maroncelli for his enormous help on my graduate study and this thesis. His extensive knowledge and passion for science has been a great example and inspiration for me. Mark, thank you for your time and patience in revising every sentence and slide for my graduate work and presentations.

I also want to thank Dr. Tom Mallouk, Dr. John Asbury and Dr. John Golbeck for all their time and advice throughout my graduate study. Thanks must also go to my colleagues and friends, present and past, from the Maroncelli group. I thank all of you for your help and support over the years, especially Dr. Sergei Arzhanstev, Jing Dong, Dr. Chet Swalina, Dr. Anjan Chakraborty, Dr. Durba Roy, Min Liang, Jens Breffke, and Anne Kaintz. I am particularly grateful to a few people individually: Sergei, thank you for teaching me the instrumentation and helping me to prepare for my comprehensive exam. Min, thanks for your help while I am away writing this thesis. Anne, thanks for your encouragement when I am down and lack confidence. You are all my lifetime friends.

Lastly, I wish to thank my family members who have supported me on every decision I have made. To my parents, thank you for raising me, trusting me and giving

me unconditional love while I am thousands of miles away. I hope you are as proud of me as I am proud of you. My most special thanks go to my husband Xiaoyi, my lifelong love and soulmate, without your devotion and understanding, it would have been impossible for me to finish my graduate study.

To all of them, I dedicate this thesis.

Chapter 1

Introduction

Room temperature ionic liquids or ionic liquids (ILs) for short are defined as a type of salt that melt at or below 100 °C. Ionic liquids have been drawing increasing attention over the last two decades, especially after the discovery of air and water-stable BF_4^- and PF_6^- salts.[1] ILs are called designer solvents for the potential variability with which anion and cations can be combined. It is estimated that there are more than 10^6 different ionic liquids could be made by combining currently known cations and anions.[2] (Figure 1-1 for commonly used ions). Ionic liquids are also regarded as green solvents for their low vapor pressure and non-flammability. Major applications of ILs include their use as solvents for inorganic and organic reactions[3], as separation and column materials in analytical chemistry[4-6], as potential media for solar cells[7,8] and drug delivery[9] and as electrolytes in electrochemical devices and processes[10-12]. Following initial study of thermodynamics and transport properties of ionic liquids of importance in various applications, physical chemists have become particularly interested in ionic liquids from a fundamental level for their extended dynamic range and the complex local environments they afford. In this section, I will briefly introduce some of the major highlights of previous studies of the fundamental physical chemistry of ionic liquids which serves as a background for my thesis research.

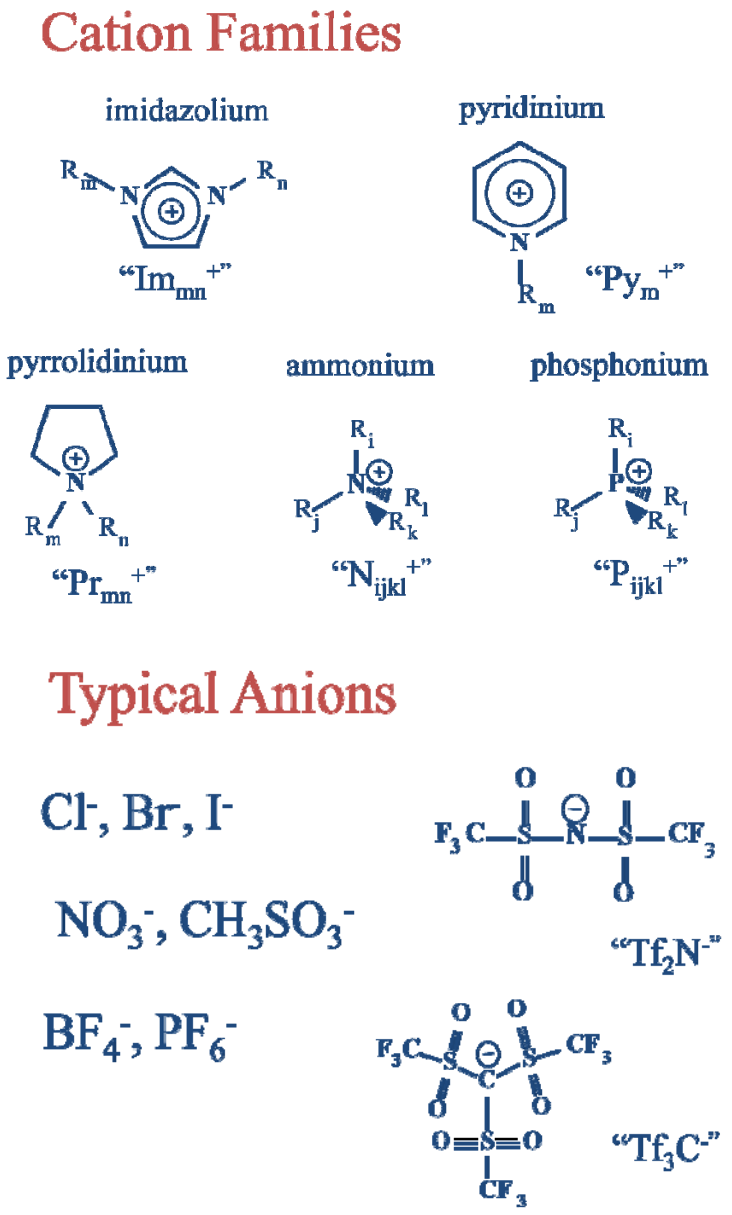

Figure 1-1 Representative cations and anions used to make ionic liquids

The strong electrostatic interactions between the cations and anions of ionic liquids lead to an array of different physical features compared with conventional dipolar solvents held together by much weaker dipole-dipole interactions. Most ionic liquids are much more viscous than conventional solvents. This property enables ionic liquids to be used as industry lubricatants. The viscosity of an IL is highly dependent upon the structure of its constituent ions. At temperatures above the glass transition, the viscosities of IL are also correlated with temperature. In most cases, the temperature dependence can be well described by Vogel–Fulcher–Tammann equation for most of the ionic liquids at room temperatures. [13] At low temperatures, ILs with more complex ions tend to behave like other glass-forming liquids while ILs with shorter alkyl-chain components tend to crystallize. Other physical features like diffusion coefficients and X-ray structures of ionic liquids have also been studied widely and nicely summarized in a review[14]. The high viscosity and low vapor pressure of ILs make them difficult to distilled like conventional solvents and thus much harder to clean. Traces amount of some impurities (water and halides) can alter the physical properties of ILs substantially.

Understanding the solvation process is important for using ILs as solvents. Time-resolved fluorescence spectroscopy can be used to study solute rotation and solvation dynamics in ionic liquids. The most common probes used to monitor these processes include C153 and 4-aminophthalimide. Earlier work from the Maroncelli group has shown that solvation times in a typical ionic liquid at room temperature can range from less than 100 femtosecond to more than 10 ns. This broadly dispersed kinetics is believed to be due to the presence of dynamic heterogeneity of ILs. [15,16] It is hard to capture the ultrafast sub-ps solvation response and only a few research groups have

reported results using high resolution pump-probe systems. [16-18] Another important reason for the study of solvation dynamics in ionic liquids is to see how chemical reactions such as electron transfer reactions are influenced by the solvent reorganization process and how this influence might be different than in common dipolar solvents.

Isomerization and charge separation reactions are typical first steps in many important chemical and biochemical processes. Initial experimental results regarding these kinds of reactions have shown that the influence of both solvation dynamics and viscosity on reaction rates and barriers can be substantial. Furthermore, a distinct dependence of reaction time on excitation wavelength can be observed in both types of reaction. This dependence has been suggested to result from dynamic heterogeneity in ILs.[1919,20]

The research described in this thesis involves study of ultrafast charge transfer processes and dynamic heterogeneity in ionic liquids. Following this brief introduction, Chapter 2 describes the main techniques and data analysis methods used in this work. Chapter 3 is focused on the study of intramolecular electron transfer of crystal violet lactone (CVL) in a collection of conventional solvents. This work served as background for the use of CVL as a probe in ILs in Chapter 4. In conventional solvents the CVL reaction was found to conform to the behavior expected for a simple two-state reaction. Reaction rates, free energies and equilibrium constants were reported in this chapter as well as the radiative decay times of CVL in different solvents. In Chapter 4, the characteristics of the CVL were then measured in several typical ionic liquids and compared to the corresponding properties in conventional solvent. Similar comparisons were also made using intramolecular charge transfer in two other solutes: 9,9'-bianthryl

and 9-biphenyl-10-methyacridinium. The reaction times of all three probes showed similar correlations with solvation time in ionic liquids as in conventional dipolar solvents. Chapter 5 describes an unpublished study in which red-edge spectroscopy is used to explore whether dynamic heterogeneity can be detected in the solvation response of a selected ionic liquid. Although this work turned out to be less than definitive, the detailed spectra and data analysis methods for solvation time calculation described in this chapter are of value for future studies of solvation dynamics in ionic liquids. Finally, in Chapter 6, red-edge spectroscopy was used to study the "up-relaxation" behavior that was first proposed by Russian scientists in the 60s. A 1 mM sample of 4-AP in propanol was made to reproduce the results of dynamic excitation dependence at 183K. Similar results were found as previous reported by Tomin and co workers. Samples with higher concentration are needed to verify this "up-relaxation" result due to the low quality of the spectra at far red-edge of absorption band.

Reference and Notes

(1) Endres, F. *Phys. Chem. Chem. Phys.* **2010**, *12*, 1648.

(2) Plechkova, N. V.; Seddon, K. R. *Chem. Soc. Rev.* **2008**, *37*, 123.

(3) Endres, F.; El Abedin, S. Z. *Phys. Chem. Chem. Phys.* **2006**, *8*, 2101.

(4) Anderson, J. L.; Armstrong, D. W.; Wei, G. T. *Anal. Chem.* **2006**, *78*, 2893.

(5) Pandey, S. *Anal. Chim. Acta* **2006**, *556*, 38.

(6) Baker, G. A.; Baker, S. N.; Pandey, S.; Bright, F. V. *Analyst* **2005**, *130*, 800.

(7) Fredin, K.; Gorlov, M.; Pettersson, H.; Hagfeldt, A.; Kloo, L.; Boschloo, G. *J. Phys. Chem. C* **2007**, *111*, 13261.

(8) Fabregat-Santiago, F.; Bisquert, J.; Palomares, E.; Otero, L.; Kuang, D.; Zakeeruddin, S. M.; Graetzel, M. *J. Phys. Chem. C* **2007**, *111*, 6550.

(9) Rogers, R. D.; Voth, G. *Acc. Chem. Res.* **2007**, *40(11)*, 1077.

(10) MacFarlane, D. R.; Forsyth, M.; Howlett, P. C.; Pringle, J. M.; Sun, J.; Annat, G.; Neil, W.; Izgorodina, E. I. *Acc. Chem. Res.* **2007**, *40*, 1165.

(11) *Electrochemical Aspects of Ionic Liquids*; Ohno, H., Ed.; John Wiley & Sons: Hoboken, 2005, pp 392.

(12) Buzzeo, M. C.; Evans, R. G.; Compton, R. G. *ChemPhysChem* **2004**, *5*, 1106.

(13) Roland, C. M.; Bair, S.; Casalini, R. *J. Chem. Phys.* **2006**, *125*.

(14) Castner, E. W.; Wishart, J. F. *J. Chem. Phys.* **2010**, *132*.

(15) Arzhantsev, S.; Ito, N.; Heitz, M.; Maroncelli, M. *Chem. Phys. Lett.* **2003**, *381*, 278.

(16) Arzhantsev, S.; Jin, H.; Baker, G. A.; Ito, N.; Maroncelli, M. Solvation Dynamics in Ionic Liquids, Results from ps and fs Emission Spectroscopy. In *Femtochemistry VII, Ultrafast Processes in Chemistry, Physics, and Biology*; Castleman, A. W., Kimble, M. L., Eds.; Elsevier B.V., 2006; pp 225.

(17) Arzhantsev, S.; Jin, H.; Ito, N.; Maroncelli, M. *Chem. Phys. Lett.* **2006**, *417*, 524.

(18) Sanders Headley, L.; Mukherjee, P.; Anderson, J. L.; Ding, R.; Halder, M.; Armstrong, D. W.; Song, X.; Petrich, J. W. *J. Phys. Chem. A* **2006**, *110*, 9549.

(19) Jin, H.; Li, X.; Maroncelli, M. *J. Phys. Chem. B* **2007**, *111*, 13473.

(20) Fukuda, M.; Terazima, M.; Kimura, Y. *Chem. Phys. Lett.* **2008**, *463*, 364.

Chapter 2

Time-Resolved Fluorescence Measurements and Data Analysis Methods

Time resolved measurements are widely used in fluorescence spectroscopy and there are many examples[1] of information provided by time-resolved experiments that cannot be obtained from traditional steady state measurements alone. In this thesis, the main technique employed for measurements of solvation times and charge transfer dynamics is time-correlated single photon counting (TCSPC). In this chapter I will introduce the most current technology used for such measurements and describe the home-built TCSPC system used in the Maroncelli group. I will also discuss the main ways in which data collected using TCSPC are analyzed, as these methods are relevant throughout this thesis.

2.1 Introduction to TCSPC

The two most popular ways for time-resolved measurement of fluorescence are "pump-probe" (typically Kerr-gating or up-conversion methods) which can reach resolutions on the femtosecond (fs) time scale and TCSPC, which optimally has a resolution of about 25 ps. The higher resolution of the pump-probe techniques is due to the employment of laser pulses for determining time resolution, while in TCSPC, time resolution is limited by the speed of the detection electronics, which currently restricts

these experiments to the picosecond scale. Although TCSPC has lower time resolution, it does have a number of advantages over pump-probe techniques:

a. High signal to noise ratio: Compared with pump-probe systems in which noise often comes from the interference of pump and probe light with the relatively weaker fluorescence signal, the majority of the noise in TCSPC comes from the signal processing electronics, which can be made negligibly small.
b. Suitable for weaker fluorophores: the technique is much more sensitive than most pump-probe methods and signals can often be averaged for longer times.
c. More robust system and easier to find signal: there are existing commercialized TCSPC system available that is easy to handle in various applications.

Based on these advantages, I chose TCSPC as the primary tool for collecting time-resolved fluorescence data for my thesis research.

The basic principle of TCSPC is shown in Figure 2-1[2]. The different components making up the system will be further explained in the following section. The sequence of events associated with registering one detected photon of fluorescence is as follows. Light from a pulsed source, usually a laser, is split into two pulses. One weak pulse pulse is collected by a photodiode (PD) whose output is conditioned by a constant fraction discriminator (CFD) which then feeds into a time-to amplitude converter (TAC) to serve as the start pulse for the experiment. The other pulse is used to excite the sample. The fluorescence signal (one photon) from the sample will go through a glass filter, monochromater and then be collected by a PMT, which is used to change the optical

signal into an electronic signal. After going through another CFD, the electronic signal will then reach the TAC and serve as stop pulse. A capacitor in the TAC begins to accumulate charge when the start pulse arrives and stops accumulating when a stop pulse is detected. The net charge of voltage accumulated is proportional to the time delay between the photon emitted from the sample and this datum is finally registered in an appropriate channel of a multi-channel analyzer (MCA). This single counting even is repeated millions of time to obtain a final fluorescence decay curve. The limiting factor in the rates at which such data can be collected is the time that the capacitor in the TAC takes to reset after the stop pulse arrives, which is usually a few microseconds. Because of this limitation, the experiment is not actually run in the intuitive manner. Instead, an inverted start-stop sequence is used in which the fluorescence signal is used as stop pulse and the excitation as the start pulse. This backward counting mode is used because the fluorescence detection rate is expected to be much lower than the laser excitation rate so that it is advantageous. The reason that this system is named single photon-counting is because the fluorescence is reduced in intensity such that at most one fluorescent photon is detected per excitation pulse. Actually proper counting statistics require that only 1/100 excitation pulses results in a detected photon.

Figure 2-2 shows the home-built TCSPC system used in the Maroncelli group. A cavity-dumped Ti:sapphire laser pumped by a Nd:YAG laser is used as the light source. This laser system generates light pulses of 150 fs duration at a 5.4 MHz repetition rate. The repetition rate is tunable using the cavity dumper, which we usually set to dump one out of every 10 pulses circulating within the laser cavity in order to reduce the original 54 MHz repetition rate to 5.4 MHz. The start pulse goes through several optics and non-

liner crystals to excite the sample at the preferred wavelength and the stop pulse is collected by a photodiode (PD).

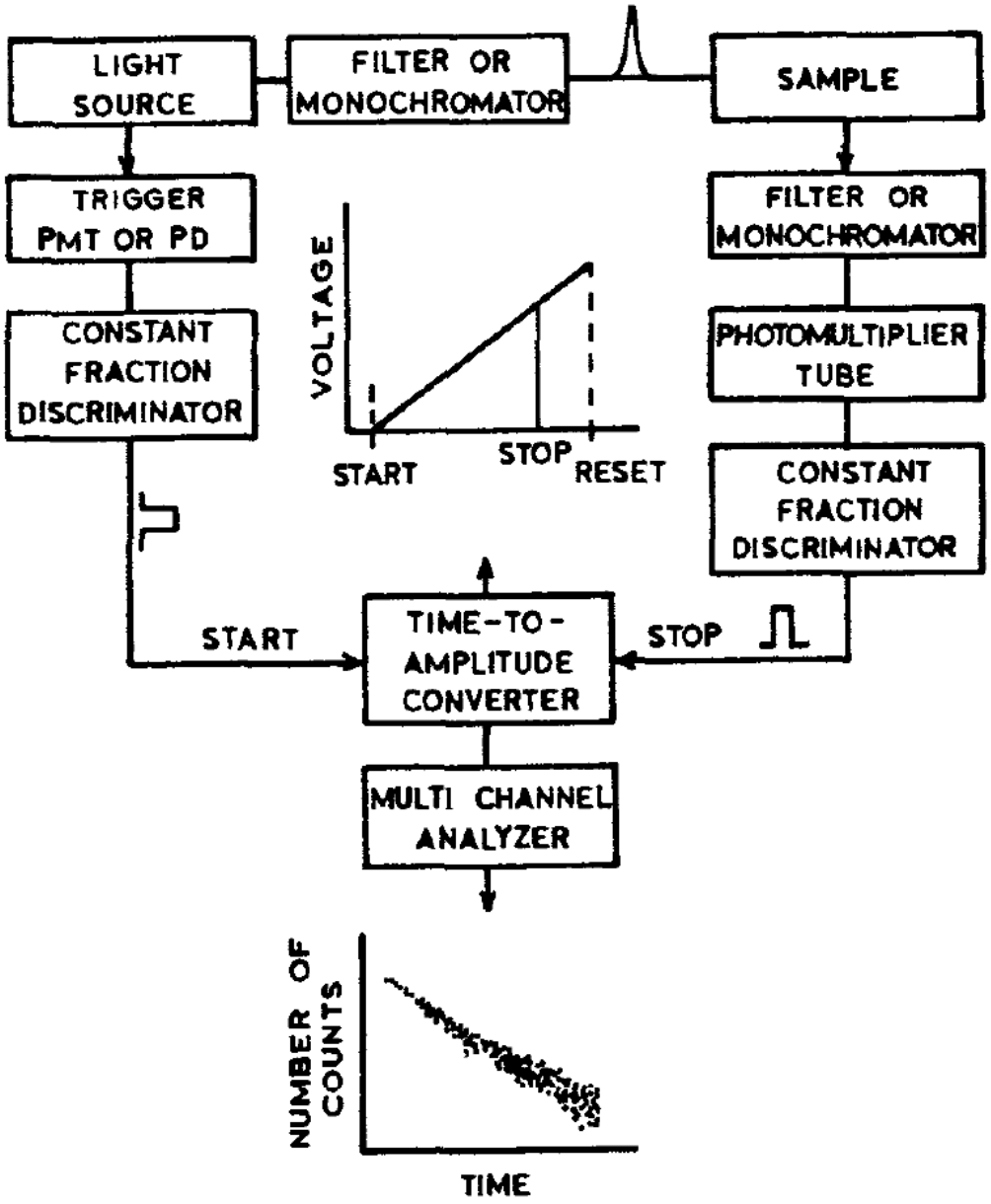

Figure 2-1 Schematic of basic principle of TCSPC system[2]

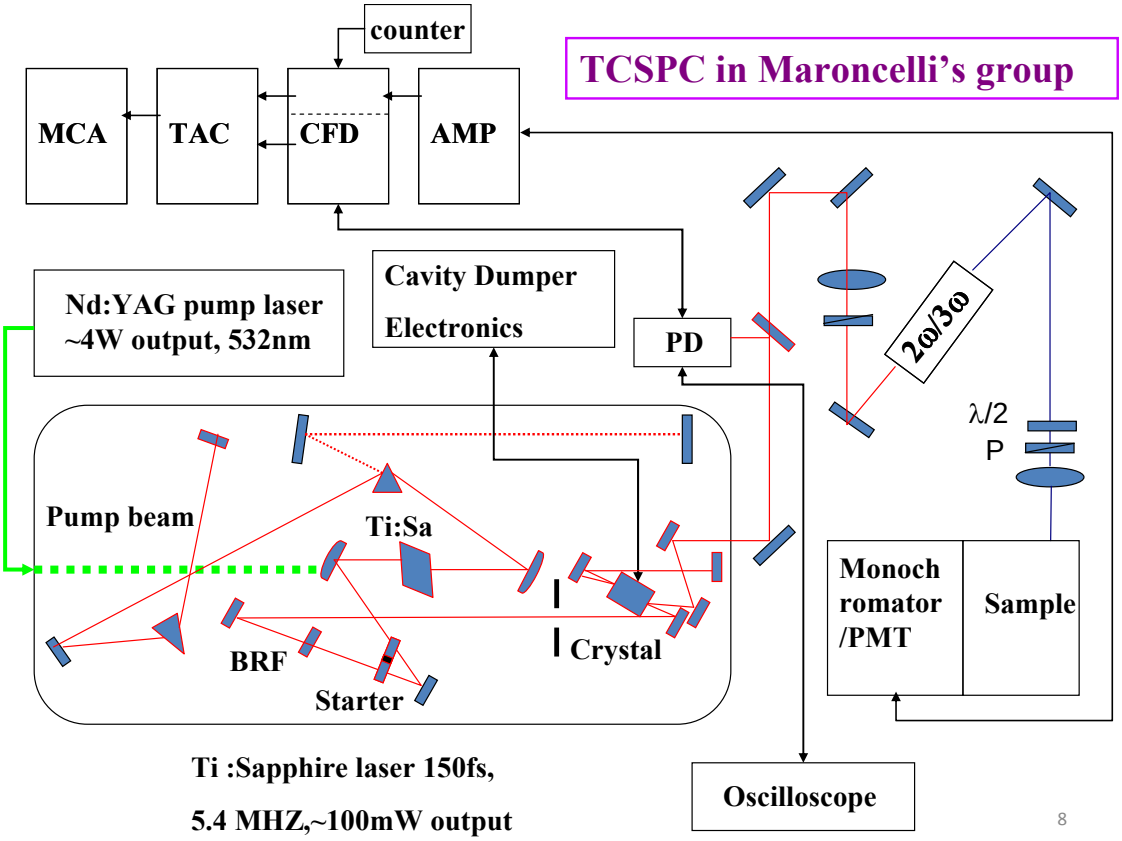

Figure 2-2 The home-built TCSPC system in the Maroncelli group

2.2 TCSPC Components[1,2]

The major components of a TCSPC instrument can be classified into three categories: light sources, optics, and detection electronics. In this section, I will explain the distinct features of each component that are needed for optimum performance of a TCSPC system.

2.2.1 The Light Source

Until the 1980s dye lasers were the most popular sources used for TCSPC. Dye lasers are passive devices that need another optical pump source. The most commonly used pumps are argon-ion lasers and Nd:YAG lasers. These two types of laser can be mode-locked by using an acousto-optic device inserted into the laser cavity. Mode-locked argon-ion lasers are typically used with the 514 nm line. They provide pulses of about 70 ps duration at repetition rates near 80 MHz. Mode-locked Nd:YAG lasers have fundamental outputs at 1064 nm, which is either doubled or tripled to 532 nm or 355 nm by non-linear crystals These output wavelengths are not the most favorable for fluorescence but can be used as pumping source for dye lasers, which cover much broader excitation ranges. The cavity length of the dye laser is adjusted to be exactly the same as the Nd:YAG or argon-ion pump laser in order to achieve mode locking of the dye laser. For a typical R6G dye laser, the output can have a repetition rate of 80 MHz with 5 ps pulse width. The output wavelength of a dye laser can also be tunable depending on the types of the dyes employed

Currently, the most widely used light sources for TCSPC are Ti:sapphire lasers. Our lab currently employs one such laser. A continuous wave (cw) argon-ion or Nd:YAG laser can be used as the pumping source for a Ti:sapphire laser because the Ti:sapphire laser self mode-locks by a phenomenon known as the Kerr lens effect. The output range of Ti:sapphire lasers are between 720 nm to 1000 nm and the output is usually doubled (2ω) or tripled (3ω) to a more useful range for fluorescence spectroscopy using non linear optical crystals. The third harmonic generation is much harder to achieve for Ti:sapphire lasers since the pulse can be as narrow as 150 fs. To generate third harmonic ($\omega_1 + \omega_2 = 3\omega$), the original light pulse and second harmonic light pulse need to have exact phase and delay matching. The final output range of the TCSPC system in our lab is 370 nm - 460 nm when the second harmonic is used and 240 nm - 333 nm with the third harmonic.

Another important feature of Ti:sapphire lasers is their high repetition rates, which can go up to 80 MHz. Typically, it takes five times of the lifetime for a probe to fully (>99%) relax to the ground state. If the lifetime of a common fluorophore is about 10 ns, the space between two pulses needs to be more than 50 ns, which requires a repetition rate of less than 20 MHz. Until recently a pulse picker was used after the laser cavity to reduce the repetition rate of the Ti:sapphire laser in our laboratory. Many of the initial experiments reported here were conducted using this pulse picker. With the improvement in the quality of Ti:sapphire crystals, which allow for much higher energy tolerance, it has become possible to introduce a cavity dumper into the laser cavity to reduce the repetition rate. Using a cavity dumper can increase the power of each pulse to five times more than the pulse picker and this is particularly beneficial for 3ω generation.

The current cavity-dumped laser used in our lab has a base repetition rate of 54 MHz. The most commonly used repetition rate for our experiments is 5.4 MHZ. Even though the Ti:sapphire laser typically generates pulses of narrow as 150 fs duration, , which are significantly faster than the 5 ps pulses from a dye laser, the time resolution of the TCSPC is still limited to about 25 ps due to limitations of the detection electronics, which I will discuss in the next section. Ti:sapphire lasers also have a practical advantage over dye lasers: there is no need to work with carcinogenic, environmentally harmful, and short-lived laser dyes.

2.2.2 The Optics and Non-linear Crystals

The basic optics used in a TCSPC system include mirrors for beam steering, non-linear crystals for changing wavelength, and polarizers and wave plates for controlling polarization. All of these elements play important roles in proper functioning of the TCSPC experiment.

Steering optics (i.e. mirrors) are used for beam alignment throughout the system. Mirrors are chosen based on the wavelength ranges that are needed. Gold or multi-layer dielectric-coated mirrors are usually used in the UV-range while aluminum-coated mirrors are more often used in connection with dye lasers operating in the visible. When performing alignment, the incident angle is also must be taken into consideration to maximize power output.

As discussed in the previous sections, frequency doubling and tripling are usually used to achieve desired wavelengths for sample excitation. The most popular crystal

used for this purpose is β-barium borate (BBO). Not only can BBO be used for sum frequency generation and second harmonic generation, it can also handle fourth and fifth harmonic generation.

Polarizers are also essential optics in a TCSPC system. They are used to adjust the beam to the correct polarization of the electromagnetic field. Typically, a polarizer is used in the excitation beam to ensure vertical excitation. For lifetime measurements, emission is collected through a second polarizer set at "magic angle" which is 54.7 ° from the vertical direction. The reason for using this angle is to remove the solute rotation effect from the decay profile. For an angle $\theta = 54.7°$ $\cos^2\theta$ is 0.333 and $\sin^2\theta$ is 0.667, the total intensity measured I_T will be proportional to the sum of $I_\perp + 2I_\parallel$, this specific 2:1 weighing of light parallel and perpendicular to the excitation direction ensures that the light collected is representative of only population decay and no anisotropy effects. One may ask why the total intensity should equal to $I_\perp + 2I_\parallel$ to be free of anisotropy effects. Consider a collection of fluorophore whose transition moment lie at various angles α_i with respect to the vertical, the total intensity emitted by this collection is a sum of the projections of these transition moments onto the three Cartesian axes:

$$I_x + I_y + I_z = \sum_{i=1}^{n} I_i(cos^2\alpha_{xi} + cos^2\alpha_{yi} + cos^2\alpha_{zi}) \quad 2.1$$

Because $I_x = I_y$ for vertically polarized excitation along I_z , $I_\perp + 2I_\parallel$ is the total intensity independent of the way in which chromophores are oriented. In Chapter 5 we will discuss polarization further and describe why signal collection at an angle perpendicular to excitation is sometimes preferred over magic angle. For anisotropy measurements,

fluorescence is separately collected at the angles parallel and perpendicular to the excitation beam.

Absorptive and beam-splitting polarizers are the most common types of polarizers in current use. Absorptive polarizers usually use an array of parallel wires which only allow light that is perpendicularly polarized to pass. Beam-splitting polarizers split the beam into two beams with different linear polarizations. Such polarizers are more suitable for high intensity light such as lasers. Wave plates are also used in the TCSPC system to provide continuous variation of the excitation intensity. A half wave plate changes the angle of a beam by 90° and is used in our lab to change the excitation angle to vertical.

Other optics like lenses and colored glasses are also important components in the alignment of the system and are usually not given enough attention. Light should go through the center of the lens to give maximum intensity.

Another important part of the TCSPC system is the monochromator, which is usually placed in front of the PMT to collect data at selected wavelength. A monochromater uses either dispersion from a prism or diffraction from a grating to achieve spatial separation of the colors of light. Optical filters are also used to help select or reject certain wavelengths. Most optical filters we employ are colored glasses that are transparent to certain wavelengths. A monochromater may introduce a time-delay or add to the instrument response time because of the dispersive nature of gratings.

2.2.3 Electronics and Detection Systems

The detection system and electronics are very important components of a TCSPC system as they are now typically the determining factors for time resolution. They can be made to insert into a NIM (Nuclear Instrumentation Module) bin which is used to supply power to the modules for TCSPC. In this section, we will introduce the different electronics used in the detection system of TCSPC.

The first component we will talk about is the PMT (photomultiplier tube). When a single photon is collected by a PMT, the optical signal is multiplied into thousands of electrons by transit through the dynode chain of the PMT. The most popular choice of PMTs for TCSPC are microchannel plate (MCP) photomultipliers. . MCP-PMTs have significantly shorter response times than PMTs based on discrete dynodes due to the reduction of the transit time spread of electrons in the electron multiplication process. This reduction is accomplished by replacing the dynode chain with electron multiplication in micron sized channels. The use of MCP-PMT yields a much narrower instrumental function compared to other PMTs. The other important advantage of the use of MCP is the absence of after pulses (long tails) in the instrumental response function.

A photodiode (PD) is used as the photon detector for the stop pulse. Photodiodes are less expensive and respond faster than PMTs. The reason that we only use PDs for detection of the laser pulse but not the fluorescence signal is mainly due to the low sensitivity of PDs. Also, a PMT usually has a sensing area at about 1cm* 1cm but a PD has only 1mm*1mm sensitive area.

After the PMT, the electronic signal will go through a constant fraction discriminator (CFD). The function of the CFD is to make the estimate of the arrival time of each pulse more accurate. If the estimation of a pulse's arrival time is based on threshold intensity, (see top panel of Figure 2-3), then there will be an error Δt when the pulse intensity fluctuates. A constant fraction discriminator separates the pulse into two pulses (see bottom panel of Figure 2-3), one of which is delayed by about half of the pulse width and the other one is inverted. The sum of the two pulses will have a zero-crossing point which does not fluctuate much with intensity changes. There are two CFDs in the TCSPC system, one is used after the PMT for the start pulse and the other is used after photodiode for stop pulse.

The Time-to-Amplitude convertor (TAC) is another time-limiting component in TCSPC data acquisition. The TAC converts time into voltage by charging a capacitor. The capacitor is pre-calibrated to have a certain time to charge to its full capacity. For example, if a capacitor needs 50 ns to charge to 10 V, and the voltage accumulated between the start pulse and stop pulse is 5 V, then the time between the two pulses is 25ns. After each stop pulse, the capacitor needs to dump all of the charge and reset to 0 V. As discussed in the previous section, in reality, we choose to use the reverse-mode of counting in order to avoid over-loading the TAC. We also limit the signal collection to be one photon per 100 pulses. A 5 MHz repetition rate means 200 ns intervals between pulses and about 20 μs between each detection time. This time difference is sufficient for the TAC to respond.

Voltage pulses from the TAC then go to the multi-channel analyzer (MCA), which converts the voltage information to into temporal information and stores

successive time values in a multi-channel array. The MCA in our lab has 4096 channels with each channel representing a time increment from a minimum of 0.8 ps to a few of ns, as determined by the TAC. Each pulse from the TAC will contribute to one data point collected by the MCA. The analog-to-digital conversion involved takes about 5 μs. We usually accumulate data until the peak reaches several thousands of counts at the maximum channel. TCSPC collects only one photon after each excitation to make sure the decay collected represents the real time decay process is sampled in a statistical way. Practically, the counting rate is limited to 50,000/s to satisfy the one photon per 100 pulses requirement and to make sure only a single photon is collected after each pulse. If two photons should have been collected after the excitation, the decay profile will be distorted, typically, more intensity will appear in the early time and the lifetime calculated will be shorter than the real one.

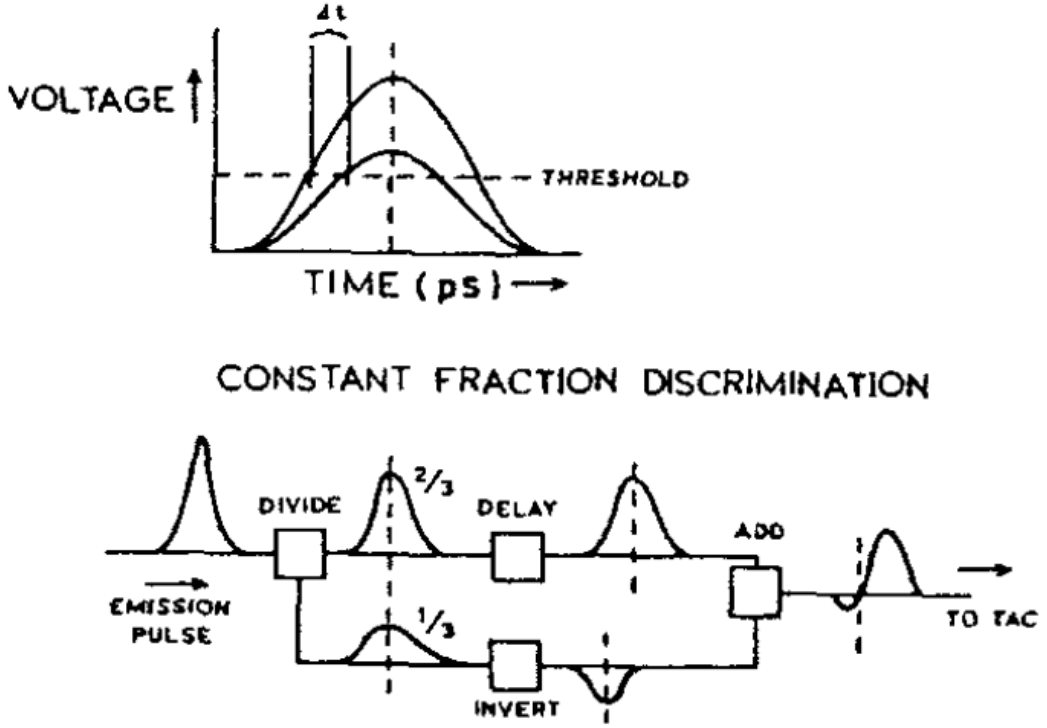

Figure 2-3 Schematics showing the operation of the constant fraction discriminator. The top panel shows the error t caused by intensity fluctuation in a constant voltage measurement. The bottom part shows the operation of a CFD[2]

2.3 Data Analysis

There are many methods of data analysis developed within the Maroncelli group that are frequently used in this thesis. In this section, I will briefly introduce the most common of these methods and also describe the basic ideas behind measurements of solvation dynamics in ionic liquids and conventional solvents.

2.3.1 Deconvolution and Least Square Fitting[2]

As discussed in the previous section, decays collected from TCSPC are usually fit to multi-exponential functions in order to obtain lifetime and other information. The collected decay intensity profile $I(t)$ is a convolution of the instrumental response function $R(t)$ and the sample signal $M(t)$. Because the instrumental response is usually not an ideal δ-function, deconvolution is necessary in order to provide a better time-resolution and the best approximation to the real sample signal $M(t)$. Experimentally, a scattering sample with some non-dairy creamer is used to determine the instrumental response function. Using the term deconvolution is not accurate since in reality, the assumed $M(t)$ with initial guessed fitting parameters are convoluted with $R(t)$ and compared with $I(t)$, and the fitting result is judged by least squares analysis:

$$\chi^2 = \sum_{k=1}^{N} \frac{1}{\sigma_k^2} [N(t_k) - N_c(t_k)]^2 = \sum_{k=1}^{n} \frac{[N(t_k) - N_c(t_k)]^2}{N(t_k)} \qquad 2.2$$

where $N(t_k)$ is the number of counts collected at t_k and $N_c(t_k)$ is the corresponding value calculated from initial parameters. σ_k is the standard deviation of each data point. χ_R^2 is a more practical parameter than χ^2 and is defined as:

$$\chi_R^2 = \frac{\chi^2}{n-p} = \frac{\chi^2}{\nu} \quad 2.3$$

where n is the number of data points, p is the number of variable parameters and $\nu = n - p$ is the number of degrees of freedom. If only random errors occur, χ_R^2 should be close to unity. But instrumental and systematic errors always occur in real experiments. For a total of 200 data points, a value of $\chi_R^2 = 1.25$ means there is only a 1% possibility for the error to be random, while a value of 1.08 means that there is 20% possibility to be random. On this basis one can say that systematic errors are likely to be present in the first case but not the second. In my experience, more important than the value of χ_R^2 is the appearance of the weighted residues D_K, which measure the deviation between measured data $I(t_k)$ and calculated data $I_c(t_k)$.

$$D_k = \frac{I(t_k) - I_c(t_k))}{\sqrt{I(t_k)}} \quad 2.4$$

In a plot of D_k versus t_k, it is easy to see systematic variations in D_K as a function of time . A good fit is when D_K is randomly fluctuates around zero, significant change in the D_K at the peak of the fit is sometimes due to the systematic error of instrumentation while it is much rarer to see this kind of systematic error in the tail of the decay.

2.3.2 Reconstruction of Time-resolved Spectra[3,4]

In TCSPC one typically collects data over a narrow band of wavelengths. If time-resolved emission spectra are desired, decays at a series of different wavelengths across the steady state emission spectrum must be collected and spectra reconstructed from these data. Typically, decays are fitted to multi exponential function:

$$I(t) = \sum_{i=1}^{n} \alpha_i \exp\left(\frac{-t}{\tau_i}\right) \quad 2.5$$

where $I(t)$ is the time-dependent intensity , α_i and τ_i are the amplitudes and time constants, which can be obtained from fitting. I_0 is the intensity at time-zero. Spectral reconstruction proceeds as follows. Suppose the intensity of a certain wavelength in the steady state spectrum is $F(\lambda_j)$. The normalization factor $H(\lambda_j)$ is calculated by

$$H(\lambda_j) = \frac{F(\lambda_j)}{\int_0^\infty I(\lambda_j,t)} = \frac{F(\lambda_j)}{\sum_i \alpha_i(\lambda_j)\tau_i(\lambda_i)} \quad 2.6$$

Then the intensity of any measured wavelength and time can be calculated using e.q 2.7

$$I'(\lambda_i, t) = H(\lambda_j)I(\lambda_j, t) = \sum_{i=1}^{n} \alpha_i'(\lambda_j)\exp\left[-\frac{t}{\tau_i(\lambda_j)}\right] \quad 2.7$$

Where $\alpha_i'(\lambda_j) = H(\lambda_j)\alpha_i(\lambda_j)$. Examples of reconstruction of time-resolved spectra from fluorescence decays collected are given in Chapter 3.3.2.

Fitting all of the data points calculated with log-normal function will result in the re-constructed time-resolved spectra. From the fitting, we can get peak frequency shift, average frequency shift, width and asymmetry factor. The frequency shift information can be transformed to solvation response function. The detailed methods and examples are discussed in Chapter 5.3.2.

2.3.3 The Solvation Response Function[3,4]

Solvation dynamics refers to how solvent molecules response to an electrical perturbation of a solute. The most common way to study solvation dynamics is by time-resolved fluorescence spectroscopy. The process is depicted in Figure 2-4: a solvation sensitive fluorophore is instantaneously excited to the S_1 state with a short laser pulse. Typically one uses fluorophores whose dipole moment increases in S_1 compared to S_0. This solute perturbation creates a nonequilibrium solvation state and the surrounding solvent molecules will reorganize to response to this changed dipole until a new equilibrium is reached. The time required for this reorganization is called the solvation time and this process is called solvation dynamics. The solvation energy relaxation can be monitored by observing the shifting of the emission spectrum of the fluorophore during the solvent equilibration. As described in the last section, reconstructed time-resolved spectra are typically fit to log-normal functions in order to determine the time-dependent peak $\nu_p(t)$ and average $\nu_a(t)$ frequencies. The solvation time can be calculated by fitting these $\nu_p(t)$ and/or $\nu_a(t)$ data with a multi-exponential:

$$\nu(t) = \sum_{i=1}^{n} \alpha_i \exp\left(\frac{-t}{\tau_i}\right) \qquad 2.8$$

or stretched exponential function:

$$\nu(t) = \nu(\infty) + \Delta\nu \exp\left\{-\left(\frac{t}{\tau_0}\right)^{\beta}\right\} \qquad 2.9$$

The normalized solvation response function is determined from ν(t) data via

$$S_\nu(t) = \frac{\nu(t)-\nu(\infty)}{\nu(0)-\nu(\infty)} \qquad 2.10$$

where $\nu(0)$ is the frequency at time-zero and $\nu(\infty)$ is the frequency at time infinity. Time-zero can be properly estimated using a method described in the next section. $\nu(\infty)$ is sometimes determined by fitting when the probe molecule has limited lifetime to measure the value. The normalized solvation response function can be used to compare the difference of solvation dynamics between systems. Solvation times have been measured in a wide range of conventional solvents and ionic liquids and they are used frequently in this thesis for the studying of charge transfer process in chapters 3 and 4. In chapter 5, a study of solvation dynamics in ionic liquid is discussed in detail.

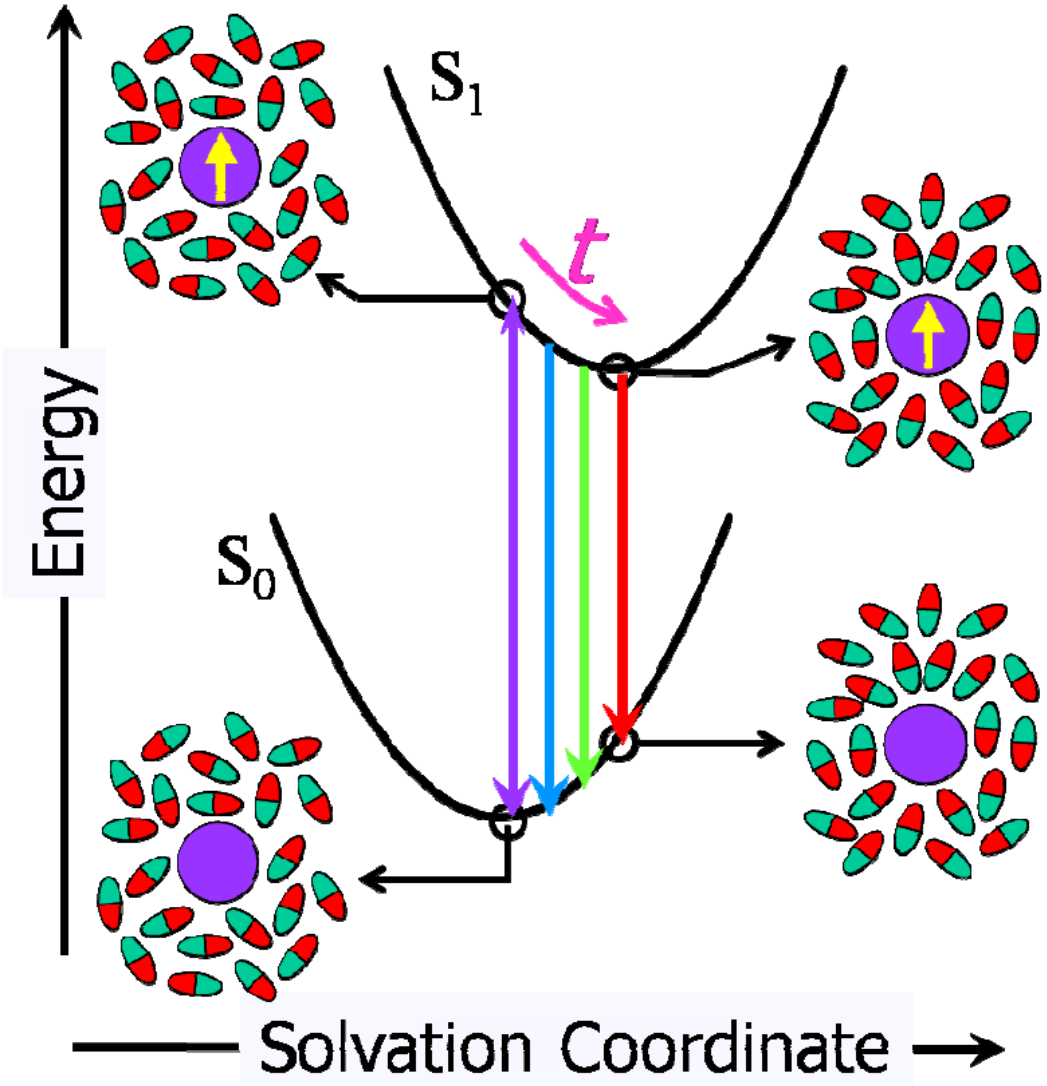

Figure 2-4 Schematic description of solvation dynamics. S_0 and S_1 represent the first two electronic energy levels of the fluorophore shown as a purple circle. The yellow arrow represents the dipole moment of the excited state. The ovals are solvent molecules with partial charges show as different colors. When the probe molecule is excited, its dipole moment changes and it takes some time *t* for the surrounding solvent molecule to reorganize into a more stable configuration for the excited state and finally emit to the ground state.

2.3.4 Estimation of Time Zero Spectrum[5]

A very important problem associated with experimental determination of $S_\nu(t)$ is to determine the initial frequency $\nu(0)$ of the emission spectrum. Determining this frequency is especially important when using TCSPC because the ~25 ps resolution of this technique is usually insufficient to capture the initial fast portions of the solvation process, which can be in the 0.1-10 ps range. Even for ionic liquids, which have much slower overall solvation than common solvents, there is still some fast relaxation missing in TCSPC experiments as has been confirmed using techniques with higher time resolution[6,7]. Fee and Maroncelli have developed a method to estimate the time-zero spectrum based on steady-state spectral data. Since they initially proposed this method, it has been applied to many studies involving solvation dynamics, and the calculated time-zero has been demonstrated to overlap with the observed one measured in high-resolution experiments.

The time-zero spectrum is defined as the hypothetical spectrum that would be observed immediately after the solute molecule is excited and has completely relaxed vibrationally but before any relaxation of the solvent occurs. The basic idea behind this method is that before any relaxation occurs, the relations between emission and absorption spectra in any solvent should coincide with these same relations in a non-polar solvent. If we use $g(\nu)$ to describe the lineshape of the absorption of a probe in any solvent and σ the shift of the lineshape in polar solvents, the inhomogeneously broadened absorption spectrum of the probe in polar solvents can be written as:

$$A_p(\nu) \propto \nu \int g(\nu - \delta) p(\delta)\, d\delta \quad (2.11)$$

where $p(\delta)$ describes the distribution of solutes among different solvation states. If we use $f(\nu)$ to represent the lineshape of the emission, the fluorescence spectrum immediately after excitation ν_{ex} (time-zero spectrum) can be represented as:

$$F_p(\nu, t = 0; \nu_{ex}) \propto \nu^3 \nu_{ex} \times \int g(\nu_{ex} - \delta)\, p(\delta) f(\nu - \delta) k_{rad}(\delta) d\delta \quad (2.12)$$

where $k_{rad}(\delta)$ is the radiative rate constant of the probe. Equation 2.11 states that the time-zero spectrum is a convolution of solvent distribution deposited into the excited state, $g(\nu_{ex} - \delta)p(\delta)$, with the fluorescence intensity function $f(\nu - \delta)k_{rad}(\delta)$. The four parameters, $g(\nu)$, $f(\nu)$, $p(\nu)$, $k_{rad}(\delta)$ used to determine F_P can be obtained from steady state spectra of the corresponding probe in a reference non-polar solvent. $g(\nu)$ and $f(\nu)$ can be directly obtained from the steady state spectra of non-polar solvents such as hexane since

$$g(\nu) \propto \nu^{-1} A_{np}(\nu) \quad (2.13)$$

and

$$f(\nu) \propto \nu^{-1} F_{np}(\nu) \quad (2.14)$$

where $A_{np}(\nu)$ and $F_{np}(\nu)$ is the absorption and emission spectrum of the non-polar reference. The radiative rate $k_{rad}(\delta)$ can be calculated from

$$k_{rad}(\delta) \propto \frac{\int f(\nu - \delta)\, \nu^3 d\nu}{\int f(\nu - \delta) d\delta} \quad (2.15)$$

and the site distribution $p(\delta)$ is assumed to be a Gaussian function:

$$p(\delta) = (2\pi\sigma^2)^{-1/2} \exp\left[-\frac{(\delta - \delta_0)^2}{2\sigma^2}\right] \quad (2.16)$$

where δ_0 is the shift induced by the polar solvent and the σ is the variation of the shift. The Gaussian width parameter σ is related to the full width (FWHM) of the solvent broadening function by:

$$\Gamma_{inh} = \sqrt{8ln2\sigma} \quad 2.17$$

Reference and Notes

(1) Chang, M. C.; Courtney, S. H.; Cross, A. J.; Gulotty, R. J.; Petrich, J. W.; Fleming, G. R. *Analytical Instrumentation* 1985, *14*, 433.

(2) *Principles of Fluorescence Spectroscopy*; Lakowicz, J. R., Ed.; Kluwer Academic Pub: New York., 1999.

(3) Castner, E. W.; Maroncelli, M.; Fleming, G. R. *J. Chem. Phys.* 1987, *86*, 1090.

(4) Maroncelli, M.; Fleming, G. R. *J. Chem. Phys.* 1987, *86*, 6221.

(5) Fee, R. S.; Maroncelli, M. *Chem. Phys.* 1994, *183*, 235.

(6) Arzhantsev, S.; Jin, H.; Baker, G. A.; Maroncelli, M. *J. Phys. Chem. B* 2007, *111*, 4978.

(7) Jin, H.; Baker, G. A.; Arzhantsev, S.; Dong, J.; Maroncelli, M. *J. Phys. Chem. B* 2007, *111*, 7291.

Chapter 3

Solvent-Controlled Electron Transfer in Crystal Violet Lactone

Reproduced in part with permission from:

Xiang Li and Mark Maroncelli* *J. Phys. Chem. A, Article ASAP, Publication Date (Web): September 10,* ***2010.***

3.1 Introduction

Crystal violet lactone (CVL; Figure 3-1) exhibits dual emission in fluid solution[1,2] as a result of a rapid excited-state charge transfer reaction.[3] Although several groups have begun to use this solute to probe various aspects of solvent-reactant coupling in ionic liquids[4-8], the solvent dependence of the CVL reaction in conventional solvents is not yet fully characterized. The present chapter describes photophysical measurements of CVL in a variety of conventional polar aprotic solvents intended to provide a more complete description of the reaction in conventional solvents, in particular how the energy and rate of the charge transfer depend upon solvent properties.

Although the photophysics of CVL had been studied earlier in the context of color formation and polymerization[9,1] it was only recently that Karpiuk first explored the excited-state reaction giving rise to the dual fluorescence of CVL.[3] Using model compounds resembling the structural components of CVL,[10,11] Karpiuk demonstrated that excitation of the lowest-energy electronic absorption leads to a polar excited state localized on the dimethylaminophthalide chromophore.[3] Solvatochromic analysis lead to an estimate of ~11 D for the dipole moment of this "locally excited" state (denoted "LE" here and "CT_A" by Karpiuk). He also showed that the second emission band, which is observed to the red of the LE band in polar solvents, is due to the transfer of an electron from one of the dimethylaminobenzonitrile moieties to the aminophthalide subsystem (Figure 3-1). The dipole moment of this charge transfer state ("CT" here; "CT_B" in Karpiuk's notation) was estimated to be ~25 D.[3] Later transient absorption

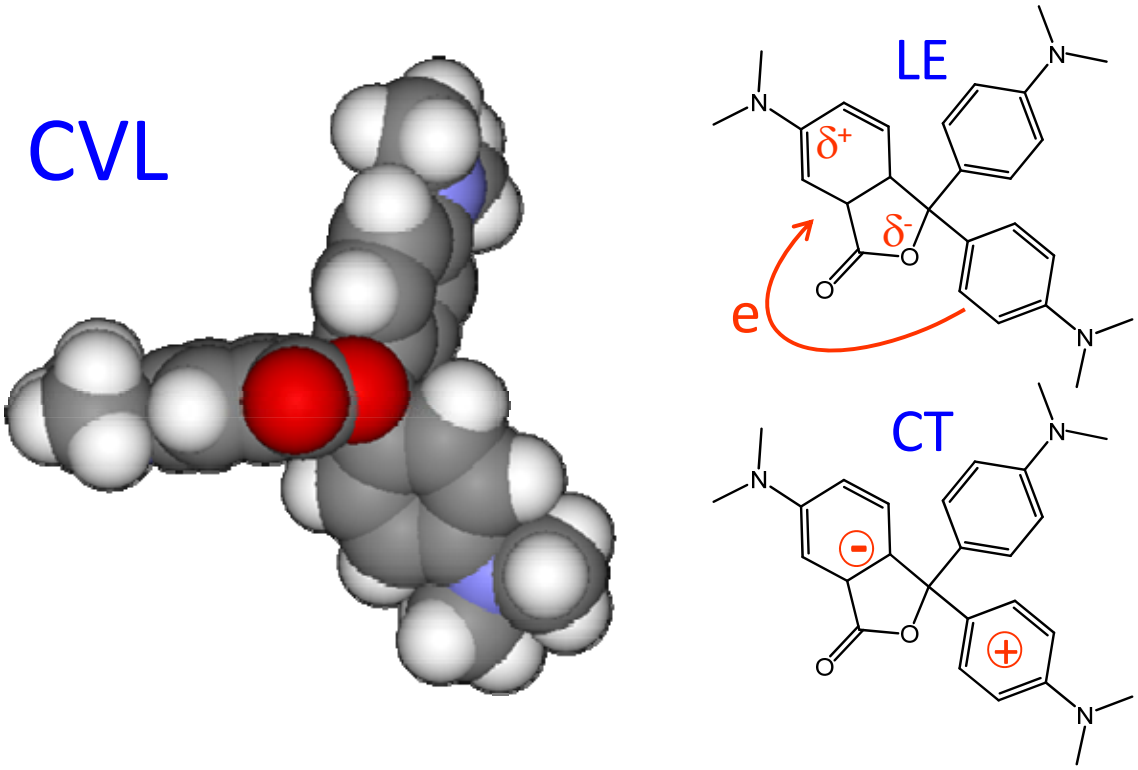

Figure 3-1 Space-filling model of CVL and schematic of illustration of the LE and CT excited states and the electron transfer reaction connecting them. The space-filling model shows the optimized ground state geometry as calculated from a CAM-B3LYP/6-311G(d) calculation

measurements in three polar aprotic solvents by Schmidhammer *et al*[12] indicated that equilibrium between the LE and CT states is established on the 10 ps time scale. As these times are roughly comparable to solvation times, these authors proposed that the charge transfer reaction is controlled by the solvent's dynamics.[12] Karpiuk also observed that the behavior of CVL in alcohol solvents differs markedly from that in aprotic solvents. In alcohols only the LE band is observed. In addition, the emission lifetime and quantum yield (φ) are much smaller in alcohols compared to aprotic solvents of like polarity. For example $\varphi = 5\times10^{-4}$ in methanol compared to 4×10^{-3} in acetonitrile.[3] The similarity of the nanosecond transient absorption spectra of CVL in 1-propanol to that of crystal violet lead Karpiuk to conclude that rapid C-O bond cleavage occurs in alcohols and potentially in other solvents capable of hydrogen bond donation. Very recently Santhosh and Samanta[6] noted that CVL has reduced lifetimes in 1,3-dialkylimidazolium ionic liquids, suggesting that such reaction might occur even these weakly protic solvents. The present work represents an extension of the characterization studies already reported by Karpiuk and coworkers on CVL and related molecules.[2,10,3,11,13,12] We focus here on conventional polar aprotic solvents in order to avoid complications of the lactone ring opening noted above. We use steady-state and picosecond time-resolved emission spectroscopy in order to more definitively establish the effects of solvent polarity and solvation dynamics on the LE $\rightarrow$ CT reaction of CVL. We find that the emission spectra and kinetics of CVL bear many resemblances to those of the "PnC" series of alkylaminobenzonitriles we have previously studied.[14] For this reason, that earlier study is a useful reference for more is a

is a useful reference for more detailed discussions of the models and analysis methods used here. As in the case of the PnC molecules, the excited state reaction is sufficiently rapid relative to the lifetime of the excited state that the relative LE and CT band intensities in the steady-state spectrum reflect the equilibrium populations of these two states. We therefore first survey the steady-state spectra observed in a range of nonpolar and polar aprotic solvents to help establish the energetics of reaction. We then describe time-resolved emission experiments used to measure reaction rates and discuss how these rates are correlated to both solvent polarity and dynamical solvent properties.

3.2 Materials and Methods

CVL was obtained from Sigma-Aldrich (97%) and crystallized twice from acetone prior to use. After recrystallization, no fluorescent impurities could be detected by any observable excitation dependence of its emission spectrum in low viscosity solvents. The solvents used here were spectroscopic or HPLC grade (typically >99%) obtained from Sigma-Aldrich. Samples for steady-state spectroscopy were prepared in 1 cm quartz cuvettes at concentrations providing optical densities of less than 0.2 at the excitation wavelength. Absorption measurements were made using a Hitachi U-3000 UV/visible spectrophotometer with a resolution of 1 nm. Corrected emission spectra were recorded with a PTI spectrometer at 2 nm resolution. Solvent blanks were subtracted from all spectra and the spectra converted to a frequency representation prior to analysis.

Time-resolved emission decays were collected using a time correlated single-photon counting instrument based on a femtosecond Ti:sapphire laser. Samples were contained in 1 cm cuvettes into which a yellow filter glass was inserted to remove reflections near time zero. Selected filters were also used in the emission path to remove stray excitation light. Emission was collected at magic angle through an ISA H10 monochromator using an emission band-pass of 8 nm. Data were collected with a resolution of 0.8 ps/channel for capturing the reaction kinetics and lower resolutions for better determining long decay components present in less polar solvents. The response time of the instrument used is 25 ps (FWHM) as measured using a scattering solution. Emission transients were fit using an iterative reconvolution algorithm which enables reliable measurement of decay components as fast as 5 ps. In most solvents, three or four pairs of decays at selected wavelengths were collected and averaged to determine reaction times and equilibrium constants. In several solvents, decays at 10-20 wavelengths spanning the emission spectrum were collected in order to produce more complete time-resolved spectra via spectral reconstruction.[15] Unless otherwise stated, both steady-state and time-resolved samples were maintained at 25.0 ± 0.2 °C using a circulating water bath. Samples were deoxygenated by bubbling with dry nitrogen gas for 15 minutes prior to data collection. Variable temperature data at temperatures lower than 10 °C were collected using an Oxford DN-1400 liquid nitrogen cryostat.

3.3 Results

3.3.1 Steady State Spectra

Representative spectra of CVL in three solvents are shown in Figure 3-2. In nonpolar solvents such as n-hexane, a single emission band is observed. This band bears a mirror image relationship to the lowest energy absorption band and it appears to originate from the same excited electronic state. As already mentioned, based on the similar S_1 absorption and emission bands of 6-dimethylaminophthalide, Karpiuk[3] assigned this transition to an excited state "LE" primarily localized on the aminophthalide ring of CVL. In solvents having relative permittivities $\varepsilon \geq 4$ a second emission band at lower energies becomes evident. Similarity to the emission of malachite green lactone lead Karpiuk to assign this second band to emission from a charge transfer (CT) state reached by partial electron donation from one or both dimethylaniline portions of the molecule to the aminophthalide ring.[3] We note that the emission spectra shown in Figure 3-2 differ somewhat from those reported by Karpiuk (Figure 3-3 of Ref.[3]). Whereas peak frequencies are nearly the same, the shapes of broad bands such as the emission in CH_2Cl_2 and the relative LE/CT intensity ratios in solvents like CH_3CN shown in Figure 3-1, appear to differ significantly. Reference [3] does not state whether any correction was made for the wavelength-dependent responsivity of the spectrometer, and it is likely that differences in spectral correction are the source of this discrepancy.[16]

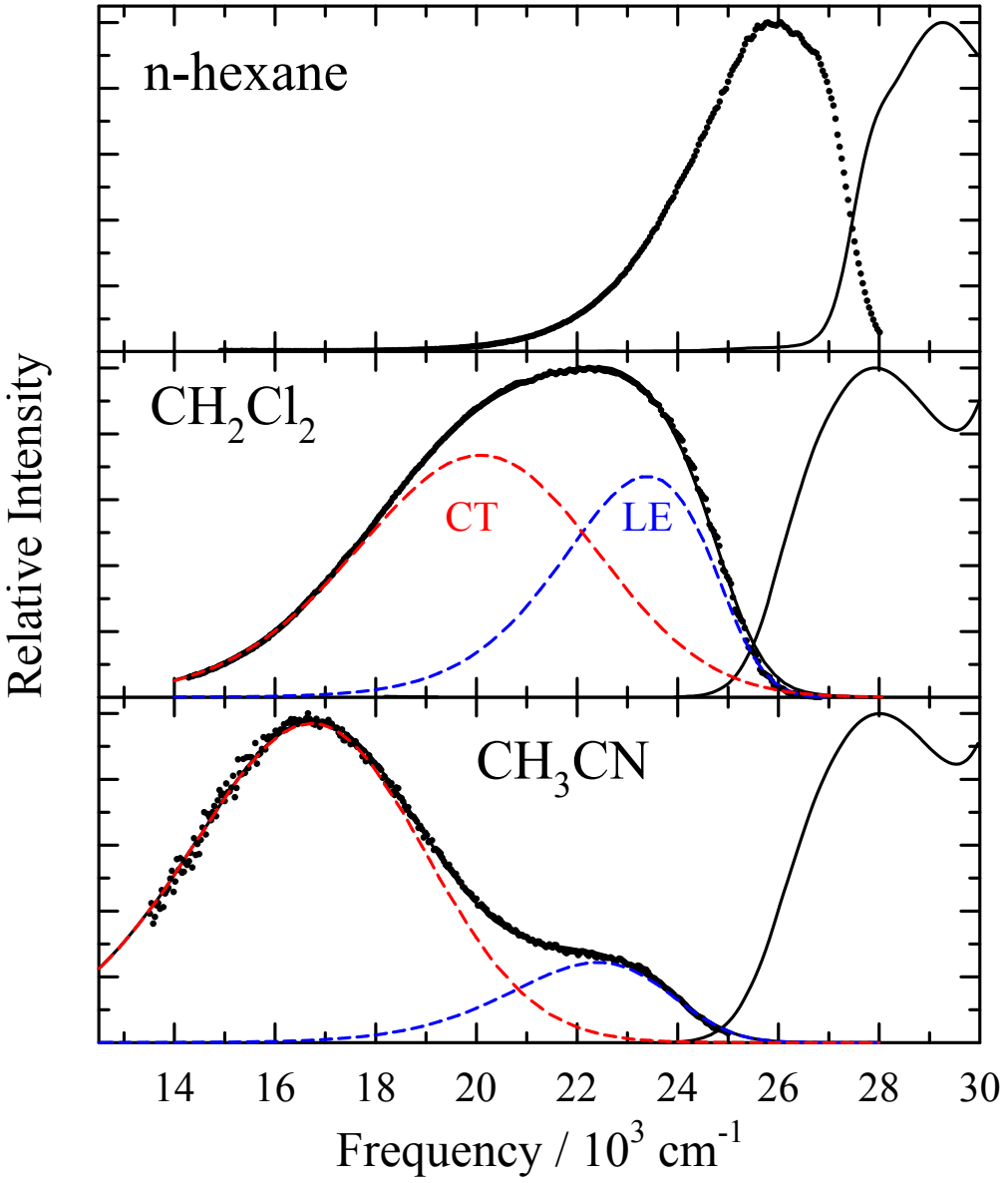

Figure 3-2 Representative absorption and emission spectra of CVL in n-hexane, dichloromethane, and acetonitrile. Observed emission spectra are shown as points. Fits (solid curves) and their decompositions into CT_A and CT_B contributions are shown as dashed curves

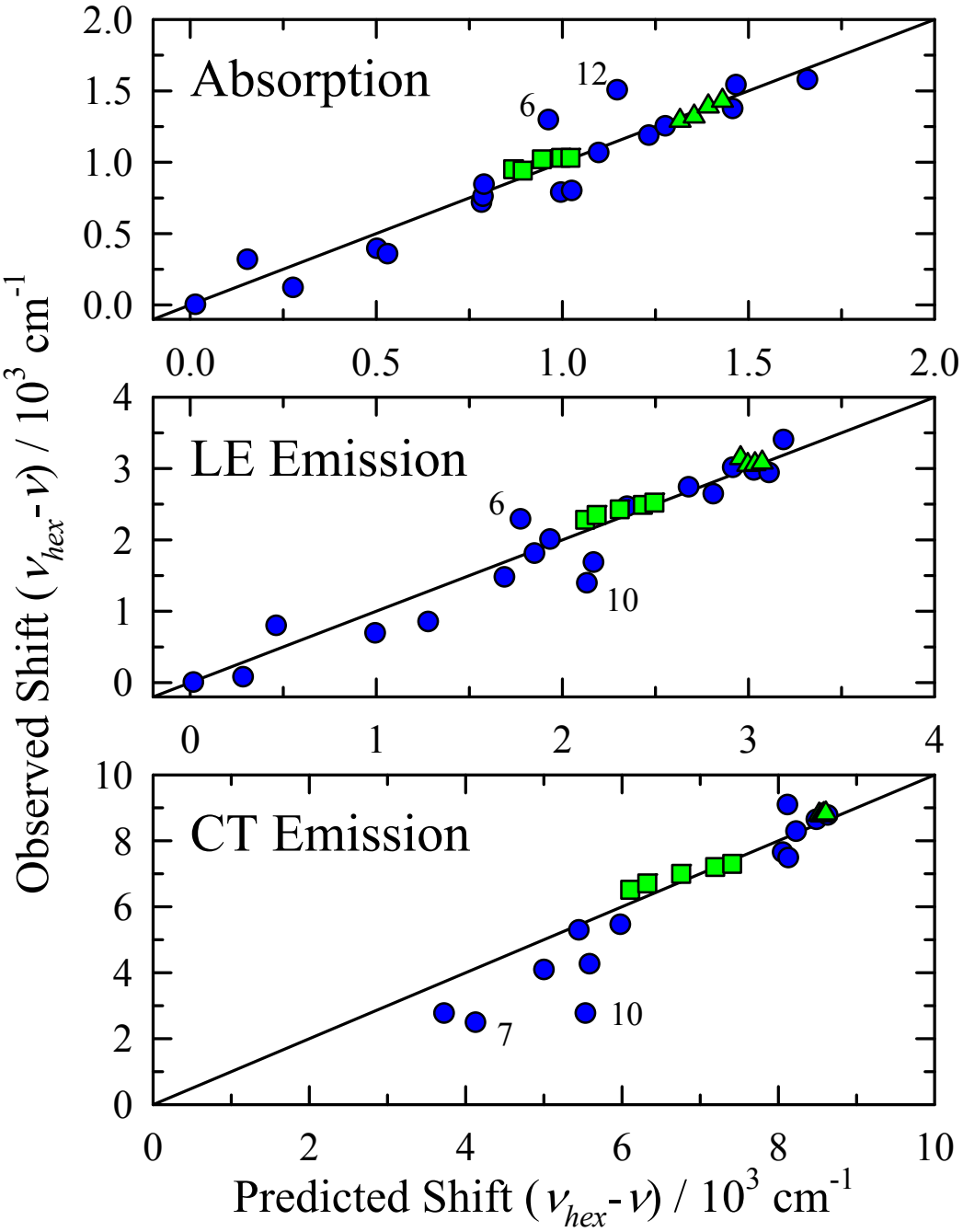

Figure 3-3 Correlation of spectral shifts measured relative to frequencies in n-hexane with solvent dielectric properties. The blue points are data in the pure solvents listed in Table 3-1: the green squares are from mixtures of acetone and methyl acetate, and green triangles from propylene carbonate + acetonitrile mixtures. Numbers indicate specific solvents as listed in Table 3-1.

To quantify the solvent dependence of the frequencies and relative intensities of the emission bands, we employed fits based on a simple inhomogeneous broadening model.[17] Specifically, we assume that both bands can be represented by shifting and broadening an "unsolvated" vibronic lineshape function using a Gaussian function to represent the distribution of solvent-induced frequency shifts present in a given solvent. For the lineshape function of both bands we use $L(\nu) \propto F_{np}(\nu)/\nu^3$ where $F_{np}(\nu)$ is the (LE) fluorescence spectrum observed in n-hexane. This approach does not provide absolute measures of the solvent shift or broadening of the CT emission, but it is nevertheless a useful and consistent way to dissect the spectra and determine relative information, especially the relative band intensities of most interest here. Two such fits are illustrated by the dashed curves in Figure 3-1. Characteristics of the steady-state emission spectra obtained from such fits along with peak frequencies of the S_1 absorption and emission peaks are summarized in Table 3-1.

To correlate these data with solvent properties we use the spherical-polarizable-dipole solute, dielectric continuum solvent model described in Refs.[14] and [18]. Transition frequencies (*tr* = *abs* or *em*) are assumed to depend on solvent dielectric properties according to:

$$h\nu_{tr} = h\nu_{tr}^0 + A_{tr} d_c(n^2) + C_{tr}\{d_c(\varepsilon) - d_c(n^2)\} \qquad 3.1$$

$$A_{tr} = -(\mu_f^2 - \mu_i^2)a^{-3} \qquad C_{tr} = -2\vec{\mu}_i \cdot (\vec{\mu}_f - \vec{\mu}_i)a^{-3} \qquad 3.2$$

where $h\nu_{tr}^0$ is the transition energy in the gas phase. Solute parameters in this description are the dipole moments in the initial *i* and final *f* electronic states of the transition, and the

#	solvent	ε_r	n_D	ν_{abs}	ν_{LE}	ν_{CT}	$\Delta\nu_{LE}$	$\Delta\nu_{CT}$	f_{CT}
1	n-hexane	1.88	1.372	29.27	25.87		0		
2	cyclohexane	2.02	1.424	29.15	25.79		0.07		
3	1,1,2-trichlorotrifluoroethane	2.41	1.356	28.96	25.22		0.79		
4	di-n-butyl ether	3.08	1.397	28.88	25.32		0.69		
5	di-isopropyl ether	3.88	1.366	28.92	25.22		0.85		
6	chloroform	4.89	1.442	27.98	23.21		2.29	2.76	0.77±.30
7	butyl acetate	5.01	1.392	28.56	24.30		1.47	2.48	0.34±.11
8	ethyl acetate	6.02	1.370	28.51	23.91		1.81	4.08	0.32±.12
9	methyl acetate	6.68	1.359	28.43	23.77		2.00	5.28	0.34±.05
10	1-chlorobutane	7.39	1.400	28.48	24.57		1.39	2.76	0.17±.08
11	tetrahydrofuran	7.58	1.405	28.47	24.01		1.68	4.25	0.30±.10
12	dichloromethane	8.93	1.421	27.77	(22.3)		2.46	5.45	0.64±.05
13	acetone	20.56	1.356	28.21	(23.0)	18.21	2.74	7.64	0.81±.05
14	butyronitrile	24.83	1.382	28.09	(23.5)	18.18	2.64	7.47	0.81±.05
15	acetonitrile	35.94	1.382	28.02	(23.2)	16.78	3.01	8.63	0.93±.05
16	N,N-dimethylformamide	36.71	1.428	27.90	(23.5)	17.32	2.97	8.27	0.89±.05
17	dimethylsulfoxide	46.45	1.477	27.70	(22.8)	16.64	3.40	9.08	0.85±.05
18	propylene carbonate	64.92	1.419	27.73	(23.2)	16.77	2.94	8.77	0.81±.05

Table 3-1 Characteristics of Steady-State Spectra (25 °C): ε_r and n_D are the relative permittivity and refractive index of the solvent from Ref.[23] ν_{abs}, ν_{LE}, and ν_{CT} are peak frequencies of the S_1 absorption band and of the peaks of the high- (LE) and low-frequency (CT) bands measured directly from the emission spectra. Values in parenthesis indicate estimates in cases where no true 2nd maximum is present. $\Delta\nu_{LE}$ and $\Delta\nu_{CT}$ are the shifts of the LE and CT bands relative to n-hexane, and f_{CT} is the fractional area of the CT emission band based on the fitting method described in the text. In these fits, the inhomogeneous broadening of the CT band was fixed at 4300 cm^{-1} and that of the LE band was assumed to depend on solvent according to $\Gamma_{LE}/\mathrm{cm}^{-1} = 336 + 2080 d_{25}(\varepsilon, n_D^2)$. The latter parameters were chosen based on unconstrained fits to the spectra and applied in order to help minimize variations in f_{CT} due the underdetermined nature of some fits. All frequencies are in units of 10^3 cm^{-1}. Cavity size a and polarizability α, both assumed independent of state. d_c is a reaction field factor

$$d_c(x) \equiv \frac{d_0(x)}{1-2cd_0(x)} \qquad d_0(x) \equiv \frac{x-1}{2x+1} \tag{3.3}$$

which depends on solute polarizability via the ratio $c = \alpha/a^3$. Here we assume $c = 0.25$, a value intermediate between the non-polarizable (c=0) and Clausius-Mossotti (c = ½) limits. The particular value used is of little consequence for the present purposes.

Figure 3-3 shows that the solvatochromic shifts of the S_1 absorption (peak) and the LE and CT bands of CVL are reasonably represented by this model. The coefficients A_{tr} and C_{tr}, obtained from bilinear fits to the data in Table 3-1 combined with data from mixtures of methyl acetate + acetone (green squares in Figure 3-3) and acetonitrile + propylene carbonate (green triangles), are compiled in Table 3-2. In principle, these fit parameters can be used to calculate changes in the dipole moments associated with the various transitions, and Karpiuk discusses such calculations in some detail.[3] In the case of CVL, there is a great deal of ambiguity in using the model described above (or any other simple model) to deduce dipole moments due to the highly non-spherical shape of this molecule (Figure 3-1). Based on comparisons to the component chromophores of CVL, Karpiuk proposed the use of two different effective spherical radii, a = 3.6 Å for analyzing the LE emission (and $S_0 \rightarrow$LE absorption) and a = 5.8 Å for the CT emission. Adopting these same choices for cavity radii and a ground state dipole moment of 6.0 D from B3LYP/6-311G(d) calculations[19] the results in Table 3-2 suggest a dipole moment of 9-12 D in the LE state and about 24 D in the CT state. While we have little confidence in the accuracy of these estimates, they are close to the values obtained by Karpiuk, based

	Abs ν_{pk}	Em $(\nu_{hex} - \nu_{LE})$	Em $(\nu_{hex} - \nu_{CT})$
$h\nu_{tr}^{0}$	31.71±.43	-2.49±.86	-3.1±2.8
A_{tr}	-12.2± 2.0	12.3± 4.1	8.9±12
C_{tr}	-2.87±.21	6.73±.42	23.2±2.1
N_{obs}	27	27	23
R	0.95	0.96	0.93
σ_{fit}	0.14	0.28	0.81

Table 3-2 Summary of Solvatochromic Fits $h\nu_{tr}^{0}$, A_{tr}, and C_{tr} are the coefficients in Eqs. 1-2 in units of 103 cm^{-1}. The column "Abs ν_{pk}" lists coefficients of the fits to absorption peak frequencies and the columns "Em $(\nu_{hex} - \nu_{tr})$" are those of fits of the emission shifts relative to n-hexane. N_{obs}, R, and σ_{fit} denote the number of data points, the linear correlation coefficient, and the standard error of each fit.

on a different solvatochromic approach. We also note that a dipole moment of 24 D for the CT is equivalent to separation of $\pm 1e$ over a distance of 5 Å. The distance between the centers of mass of the donor dimethylaniline and aminophthalide rings is 5.6 Å, consistent with the idea of complete electron transfer in the LE $\rightarrow$ CT reaction.

Figure 3-4 illustrates the changes in emission observed as a function of temperature in the solvent n-butyronitrile. Over the temperature range shown, both the LE and CT bands shift to higher frequencies with increasing temperature as a result of the decreasing density and polarity of the solvent. These approximately linear shifts are characterized by temperature derivatives of 5.4 cm^{-1} K^{-1} (LE) and 11 cm^{-1} K^{-1} (CT). Of most interest in Figure 3-4 is the non-monotonic variation of the relative intensities of the LE and CT bands. These intensities are shown in the form of a "Stevens-Ban plot"[20] in Figure 3-5. Also included are analogous data in propylene carbonate. If certain requirements are met, the high-temperature limiting slopes in such plots provide estimates of the reaction enthalpy, $\Delta_r H$, and the low-temperature slope the activation enthalpy $\Delta_r H^*$ of the LE $\rightarrow$ CT reaction.[20-22] The data in Figure 3-5 provide $\Delta_r H$ = -17 ± 1 kJ/mol and $\Delta_r H^*$ = 11 ± 2 kJ/mol in butyronitrile and $\Delta_r H^*$ = 12 ± 3 kJ/mol in propylene carbonate. Although we do not expect the activation enthalpies determined in this way to be as accurate as those deduced from the time-resolved data discussed below, we note that these values of $\Delta_r H^*$ are close to the viscosity activation energies of the two solvents, E_η = 8.7 kJ/mol in butyronitrile and 16 kJ/mol in propylene carbonate (at 25 °C).[23]

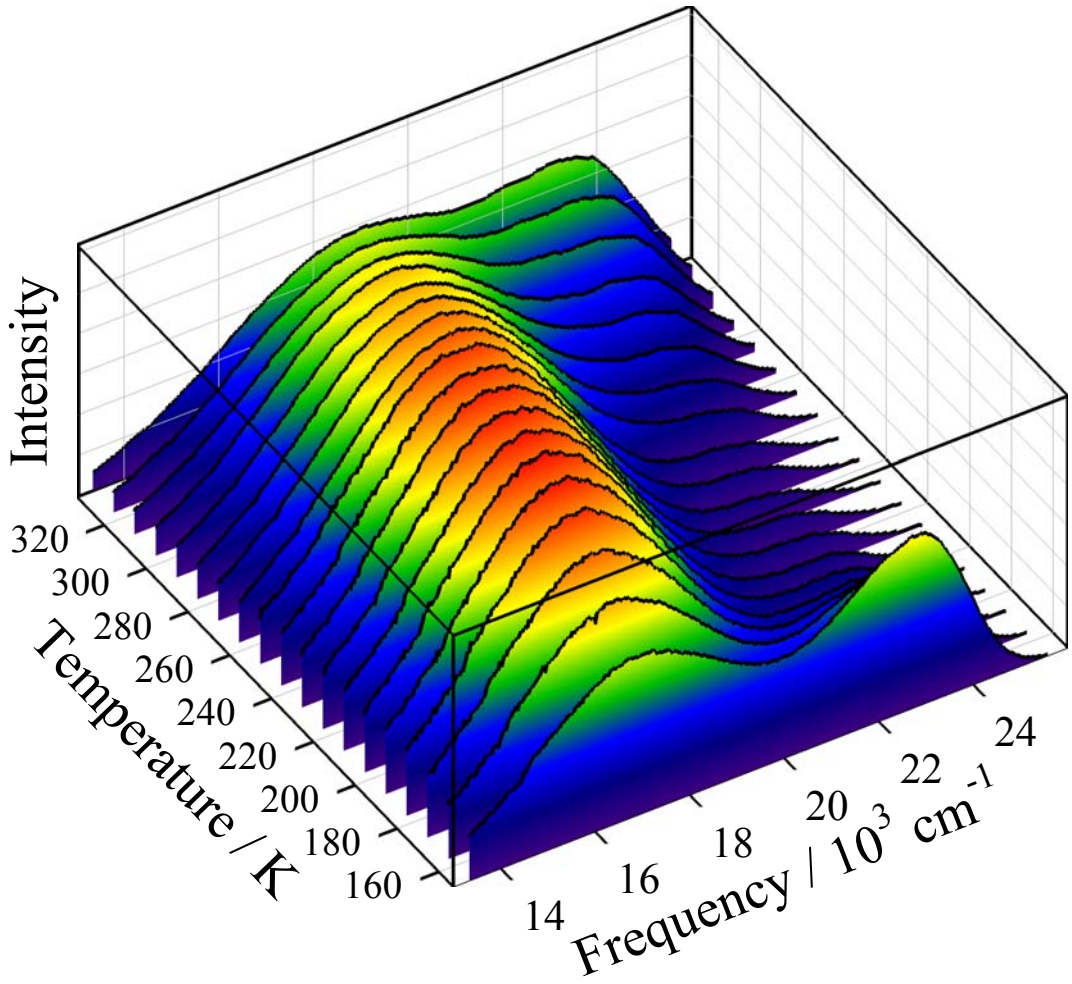

Figure 3-4 Temperature dependence of the steady-state emission of CVL in n-butyronitrile. Spectra have been area-normalized to display the relative intensity changes of the LE and CT bands.

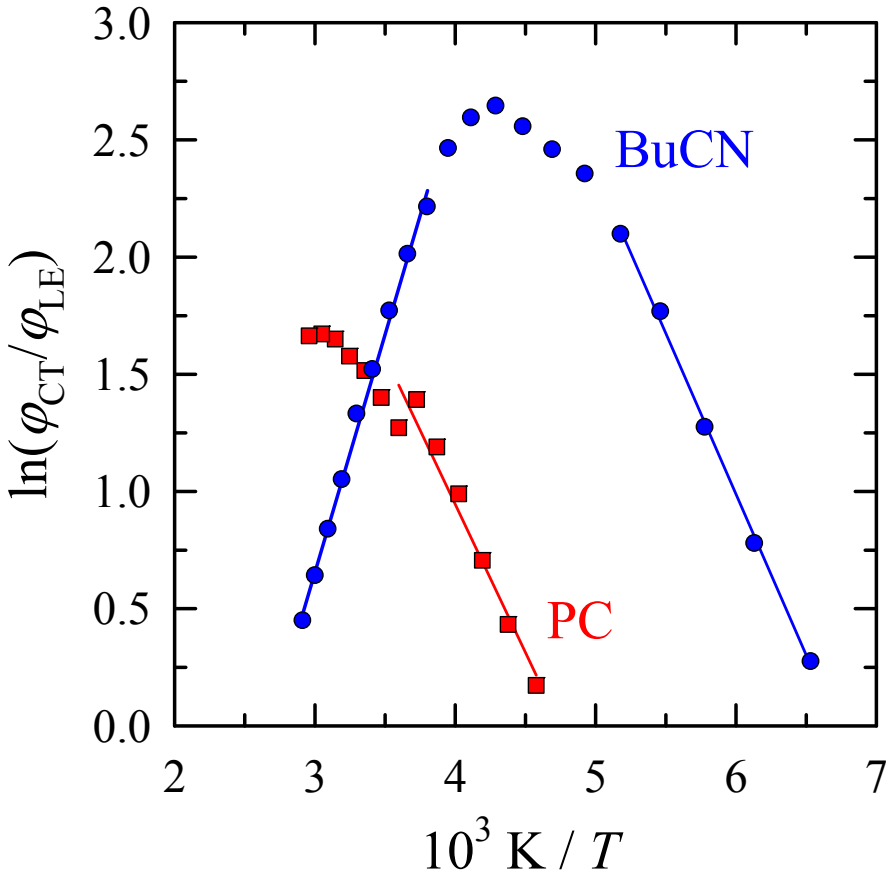

Figure 3-5 "Stevens-Ban" plots of the ratio of integrated intensities of the CT and LE emission bands of CVL in n-butyronitrile (BuCN) and propylene carbonate (PC). The lines shown here are fits to the limiting low- and high-temperature slopes which provide estimate of $\Delta_r H^*$ and $\Delta_r H$, respectively.

3.3.2 Time-Resolved Emission & Kinetic Model

Representative time-resolved emission decays of CVL in acetone are shown in Figure 3-6. These decays are typical of what is observed in moderate- to high-polarity solvents. Emission near the peak of the LE maximum undergoes a pronounced rapid decay with a time constant in the 10-30 ps range, followed by a small amplitude component having a nanosecond time constant. In the region of the CT emission there is a fast rise and slow decay with essentially the same two time constants. Multi-exponential fits are illustrated by the weighted residuals at the top of Figure 3-6 and the parameters obtained from these fits are shown in the inset Table. In many cases a purely bi-exponential function does not fit the transients in the LE region to within statistical uncertainties. A third, small amplitude (2% here) component with an intermediate time constant is often necessary. We believe that this intermediate component represents impurity fluorescence which we have not been able to completely eliminate.[24] Nevertheless, it is clear that in most conventional liquid solvents the emission kinetics of CVL conform closely to those of a two-state interconversion process. Further evidence of this simple kinetics is provided in Figure 3-7 where we display representative time-resolved emission spectra of CVL collected in acetone and butyronitrile. These spectra were obtained via spectral reconstruction of unconstrained fits of emission decays collected at individual wavelengths.[15] Fitting these time-resolved spectra in the same manner as the steady-state spectra (solid curves in Figure 3-7) shows that the LE

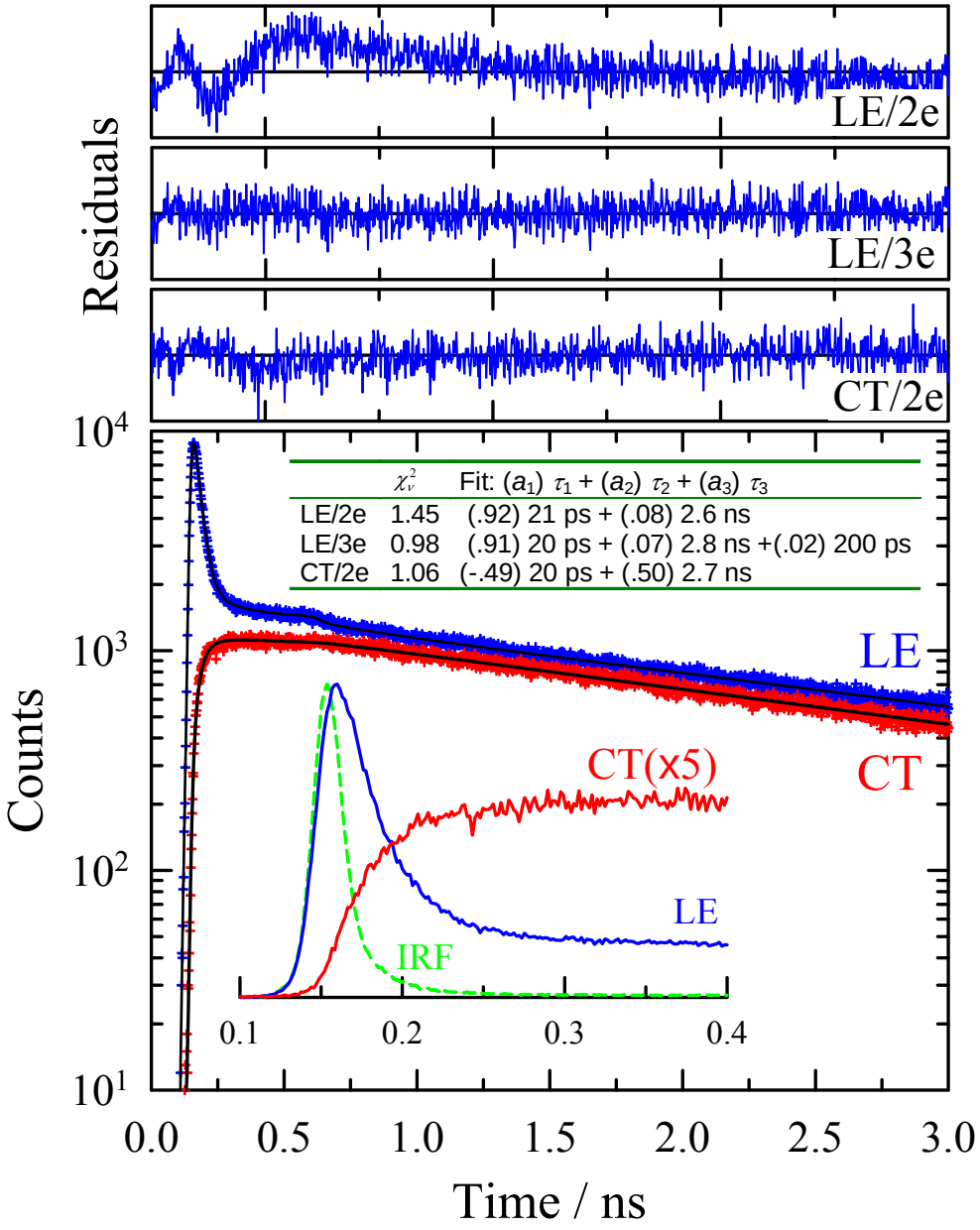

Figure 3-6 Representative emission decays of CVL in acetone (25 °C). The points on the bottom are experimental data in the LE (435 nm, blue) and CT (580 nm, red) spectral regions and the superimposed curves are multiexponential fits to these data. The inset graph is an expanded view of the early-time data using a linear vertical scale and showing the instrumental response function "IRF". The upper panels are the weighted residuals of double and triple exponential fits to the LE decay and a double exponential fit of the CT decay. In the case of the CT fit, the rise time was fixed to the decay time of the LE emission. Parameters of these three fits are provide in the inset Table.

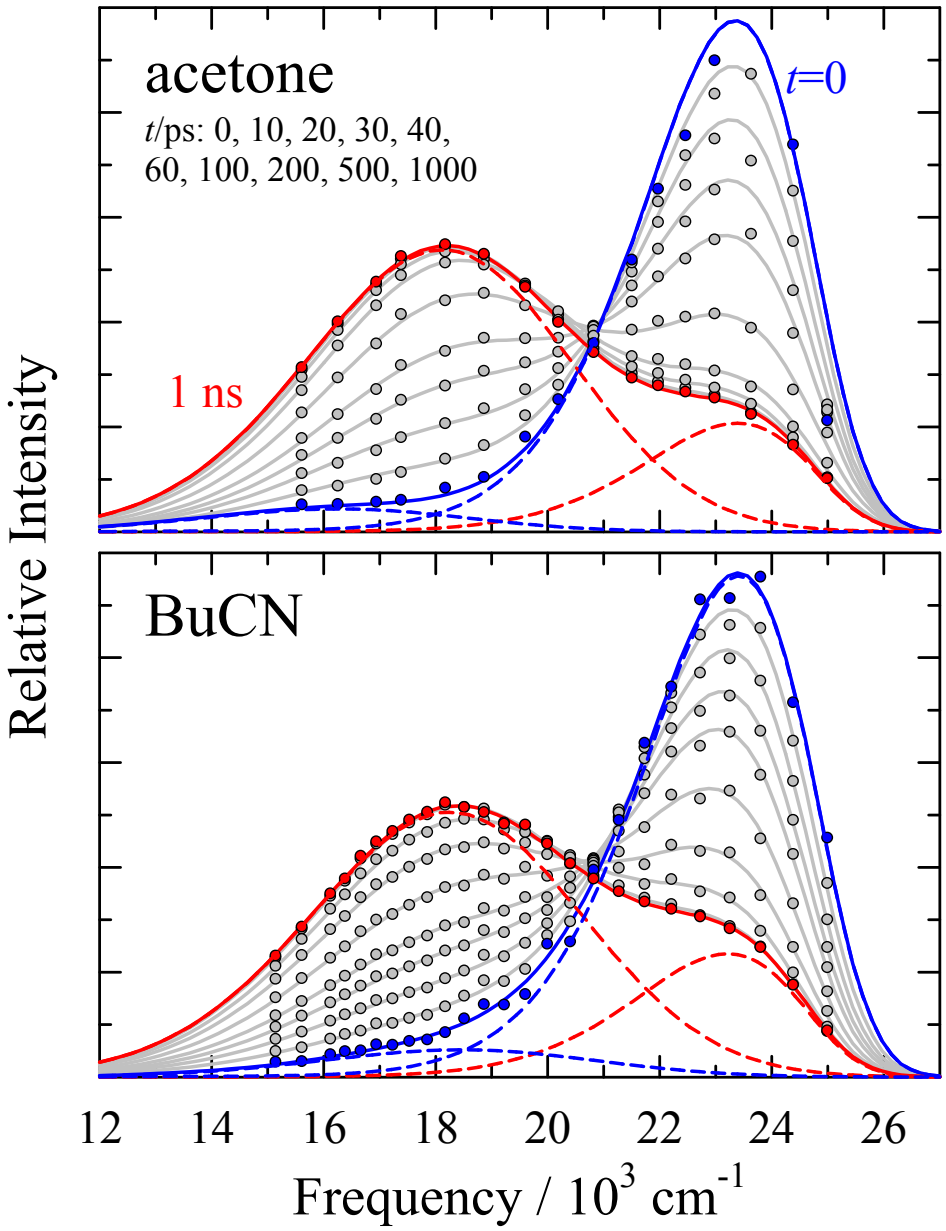

Figure 3-7 Area normalized time-resolved emission spectra of CVL in acetone and n-butyronitrile. The points are spectral data reconstructed from unconstrained fits of emission transients at each wavelength. The solid curves are fits of these reconstructed spectra data using the same procedure described for steady-state emission. The dashed curves show the component LE and CT spectra at $t = 0$ and 1 ns.

emission decreases in intensity synchronously with the rise of the CT emission. In solvents like acetone and butyronitrile, whose solvation times are much shorter than the 25 ps instrument response time of these experiments, the area-normalized spectra exhibit approximate isoemissive points (near 21,000 cm^{-1} in Figure 3-6) characteristic of a 2-state process.[25] This observation is consistent with the results of Schmidhammer *et al*.[12] who reported clear isosbestic points in the transient absorption of CVL in two solvents.[26] Figure 3-7 also shows decompositions of the t=0 and late-time spectra into LE and CT components (dashed curves). Note that a small (~10%) CT component is apparently present at time zero. This prompt CT emission is most likely an artifact related to fitting individual decays without constraints. Fitting rise components having time constants near to the instrument response time, as is the case here, is highly uncertain because rises times, amplitudes, and time shifts are all strongly correlated. When the rise times in the CT region are fixed to equal those in the better-defined decays in the LE region (as in Figure 3-6) no CT component is observed at time zero.

Based on the observations just mentioned, we interpret the time-resolved data in terms of the 2-state kinetic model shown in Scheme 3-1, assuming no direct excitation of the CT state. (The present analysis is very similar to that described in Ref.[14] and more details can be found there.[27]) In the limit of rapid excited-state equilibrium (k_f, k_r >> k_{LE}, k_{CT}) relevant here, the populations are expected to follow the relations:

$$[\mathrm{LE}(t)]/[\mathrm{LE}]_0 \cong \frac{1}{k_f + k_r}(k_r e^{-k_{dec}t} + k_f e^{-\kappa_{rxn}t}) \qquad 3.4$$

$$[\mathrm{CT}(t)]/[\mathrm{LE}]_0 \cong \frac{k_f}{k_f + k_r}(e^{-k_{dec}t} - e^{-\kappa_{rxn}t}) \qquad 3.5$$

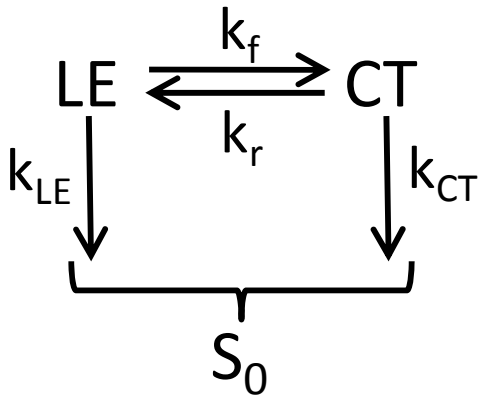

Scheme 3-1

with

$$\kappa_{rxn} = k_f + k_r \tag{3.6}$$

and

$$k_{dec} = \frac{k_{LE}k_r + k_{CT}k_f}{k_f + k_r} \tag{3.7}$$

Table 3-3 lists parameters based on bi-exponential fits of time-resolved emission data of the sort shown in Figure 3-6 and interpreted within the context of the above model. In addition to the time constants $\tau_{rxn} = \kappa_{rxn}^{-1}$ and $\tau_{dec} = k_{dec}^{-1}$, also listed are values of the normalized amplitudes a_{fast} of the fast component of emission measured on the blue side of the LE band where CT emission is negligible. Some comparisons of the time constants observed are available from the work of Karpiuk and coworkers.[3,12] For the six solvents in which there is overlap, the values of τ_{dec} reported here average 15% smaller than those previously reported.[3] This systematic difference can be reasonably ascribed to either a difference in deoxygenation techniques or to the different time resolutions available (~1 ns in the case of Ref. [3]) More important is a comparison of the fast time constants τ_{rxn} with the transient absorption data of Schmidhammer *et al.*[12]. Using an instrument with 300 fs resolution, these authors reported LE and CT rise and decay times of 8.6 ± 0.4 ps in acetonitrile, (28 ± 6 ps) in propylene carbonate, and DMSO (14 ± 2 ps) in dimethylsulfoxide. In the case of the first two solvents, our data agree quantitatively with their results. This agreement, especially in the case of acetonitrile, supports the idea that one can measure time constants which are comparable to or even significantly smaller than the 25 ps instrument response time of the TCSPC instrument with

reasonable accuracy. However, the present result in DMSO, 29 ± 3 ps, is markedly different from that of Schmidhammer *et al*., and the reason for this difference is unknown.

Before discussing the kinetic parameters in Table 3-3 in more detail, we first use these data to estimate the equilibrium constant for the LE $\rightarrow$ CT reaction. According to Eq. 3-4 $a_{fast} = k_f /(k_f + k_r)$ so that a_{fast} is related to the equilibrium constant via:

$$K_{eq} = \frac{k_f}{k_r} = \frac{a_{fast}}{1 - a_{fast}} \tag{3.8}$$

In the rapid-reaction limit, ratio of band intensities or quantum yields φ in steady-state spectra are also related to the equilibrium constant as follows:

$$\frac{\varphi_{CT}}{\varphi_{LE}} = \frac{k_{rad}^{CT}}{k_{rad}^{LE}} \frac{k_f}{k_r} = \frac{k_{rad}^{CT}}{k_{rad}^{LE}} K_{eq} \tag{3.9}$$

Making the assumption that ratios of radiative rates in different solvents depend only upon emission frequencies due to the relation $k_{rad} \propto \nu_{em}^3$, equilibrium constants can be estimated from steady-state data to within a constant factor *C* via:

$$K_{eq} = C \frac{\nu_{LE}^3 \varphi_{CT}}{\nu_{CT}^3 \varphi_{LE}} \tag{3.10}$$

Both measures of K_{eq} are provide in logarithmic form in Table 3-3. A weighted average of the differences between the time-resolved and steady-state estimates yields *C* = 2.4 ± 0.3. Using this value of *C* the two estimates of K_{eq} are compared in Figure 3-8 (a). As shown here, there is reasonable agreement between the steady-state and time-

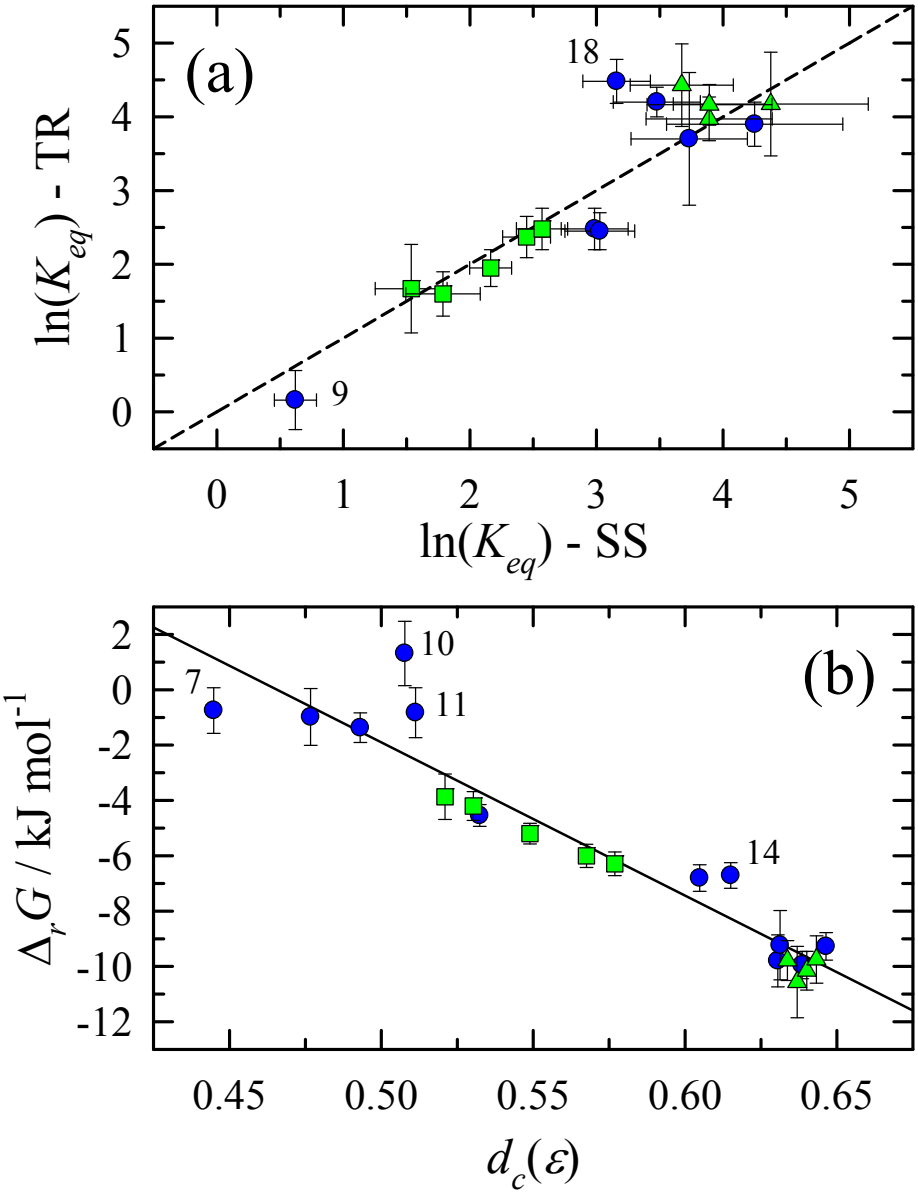

Figure 3-8 Equilibrium constant and free energy change of the LE→CT reaction. (a) Comparison of equilibrium constants determined from relative amplitudes of the LE decay ("TR") and from relative intensities of steady-state CT and LE emission ("SS"). (b) Estimates of reaction free energies determined from weighted averages of the lnK_{eq} data versus dielectric reaction field factor $d_c(\varepsilon)$. The line drawn in this panel is the regression $\Delta_r G / \text{kJ mol}^{-1} = 25.8 - 55.4 d_c(\varepsilon)$ ($r^2 = 0.90$). The green squares are data from mixtures of acetone and methyl acetate, and green triangles from propylene carbonate + acetonitrile mixtures. Numbers indicate specific solvents as listed in Table 3-3

resolved estimates. Reaction free energies, $\Delta_r G$, obtained from a combination of these K_{eq} values via $\Delta_r G = -RT \ln K_{eq}$, are also summarized in Table 3-3. We note that the values determined in highly polar solvents are somewhat larger than the values of -3 to -4 kJ/mol estimated by Schmidhammer *et al.*[12] on the basis of less direct information (but much smaller than the earlier estimate of -57 kJ/mol[3]). The present values of $\Delta_r G$ are plotted versus the dielectric reaction field factor $d_c(\varepsilon)$ in Figure 3-8(b). With a few exceptions such as dichloromethane (#10), the correlation between $\Delta_r G$ and $d_c(\varepsilon)$ is good. Using the same model employed for solvatochromic analysis, the slope in such a plot is expected to be given by

$$\frac{d(\Delta_r G)}{d(d_c)} = -\left(\frac{\mu_{CT}^2}{a_{CT}^3} - \frac{\mu_{LE}^2}{a_{LE}^3} \right) \qquad 3.11$$

The observed value, -55 kJ/mol is consistent with the estimates of the LE and CT dipole moments determined from analysis of frequency shifts. Using Karpiuk's[3] values for cavity radii once again, a_{LE} = 3.6 Å and a_{CT} = 5.8 Å, and the estimate μ_{CT} = 24 D, the observed slope implies μ_{LE} = 9.7 D, in the middle of the range 9-12 D suggested by the solvatochromic analysis.

We now consider the solvent dependence of the kinetic quantities in Table 3-3. In Figure 3-9 we plot the average decay rate, $k_{dec} = 1/\tau_{dec}$, as a function of the peak CT emission frequency. In solvents more polar than acetone, there is a good correlation between ν_{CT} and the logarithm of k_{dec}. In these solvents, for which $K_{eq} > 4$, Eq. 3.7 indicates that k_{dec} should be approximately equal to k_{CT}, the rate constant for CT-state

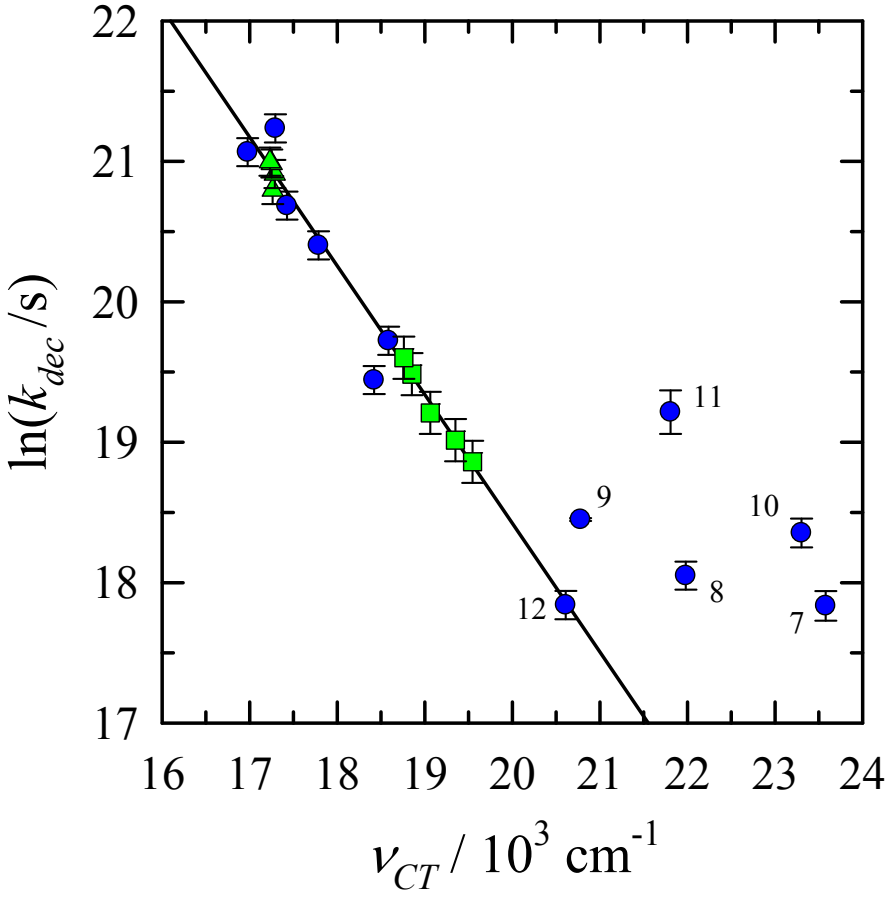

Figure 3-9 Decay rate constants k_{dec} associated with the slower emission decay component plotted versus CT frequency. The blue points are data in pure solvents, the green squares and triangles are data in mixtures of acetone + methyl acetate and propylene carbonate + acetonitrile, respectively. Numbers indicate specific solvents listed as in Table 3-3.

	solvent[a]	$d_c(\varepsilon)$	η /cP	$<\tau_{solv}>$ /ps	a_{fast}	τ_{rxn} /ps	τ_{dec} /ns	$\ln\frac{a_{fast}}{a_{slow}}$	$\ln\frac{v_{LE}^3\varphi_{CT}}{v_{CT}^3\varphi_{LE}}$	$\Delta_r G$ /kJ mol^{-1}	k_f /ns^{-1}
7	butyl acetate	0.44					18		-0.6	-0.7±.8	
8	ethyl acetate	0.48					15		-0.5	-1.0±1.0	
9	methyl acetate	0.49	0.36	0.85	0.54	36	10	0.2	-0.2	-1.4±.5	18±4
10	1-chlorobutane	0.51					11		-1.4	1.3±1.2	
11	tetrahydrofuran	0.51					4.5		-0.5	-0.8±.9	
12	dichloromethane	0.53	0.41	0.56	0.30	70	18		1.0	-4.5±.4	12±2
13	acetone	0.60	0.30	0.58	0.92	22	3.6	2.5	2.1	-6.8±.5	42±10
14	butyronitrile	0.62	0.55	0.75[b]	0.92	25	4.6	2.5	2.2	-6.7±.5	37±6
15	acetonitrile	0.63	0.34	0.26	0.98	8	1.2	3.9	3.4	-9.8±.9	120±30
16	N,N-dimethylformamide	0.63	0.80	0.91	0.97	23	1.4	3.7	2.9	-9.2±1.3	43±5
17	dimethylsulfoxide	0.64	1.99	2.0	0.98	29	0.71	4.2	2.6	-10.0±.5	34±3
18	propylene carbonate	0.65	2.53	2.0	0.99	30	0.6	4.5	2.3	-9.3±.5	33±3
21	3:1 MeOAc+acetone	0.52	0.35	0.78	0.83	41	6.4	1.7	0.7	-3.9±.8	20±6
22	2:1 MeOAc+acetone	0.53	0.34	0.76	0.83	40	5.5	1.6	0.9	-4.2±.5	21±3
23	1:1 MeOAc+acetone	0.55	0.33	0.72	0.87	37	4.6	2.0	1.3	-5.2±.4	24±5
24	1:2 MeOAc+acetone	0.57	0.32	0.67	0.91	27	3.5	2.4	1.6	-6.0±.4	34±5
25	1:3 MeOAc+acetone	0.58	0.32	0.65	0.92	27	3.1	2.5	1.7	-6.3±.4	35±5
31	1:4 PC+ACN	0.63	0.45	0.37	0.97	13	0.93	4.0	3.0	-9.8±.7	78±12
32	2:3 PC+ACN	0.64	0.62	0.52	0.98	15	0.83	4.2	3.5	-10.6±	66±9
33	3:2 PC+ACN	0.64	0.89	0.78	0.98	18	0.77	4.2	3.0	-10.2±.7	56±6
34	4:1 PC+ACN	0.64	1.40	1.25	0.98	22±2	0.76	4.4	2.8	-9.8±.9	45±5

Table 3-3 Characteristics of Time-Resolved Decays & Reaction Quantities (25 °C), MeOAc = methylacetate, ACN = acetonitrile, and n:m indicates mixture compositions by volume. η is the solvent viscosity and $<\tau_{solv}>$ the integral solvation time of the C153 probe. In pure solvents these data are taken from Refs. [23] and [31], respectively. In the PC+ACN mixtures these values are from Ref. [32] and from volume-based interpolation between pure solvent values in the case of MeOAC+acetone mixtures. The value of $<\tau_{solv}>$ for butyronitrile is estimated. a_{fast} is the amplitude of the fast decay component of the LE emission, $\tau_{rxn} = \kappa_{rxn}^{-1}$ is the fast time constant associated with reaction, and $\tau_{dec} = k_{dec}^{-1}$ is the slow time constant associated with S_1 decay. The quantity $\ln(a_{fast} / a_{slow})$ provides an estimate of the equilibrium constant ($\ln K_{eq}$) for the LE↔CT reaction from time-resolved measurements and $\ln(\nu_{LE}^3 \varphi_{CT} / \nu_{CT}^3 \varphi_{LE})$ is the related quantity from the steady-state spectra. $\Delta_r G$ is the free energy change in the reaction determined as a weighted average of these two estimates and k_f is the forward (LE→CT) rate constant

decay. We note that the values of $k_{dec} \cong k_{CT}$ measured here as well as their dependence upon ν_{CT} are quite similar to what was reported for the CT-state analogue malachite green lactone.[10] In the latter case, Karpiuk attributed the emission decay rate to the internal conversion CT $\rightarrow S_0$, and the exponential relationship between k_{dec} and ν_{CT} to a manifestation of the energy gap law.[10] It is reasonable to adopt this same interpretation in the case of CVL, at least in sufficiently polar solvents.

Rate constants for the forward reaction (LE $\rightarrow$ CT), calculated from κ_{rxn} and K_{eq} via

$$k_f = \frac{\tau_{rxn}^{-1}}{1 + K_{eq}^{-1}}, \qquad 3.12$$

are listed in the final column of Table 3-3. These rate constants are plotted in Figure 3-10 as functions of both viscosity (η/T) and average solvation time $<\tau_{solv}>$. In addition to the data listed in Table 3-3, we have included data from temperature dependent measurements in propylene carbonate and butyronitrile (small open symbols and regression lines). Motivating the choice of independent variable here is the expectation that the LE$\rightarrow$CT reaction is significantly influenced by dynamical solvent effects.[12] If the reaction involves some large amplitude motion of the solute one might expect the friction on this motion to be proportional to (η/T) as predicted by hydrodynamics. If alternatively, the primary nuclear coordinates comprising the reaction coordinate are solvent coordinates, an inverse proportionality to solvation times might be expected. The data in Figure 3-10 shows that the reaction rates are correlated to both η/T and $<\tau_{solv}>$. As suggested by the color coding in this Figure, which groups solvents according to

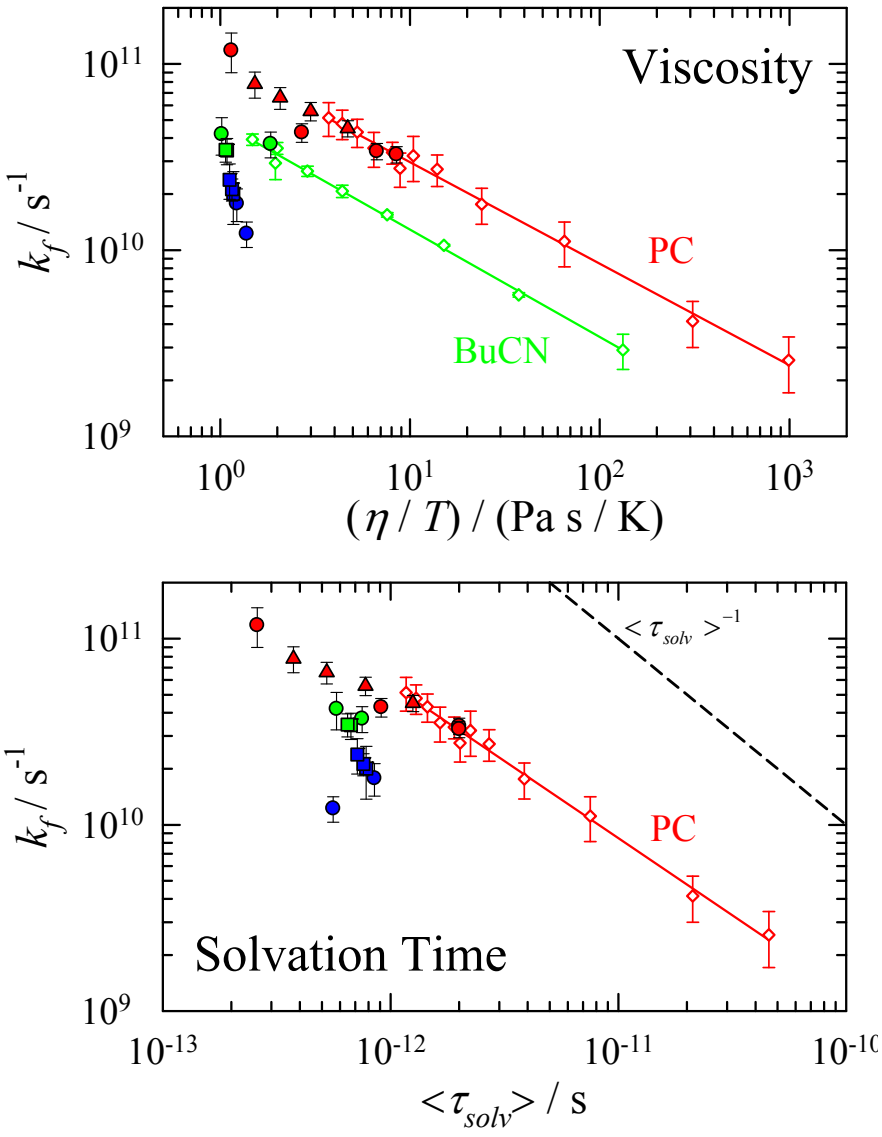

Figure 3-10 Forward reaction rate constants k_f plotted versus viscosity (η/T) and solvation time $<\tau_{solv}>$. Larger symbols are the data listed in Table 3-3. The colors indicate relative polarity: blue = least polar (n<12), green = intermediate polarity (#13,14), and red = most polar (n=15-18) solvents. The small open symbols and regression lines are temperature dependent data in butyronitrile (BuCN; 170-310 K) and propylene carbonate (PC; 210-340 K). Viscosity data for these points are from paramertizations of literature data[33] and the solvation times in propylene carbonate are from measurements of Berg and coworkers using the *s*-tetrazine probe.[34] The slopes of the temperature dependent data indicate relations $k_f \propto (\eta / T)^{-p}$ with powers $p = 0.54$ (PC) and 0.58 (BuCN) and $k_f \propto < \tau_{solv} >^{-p}$ with $p = 0.83$ (PC).

polarity, reaction energetics is also an important determinant of the rates. The most polar solvents, those with driving forces $-\Delta_r G > 9$ kJ/mol (red points) approximately follow a single correlation with either measure of solvent friction. Points with successively smaller driving force, (6-9 kJ/mol = green and < 6 kJ/mol = blue), show slower reactions for a given value of η/T or $<\tau_{solv}>$. Such variations can be readily understood as reflecting proportionate lowering of the barrier to reaction with increasing driving force - $\Delta_r G$. Such a dependence is expected based either on Marcus theory in the normal regime or on simple Brønsted arguments. In prior work on aminobenzonitriles,[14] we were able to approximately disentangle this equilibrium energetic effect from the solvent dynamical effect. Although the present data do not permit such an analysis, it seems reasonable to assume that the same situation pertains here. In any case, the additional dependence on solvent polarity does not obscure the connection to solvent friction, at least in the highly polar solvents.

Whether the frictional effect is the result of solute (η/T) or solvent ($<\tau_{solv}>$) motions cannot be decided solely on the basis of the comparisons in Figure 3-10. In the solvents suitable for CVL experiments (i.e. excluding the normal alcohols), viscosity and solvation time are approximately proportional to one another and thus the correlations of either variable with τ_{rxn} are of comparable quality. However, electronic structure calculations[19] indicate that steric hindrance prevents any large-amplitude motion of the dimethylaniline donor groups, which are the most likely candidates for solute motions that would couple to solvent viscosity. For this reason we favor interpreting the LE$\rightarrow$CT reaction as an adiabatic electron transfer process whose reaction coordinate involves

primarily solvent polarization modes and is therefore controlled by solvation dynamics. In support of this interpretation, we note that in ionic liquid solvents, we[8] and Samanta and coworkers[6] observe near equality between estimates of τ_{rxn} and $<\tau_{solv}>$. In contrast, in the highly polar conventional solvents studied here, τ_{rxn} is about 10-fold larger than $<\tau_{solv}>$, which implies a small but significant barrier to reaction (~1-2 k_BT) in these solvents.

3.4 Summary and Conclusions

In the present work we have surveyed the steady-state and time resolved emission of CVL in a variety of aprotic solvents. Analysis of the solvatochromism of the LE and CT bands measured here using a different dielectric continuum model leads to essentially the same results previously reported by Karpiuk.[3] The dipole moments of the LE and CT states are estimated to be 9-12 D and ~24 D, respectively. Because these values depend strongly upon the choice of cavity radii, they should only be considered to provide a rough indication of the relative polarities of the two excited states. Nevertheless, these dipole moments support a description of the LE $\rightarrow$ CT reaction as involving a full electron transfer between the aminobenzene and aminophthalide groups.

Analysis of the relative intensities of the LE and CT emission bands, together with information from time-resolved data enables determination of free energy changes $\Delta_r G$ associated with the LE $\rightarrow$ CT reaction. These free energies are reasonably correlated to solvent dielectric properties using the same dielectric continuum model used to analyze the solvatochromic shifts. The solvent dependence is such that $\Delta_r G$ ranges between +14

kJ/mol in n-hexane to -10 kJ/mol in propylene carbonate, with $\Delta_r G = 0$ occurring for dielectric constants between 5-6.

The emission kinetics of CVL largely conforms to expectations for a 2-state reaction between the LE and CT states. In moderately to strongly polar solvents near room temperature, emission decays are close to bi-exponential in form, consisting of a dominant component with a time constant of 8-40 ps, related to LE $\leftrightarrow$ CT equilibration, and a minor component with a nanosecond lifetime due to decay of the equilibrated excited-state population. In the more polar solvents displaying CT emission, the lifetime is determined primarily by the non-radiative decay of the CT state to S_0 and is exponentially related to the CT-S_0 energy gap, similar to what was previously observed in malachite green lactone.[10] The rates of the LE $\rightarrow$ CT reaction appear to be sensitive to both solvent polarity and to solvent friction. At least within the highest polarity solvents examined here, there is a good correlation of the reaction rates (or τ_{rxn}) with both solvent viscosity and solvation times. The simplest description of the reaction consistent with these observations is that of an adiabatic electron transfer on a 1-dimensional reaction coordinate comprised primarily of solvent polarization modes and having a modest barrier to reaction. More complicated scenarios involving fast equilibration with vibrational modes of the solute, as proposed by Schmidhammer *et al.*,[12] are equally consistent with the data. Quantitative modeling of the reaction rates and additional data with higher time resolution are needed to determine which perspective is more applicable.

References and Notes

1. Kaneko, Y.; Neckers, D. C. *J. Phys. Chem. A* **1998**, *102*, 5356.
2. Karpiuk, J. *Ann. Polish Chem. Soc.* **2001**, 271.
3. Karpiuk, J. *J. Phys. Chem. A* **2004**, *108*, 11183.
4. Jin, H.; Li, X.; Maroncelli, M. *J. Phys. Chem. B* **2007**, *111*, 13473.
5. Annapureddy, H. V. R.; Margulis, C. J. *J. Phys. Chem. B* **2009**, *113*, 12005.
6. Santhosh, K.; Samanta, A. *J. Phys. Chem. B* **2010**, *114*, 9195.
7. Jin, H.; Li, X.; Maroncelli, M. *J. Phys. Chem. B* **2010**, *114*, in press.
8. Li, X.; Maroncelli, M. *J. Phys. Chem. B* **2010**, manuscript in preparation.
9. Allen, N. S.; Hughes, N.; Mahon, P. *J. Photochem.* **1987**, *37*, 379.
10. Karpiuk, J. *Phys. Chem. Chem. Phys.* **2003**, *5*, 1078.
11. Karpiuk, J. *Phys. Chem. Chem. Phys.* **2005**, *7*, 4070.
12. Schmidhammer, U.; Megerle, U.; Lochbrunner, S.; Riedle, E.; Karpiuk, J. *J. Phys. Chem. A* **2008**, *112*, 8487.
13. Karpiuk, J.; Karolak, E.; Nowacki, J. *Pol. J. Chem.* **2008**, *82*, 865.
14. Dahl, K.; Biswas, R.; Ito, N.; Maroncelli, M. *J. Phys. Chem. B* **2005**, *109*, 1563.
15. Maroncelli, M.; Fleming, G. R. *J. Chem. Phys.* **1987**, *86*, 6221.
16. As a check on the present results we recorded several spectra using a different fluorimeter from the one used to collect the results reported here and obtained nearly identical spectra.
17. Fee, R. S.; Milsom, J. A.; Maroncelli, M. *J. Phys. Chem.* **1991**, *95*, 5170.
18. Arzhantsev, S.; Zachariasse, K.; Maroncelli, M. *J. Phys. Chem. A* **2006**, *110*, 3454.
19. Lasse Jensen, unpublished calculations (2010).

20. Stevens, B.; Ban, M. I. *Trans. Faraday Soc.* **1964**, *60*, 1515.

21. Zachariasse, K. A. *Trends in Photochemistry & Photobiology* **1994**, *3*, 211.

22. Grabowski, Z. R.; Rotkiewicz, K.; Rettig, W. *Chem. Rev.* **2003**, *103*, 3899.

23. Marcus, Y. *The Properties of Solvents*; Wiley: New York, 1998.

24. Because CVL emission is relatively weak in polar solvents, with quantum yields in the range 0.004-0.02[3], solvent impurities and contributions of Raman scattering interfere with decay measurements more than in typical fluorescence probes. In some cases we subtracted transients obtained from solvent blanks before fitting the emission decays, which tends to reduce but not eliminate the relative magnitude of the intermediate component.

25. Koti, A. S. R.; Krishna, M. M. G.; Periasamy, N. *J. Phys. Chem. A* **2001**, *105*, 1767.

26. In solvents having slow solvation responses such as ionic liquids, the LE band undergoes a dynamic Stokes shift, which typically spoils this simple behavior.[8] Interestingly, in one ionic liquid, Santhosh and Samanta[6] report a clear isoemissive point despite a significant dynamic Stokes shift of the LE band.

27. Equation 3.7 of Ref.[14] is incorrect; Eq. 6 is the corrected version.

28. Barthel, J.; Neueder, R.; Roch, H. *J. Chem. Eng. Data* **2000**, *45*, 1007.

29. Barthel, J.; Utz, M.; Gross, K.; Gores, H. J. *J. Solution Chem.* **1995**, *24*, 1109.

30. Bondeau, A.; Huck, J. *J. Phys. (Les Ulis, Fr.)* **1985**, *46*, 1717.

31. Horng, M. L.; Gardecki, J. A.; Papazyan, A.; Maroncelli, M. *J. Phys. Chem.* **1995**, *99*, 17311.

32. Gardecki, J. A.; Maroncelli, M. *Chem. Phys. Lett.* **1999**, *301*, 571.

33. Propylene carbonate viscosity data are from Refs.[28-30], which fit to the relation $\ln(\eta/\mathrm{cP}) = -2.181 + 456.2/(T/\mathrm{K} - 149.03)$ valid 205-400 K. Butyronitrile viscosities are from ESDU Physical Data, Chemical Engineering Series (http://www.esdu.com/) which fit to $\ln(\eta/\mathrm{cP}) = -3.405 + 644.3/(T/\mathrm{K} - 68.33)$ over the temperature range 175-375 K.

34. Ma, J.; Bout, D. V.; Berg, M. *J. Chem. Phys.* **1995**, *103*, 9146.

Chapter 4

Solvent-Controlled Intramolecular Electron Transfer in Ionic Liquids

Reproduced in part from:

Xiang Li, Min Liang, Anjan Chakraborty, Minako Kondo, and Mark Maroncelli*

submitted to J. Phys. Chem. B.

4.1 Introduction

Room temperature ionic liquids are an emerging class of materials currently being explored in a variety of contexts.[1-6] In many applications, such as their use as solvents for organic synthesis[1,7-9] and in electrochemical processes,[10,11] it is important to understand how electron transfer might be affected by the ionic surroundings in these liquids. In particular, one would like to know whether ionic liquids are in some way distinctive in their influence on electron transfer reactions, or whether solvent effects can be considered qualitatively the same as in the well-studied case of high-polarity conventional solvents. In this paper we address one aspect of this question, whether the relationship between solvation and reaction times in three intramolecular charge transfer reactions known to be solvent controlled in dipolar solvents extends to the longer solvation times existent in ionic liquids.

As far as energetic aspects of electron transfer are concerned, there appears to be little to distinguish ionic liquids from dipolar solvents of high polarity. For example, Lynden-Bell[12] used molecular dynamics simulations of two model dimethylimidazolium ionic liquids to investigate the extent to which the usual Marcus-type descriptions of solvation energies are applicable to ionic liquids. Just as in the case of dipolar liquids, she found that the free energy profiles associated with 1-electron oxidation and reduction of spherical ions closely conform to the parabolic shape expected by Marcus theory. More remarkable is the fact that Lynden-Bell also observed that the reorganization and activation energies, even the charge dependence of these quantities, is almost the same in

the ionic liquids and in acetonitrile, the simulators' default choice of comparison dipolar solvent. Similar observations were made in an independent study by Shim and Kim,[13] who simulated charge transfer between two atoms of a model diatomic solute in 1-ethyl-3-methylimidazolium hexafluorophosphate. These two simulations, together with extensive evidence from solvatochromic studies of ionic liquids,[14,15] including some direct measurements of energies associated with charge-transfer transitions[16,17] suggest that there is little to distinguish solvation energies in an ionic liquid environment from those found in a highly polar conventional solvent such as acetonitrile or dimethylsulfoxide.

This energetic similarity might not be expected extend to dynamical solvent effects on electron transfer,[18] given the very different time scales and distinct mechanisms of solvation in ionic liquids compared to dipolar solvents. As a result of their much higher viscosities, the solvation response in ionic liquids is hundreds of times slower than in most conventional solvents.[17,19,20] In addition, the response is broadly distributed in time, with significant contributions from components ranging from the subpicosecond to the nanosecond time scales.[20] Finally, simulation studies have shown that, in contrast to the predominantly rotational response of dipolar solvents, the primary means of relaxing the solvation energy in ionic liquids is translational motion of ions.[21,22] These differences might well be expected to produce both quantitative and qualitative differences in electron transfer processes susceptible to dynamical solvent influence. To explore this possibility, Shim and Kim used simulations of electron transfer in a model diatomic solute in two different ionic liquids to investigate how friction on barrier-crossing and well dynamics might influence adiabatic electron transfer reactions.[13,23]

They again compared the behavior in the ionic liquids to that in acetonitrile. For high-barrier (>10 k_BT) reactions they found only moderate (factors of 3-5) deviations from transition state theory predictions, which were well described by Grote-Hynes theory.[24] In these cases, the dynamical solvent effects on the electron transfer were found to be virtually identical in the ionic liquid and acetonitrile, despite the nearly 100-fold difference in the viscosities or zero-frequency friction in the two solvents. This similarity results from the fact that for high-barrier reactions only the highest frequency portions of the solvent friction, that portion coming from the ultrafast components of the solvation response, are relevant, and this fast portion of the friction is comparable in the acetonitrile and ionic models. Only for reactions with lower barriers, where more of the full friction is felt during barrier crossing, and where well dynamics become important, did they predict much larger dynamical solvent effects and large differences between the ionic liquids and acetonitrile.[23]

A variety of experimental studies of electron transfer rates have also been performed. Many of these studies involved diffusion-limited bimolecular electron transfer reactions.[25-32] In a number of cases, reaction rates were reported to be much greater than predicted based on simple viscosity scaling of the rates observed in conventional solvents. Our analysis suggests that these faster-than-expected rates are probably due to the inapplicability of the simplest treatments of diffusion-limited reaction in high-viscosity liquids rather than to unusual behavior of the electron transfer process itself.[33,34] Electrochemical methods have also been used to measure heterogeneous electron transfer kinetics in a variety of ionic liquids.[10,35] Of most interest in the present context are experiments of van Eldik and coworkers[36,37] who used cyclic voltammetry to

measure electron transfer rates of the ferrocene/ferrocinium couple on bare gold[36] and on alkanethiol coated [37] electrodes in 1-butyl-3-methylimidazolium bis-(trifluoromethylsulfonyl)imide ($[Im_{41}][Tf_2N]$). The observed rates were interpreted in terms of a transition from the regimes of solvent-controlled adiabatic electron transfer on bare electrodes[36] to nonadiabatic electron transfer as a function of the alkanethiol chain length.[37] A complicating factor in fully interpreting these and other heterogeneous electron transfer rates is the fact that ionic liquids bind strongly to solid surfaces and form multilayer structures that are only now beginning to be understood.[38,39] Virtually nothing is known about solvation dynamics within these layers.

Intramolecular electron transfer reactions, typically using photo-induced processes, afford information that can be more readily interpreted in terms of dynamical solvent effects. Relatively few experiments of this sort have so far been performed in ionic liquids.[40-53] Of the studies published to date, several bear on the question of how the slow solvation dynamics in ionic liquids affects electron transfer. In addition to studies of crystal violet lactone[41,42,51] and bianthryl[45-47] to be discussed in more detail below, studies of two other electron transfer reactions should be mentioned. Lockard and Wasielewski[40] used femtosecond transient absorption to measure charge separation and recombination rates in a covalently linked organic donor-acceptor dyad in several conventional solvents and in an imidazolium ionic liquid. At room temperature, these reactions were observed to take place on comparable time scales (1-50 ps) in dipolar solvents and the ionic liquid, suggesting that the much slower solvation in the ionic liquid had little effect on these reactions. They also observed a clear difference in the temperature dependence of the rate of the recombination reaction, which might signal

partial solvent control or might instead be related to the viscosity affecting conformational dynamics also thought to be relevant. In similar experiments, Vauthey and coworkers[44] reported electron transfer times in the covalently linked perylene – dimethylaniline dyad (PeDMA) in six dipolar solvents and in 3-ethyl-1-methylimidazolium ethyl sulfate. They noted that much slower and highly non-exponential charge separation occurs in the ionic liquid compared to the conventional solvents studied. In the latter solvents, the electron transfer was observed to be approximately equal to solvation times measured with coumarin 153.[54] Based on an estimated solvation time in the ionic liquid, we find that roughly the same equality of electron transfer and solvation time appears to hold for the ionic liquid as well. The PeDMA reaction bears some resemblance to bianthryl reaction, discussed in detail below.

In the present work we use picosecond time-resolved emission spectroscopy to measure intramolecular electron transfer rates in the three solutes 9-(4-biphenyl)-10-methylacridinium ($BPAc^+$), crystal violet lactone (CVL), and bianthryl (BA; Figure 4-1). All three solutes have been previously characterized in conventional solvents, where it has been shown that the electron transfer processes in Figure 4-1 are primarily controlled by solvation dynamics. These three reactions share a number of common features. First, all three solutes exhibit dual fluorescence whose composition varies with solvent polarity. In low polarity solvents, emission occurs primarily from a “locally excited” or LE state reached by excitation in the lowest energy absorption band.

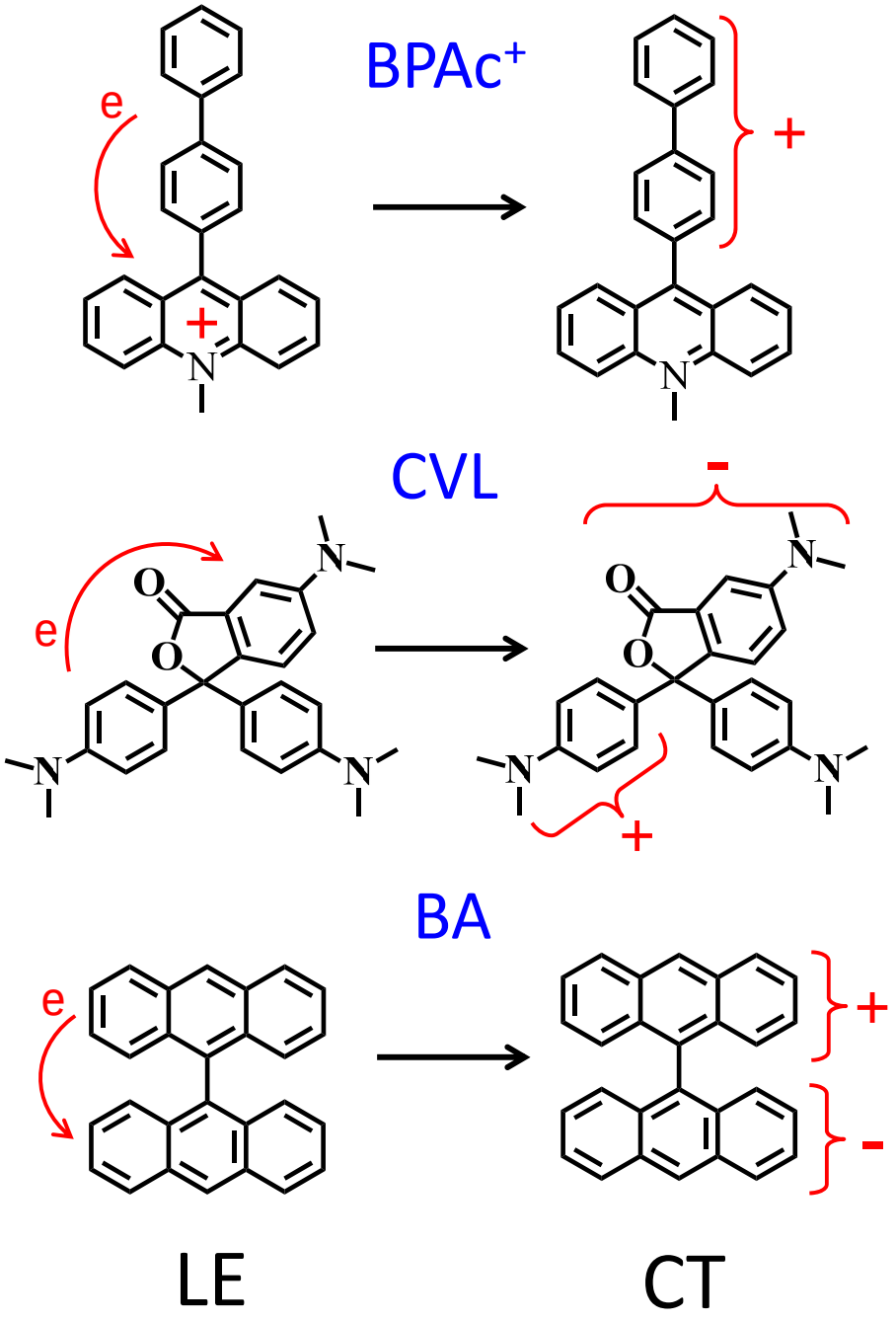

Figure 4-1 Schematic of the charge transfer processes in 9-(4-biphenyl)-10-methylacridinium ($BPAc^+$), crystal violet lactone (CVL) and bianthryl (BA).

The term "local" here is used to indicate that excitation can be thought of as residing on one portion of the molecule: the acridinium ring in the case of $BPAc^+$, the aminophthalide ring in CVL, and one of the two anthracene rings in bianthryl.[55] In high-polarity solvents, emission from a "charge transfer" (CT) electronic state is also observed, and this emission typically dominates the spectrum. In all three cases, the LE $\rightarrow$ CT conversion entails a charge redistribution which amounts to transfer of approximately one electron in the directions indicated in Figure 4-1. In most conventional solvents the LE $\rightarrow$ CT reaction and its reverse are rapid relative to depopulation of the excited state, so that the relative amounts of LE and CT emission reflect the equilibrium between these states. Finally, in all three cases the this equilibrium shifts strongly in favor of the CT state with increasing solvent polarity. More background on the individual reactions is provided below.

$BPAc^+$ is one of a series of fluorescent donor-substituted acridinium molecules introduced by Jones and coworkers[56] for studying electron transfer reactions with variable driving force.[57-60] Horng *et al*.[58] measured the time-resolved emission of $BPAc^+$ in 21 conventional solvents at 25 °C. Predominantly bi-exponential kinetics with widely separated time constants conforming to expectations for a 2-state reaction were observed. The shorter time constant, which ranged between 4 and 500 ps, could be associated with the LE $\rightarrow$ CT reaction time. In 14 solvents more polar than acetone, Horng *et al*. observed a strong correlation between this LE $\rightarrow$ CT reaction time and solvation times measured with the non-reactive solute coumarin 153 (C153). This relationship could be

approximately expressed $\tau_{rxn} \cong 8.4 < \tau_{solv} >^{0.65}$. No measurements of $BPAc^+$ or related molecules in ionic liquids have been reported previously.

CVL is a molecule whose dual fluorescence was characterized only recently in an extensive study by Karpiuk[61] with additional contributions from our group.[62] Based on the spectra and dynamics of the component chromophores of CVL,[63,64] Karpiuk concluded that the LE state entails excitation of aminophthalide portion of the molecule whereas the CT is one in which an electron transfer has transferred from one or both dimethylamino fragments to the aminophthalide ring (Figure 4-1). Using an analysis of the solvatochromism of the two emission bands, Karpiuk estimated dipole moments of ~11 D for the LE state and ~25 D for the CT state,[61] which can be compared to a calculated dipole moment of 6.0 D[62] in the ground state. As these dipole moments indicate, the LE state already entails a significant charge redistribution compared to the ground state, which renders both the LE and CT emission significantly solvatochromic. Li *et al*.[62] measured the time-resolved emission of CVL in a range of solvents and, as in the case of $BPAc^+$, found primarily well-resolved bi-exponential kinetics with a short time constant of 10-100 ps due to reaction and a long time constant in the 1-20 ns range. They used information from both emission decays and LE/CT contributions to the steady-state emission spectra to measure the driving force for the LE $\rightarrow$ CT reaction, which was found to vary from about -15 kJ/mol in nonpolar solvents to +10 kJ/mol in highly polar solvents. Based on transient absorption data in three solvents Karpiuk and coworkers[65] suggested that the charge transfer reaction in CVL is controlled by solvation dynamics. A more extensive survey of reaction kinetics in a number of solvents and solvent

mixtures[62] supported this suggestion, but the distinction between control by solvation dynamics as oppose to other frictional effects could not be as definitively established in CVL as the other two solutes studied here, because an additional nonradiative channel[61] precluded measurement of the reaction rate in protic solvents.[62]

CVL has also been studied in ionic liquids.[41,42,51,66] Jin *et al*.[41] reported a large variation of the relative intensities of the LE and CT bands in the steady-state spectra of CVL with excitation wavelength, and interpreted this variation as an example of dynamic heterogeneity in ionic liquids. Annapureddy and Margulis[66] performed simulations of the experimental system studied by Jin *et al*. They showed that, in contrast to conventional solvents like acetonitrile, the sluggish dynamics in ionic liquids means that site-to-site variations in solvation energies can persist for several nanoseconds and that this persistence should result in excitation dependence of both fluorescence spectra[67] and excited-state electron transfer rates.[66] During the course of the experiments reported in the present study we have found that the large variations in the steady-state emission spectra reported by Jin *et al*.[41] were spurious, probably as a result of solvent impurity emission contaminating the relatively weak emission of CVL.[42] (We have checked for excitation wavelength dependence in a number of the solute + ionic liquid combinations reported here and find only very small variations to LE/CT intensity ratios. Although we believe that these variations are genuine, better examples have been reported using other reactions[33,50,68] and so we do not discuss this phenomenon further in the present work.) A final study of CVL in ionic liquids was recently reported by Santhosh and Samanta.[51] These authors measured steady-state spectra and several photophysical properties of CVL in six ionic liquids as well as complete time-resolved emission spectra in one liquid at

room temperature. They observed a good correlation between the frequency of the LE emission and the $E_T(30)$ polarity parameter[15] and also noted much lower emission quantum yields in 1-alkyl-3-methylimidazolium ionic liquids compared to other ionic liquids studied. From these observations they concluded that the hydrogen bond donating ability of the C(2)-H atom in the former liquids is sufficient to open the additional deactivation channel described by Karpiuk for CVL in alcohol solvents.[61] In the ionic liquid 1-butyl-2,3-dimethylimidazolium bis(trifluoromethanesolufonyl)imide Santhosh and Samanta reported an isoemissive point in the area-normalized spectra and a rise time of the CT emission (1 ns) which was comparable in magnitude to the solvation time they measured in this liquid measured using C153 (690 ps). On this basis they suggested that the LE→CT reaction is controlled by solvation dynamics in ionic liquids.

Bianthryl has enjoyed much greater study than the other solutes used in this work. Schneider and Liptay[69] first recognized charge transfer to be responsible for the dual fluorescence of bianthryl. They estimated excited-state dipole moments of 18 D in polar solvents, consistent with a full electron transfer between the two anthracene chromophores. Since this seminal work numerous groups have studied various aspects of the excited state behavior of bianthryl in conventional solvents[70-84] and in the gas phase,[85,86] leading to a rich, although but not entirely consistent description of the LE → CT reaction. Pioneering measurements and modeling of the time-resolved emission of bianthryl in polar solvents were performed by Barbara and coworkers roughly twenty years ago.[70-73] They postulated that the excited state charge transfer in bianthryl could be described in terms of an adiabatic process on a single S_1 potential energy surface produced via the mixing of three diabatic states: an LE state consisting of an excitonic

mixture AA*↔A*A and a pair of CT states, A^+A^- and A^-A^+.[55] Based on the near equality observed between the electron transfer times of bianthryl and solvation times measured with coumarin probes,[70] they further proposed that the reaction coordinate was comprised solely of solvent polarization modes. Using this description, they were able to provide a coherent account of the solvent dependence of the steady-state emission of bianthryl and the time-dependent emission observed in high-polarity solvents.[72,73] In propylene carbonate for example, their modeling suggested that the Frank-Condon region is predominantly of LE character, but that there exists only a small (~k_BT) energy barrier to transfer to the CT region of S_1, whose minimum lies below the FC region by about ~21 kJ/mol.[73] The highly non-exponential reaction kinetics they observed experimentally and its resemblance to the time dependence of the dynamic Stokes shift was explained by the very small barrier and the non-exponential survival probability of LE character on such a surface. This complex reaction dynamics in bianthryl contrasts with the simple 2-state type of kinetics observed in $BPAc^+$ and CVL in conventional solvents. But it is also reasonable to describe these latter reactions using a 1-dimensional adiabatic description similar to the one envisioned for bianthryl. In these cases the reaction barrier must be larger than in bianthryl in order to more effectively separate populations into LE and CT regions of the potential. If such a description is correct, analyses of the sort described by Shim and Kim[23] require that in all three cases the barrier must be quite small, no more than a few k_BT to be consistent with the observed dependence on solvation times.

It should be noted that subsequent work on bianthryl suggests that the model proposed by Barbara and coworkers[72,73] is not a complete description of this reaction. For example, torsional dynamics are neglected in the model, and such dynamics are

likely to play some role in determining the details of the spectral dynamics observed.[74,75,85] There also is some discrepancy between the LE-CT equilibrium constants deduced from fluorescence measurements and determinations of dipole moments in weakly polar solvents[78] as well as with equilibrium constants deduced from transient absorption (TA) measurements in high polarity solvents.[82] This discrepancy has yet to be resolved. Finally, the most recent femtosecond TA studies indicate that there is some CT[82] or "pre-CT"[83] state population already present at times of less than 50 fs, something not anticipated by Barbara's photodynamic model as originally proposed. These observations suggest that refinement, probably incorporation of coordinates other than solvation into the model, will be required for a completely quantitative description of the bianthryl reaction.

Bianthryl has been studied in ionic liquids using both picosecond time-resolved emission[45-47] and transient absorption on femtosecond[45] and nanosecond[45,84] time scales. Nagasawa and coworkers[45] measured the femtosecond broadband TA in the visible region and time-resolved emission spectra of three imidazolium ionic liquids. The TA measurements revealed rise times of an excited-state absorption attributed to the CT state in the range 53-100 ps.[45] Emission spectra recorded with 30 ps resolution were used to monitor the dynamic Stokes shift of the CT band of bianthryl in these same solvents. The fact that the emission Stokes shifts extended to times much longer than the CT rise observed in TA experiments lead Nagasawa *et al*.[45] to conclude that the LE $\rightarrow$ CT reaction proceeds on a different time scale from solvation in ionic liquids. This conclusion implies that a different relationship exists between solvation and reaction in ionic liquids compared to conventional solvents, where approximate equality between the

times prevails.[71,72,82] Independent measurements of the time-resolved emission spectra of bianrthyl in the same three ionic liquids were reported by Samanta and coworkers.[47] These authors estimated the LE→CT reaction time from the decay observed near the peak of the LE emission and measured solvation times in terms of the dynamic Stokes shift of the entire emission band. They found the former times to be significantly smaller than the latter times and again concluded that reaction and solvation occur on different time scales in ionic liquids.[47] In a second study, Nagasawa and coworkers used the dynamic Stokes shift of the bianthryl spectrum to measure the temperature dependence of the solvation response in five ionic liquids. They observed a good correlation between the average solvation times measured in this way and the solvent viscosity in most of these liquids. The dependence upon viscosity was weaker ($< \tau_{solv} > \propto \eta^{0.60}$) than was previously observed using C153 as a solvation probe ($< \tau_{solv} > \propto (\eta / T)^{1.0}$).[17]

In the present work we measure reaction times of intramolecular electron transfer in $BPAc^+$, CVL, and bianthryl in an assortment of ionic liquids. We do not attempt to model the connection between solvation dynamics and reaction here. Instead, we merely compare the reaction times measured in ionic liquids to solvation times measured with C153 in these same liquids and ask whether the relationships previously established in dipolar solvents extend to ionic liquid solvents. The answer we obtain is a definite yes in $BPAc^+$ and bianthryl and a qualified yes in the case of CVL. As the details of the methods used to deduce reaction times of these three reactions differ, we present the results of each solute separately. Where possible, we compare the results and conclusions provided here to prior ionic liquid work, in particular addressing the

disagreement between the conclusions of the present study and those made in previous studies of the bianthryl reaction in ionic liquids.[45,47]

4.2 Materials and Experiments

9-(4-Biphenyl)-10-methylacridinium ($BPAc^+$) and 9-phenyl-10-methylacridinium (PAc^+) hexafluorophosphate were prepared by Gil Jones as described in Ref.[87] Crystal violet lactone (CVL) was obtained from Sigma-Aldrich (97%) and recrystallized twice from acetone. 9,9'-bianthracene (or bianthryl, BA) was prepared by procedure of Bell and Waring[88] and recrystallized from carbon tetrachloride. In all cases purity was initially checked by thin layer chromatography and confirmed by lack of detectable impurity fluorescence.

Ionic liquids were obtained from a variety of sources. Unless otherwise specified these materials were used as received except for drying. 1-Ethyl-3-methylimidazolium *bis*(trifluoromethylsulfonyl)imide ($[Im_{21}][Tf_2N]$) and 1-butyl-3-methylimidazolium tetrafluoroborate ($[Im_{41}][BF_4]$) were obtained from Iolitec (99%). $[Im_{41}][BF_4]$ was dissolved in methylene chloride and treated with activated carbon several times to remove fluorescent impurities. 1-Butyl-3-methylimidazolium hexafluorophostphate ($[Im_{41}][PF_6]$) was obtained from Covalent Associates (99+%) and propyltrimethylammonium *bis*(trifluoromethylsulfonyl)imide ($[N_{3111}][T_2fN]$) from Kanto Chemical. Isopropylpropyldimethyl *bis*(trifluoromethylsulfonyl)imide ($[N_{ip311}][Tf_2N]$), 1-propyl-3-methylpyrrolidinium *bis*(trifluoromethylsulfonyl)imide ($[Pr_{31}][Tf_2N]$), and 1-butyl-3-methylpyrrolidinium *bis*(trifluoromethylsulfonyl)imide ($[Pr_{41}][Tf_2N]$) were

prepared by Gary Baker as described in Ref.[89] Finally, tributyltetradecylphosphonium *bis*(trifluoromethylsulfonyl)imide ($[P_{14,666}][Tf2N]$) was prepared from the chloride salt. Tributyltetradecylphosphonium chloride ($[P_{14,666}][Cl]$; Cytec Canada) was first purified by washing twice with water, drying and dissolving the dried liquid in dichloromethane (DCM) containing activated carbon. This mixture was stirred overnight and the carbon removed using a syringe filter. The DCM solution was then mixed with an approximately equimolar amount of aqueous of lithium *bis*(trifluoromethylsulfonyl)imide and the reaction stirred overnight at room temperature. The DCM layer was separated and washed with water ten or more times until no Cl^- could be detected with $AgNO_3$. DCM was removed from the final product by rotary evaporation for 1 h at 60 °C. All ionic liquid samples were dried on a vacuum line until the water content was below 200 ppm as determined by coulometric Karl-Fischer titration.

Samples for steady-state spectroscopy were prepared in 1 cm quartz cuvettes at concentrations providing optical densities of less than 0.2 at the excitation wavelength. Absorption measurements were made using a Hitachi U-3000 UV/visible spectrophotometer with a resolution of 1 nm. Corrected emission spectra were recorded with either PTI Quanta-Master 1 or Spex Fluorolog 212 fluorimeters at 2 nm resolution. Solvent blanks were subtracted from all spectra and the spectra converted to a frequency representation prior to analysis. Low-temperature spectra were recorded using vacuum-sealed samples in an Oxford DN-1754 cryostat.

Time-resolved emission decays were collected using a time correlated single-photon counting (TCSPC) instrument whose main features have been previously described.[90] The excitation source was the doubled output of a cavity-dumped

Ti:sapphire laser operating at a repetition rate of 5.4 MHz. Excitation wavelengths ranged between 370 and 420 nm depending on the solute. Samples were contained in 1 cm cuvettes into which a yellow filter glass was inserted to remove reflections near time zero. The optical densities of these samples were typically below 0.2 but sometimes as high as 0.4 in order to minimize the effects of impurity fluorescence from the ionic liquid solvents. Emission was collected at magic angle through an ISA H10 monochromator using an emission band-pass of 8 nm. The overall response time of the TCSPC instrument was 25-30 ps (FWHM), as measured using a scattering solution. Data were collected over time windows of 6-30 ns, depending on the solute and its lifetime. Emission transients were fit using observed instrument response functions and an iterative reconvolution algorithm. In the case of CVL, whose fluorescence is weak, solvent blanks were recorded under identical conditions to those of the sample and these blank decays subtracted prior to data analysis. Emission transients at 15-25 wavelengths were collected and time-resolved spectra reconstructed from fits to these data using methods described in Ref.[91] Temperatures for the steady-state and TCSPC measurements were maintained to ± 0.2 °C using water from a circulating bath.

Preliminary fluorescence upconversion measurements were made with the same laser source using 390 nm excitation. The collection optics and detection electronics were essentially identical to those described in previous work.[54] The only significant difference is that the prism pulse compressors were omitted. Samples were contained in a 1 mm thickness quartz flow cell connected to a peristaltic pump and the system purged with nitrogen at room temperature, 21 ± 1 °C. Emission was recorded at magic angle.

The instrument response function of of this system was ~300 fs (FWHM) as judged by upconversion of Raman signal from neat solvents.

4.3 Results and Discussion

Before discussing the results obtained with different solutes, we pause to consider the ionic liquids used in this study. Because the experiments described here were carried out over the course of several years, a common set of solvents and conditions was not used for all three solutes. Instead, the choice of solvents was dictated by availability and by the need to use solvents of the highest optical purity possible, especially for the weakly fluorescent solute CVL. Table 4-1 lists the ionic liquids studied along with some properties pertinent to their use as solvents in charge transfer contexts. (We specify cations here by type as Im = 1-alkyl-3-methylimidazolium, N = ammonium, Pr = pyrrolidinium, and P = phosphonium, and use numerical subscripts to indicate the carbon numbers in n-alkyl groups or ip=isopropyl to indicate the variable substituents.) Some indicators of the ability to stabilize dipolar and charged species are provided by the bulk ion concentrations [IP] and the solvent reorganization energies λ_{C153} and free energy changes ΔG_{C153} associated with the $S_0 \leftrightarrow S_1$ transition of the solvatochromic probe coumarin 153 (C153)[17]. The concentration of ions (defined here as +- pairs) has been suggested as a useful measure of solvent polarity in ionic liquids. Within the present collection of liquids the only significant variations from a value of ~3 M occur in the liquids not based on the Tf_2N^- (*bis*(trifluoromethylsulfonyl)imide) anion and with the unusually large cation in $[P_{14,666}][Tf_2N]$. The molecular measures of solvation energies

Ionic Liquid	[IP]	λ_{C153}	ΔG_{C153}	T	η	$<\tau_{solv}>$	f_{obs}
	/mol dm^{-3}	/kJ mol^{-1}	/kJ mol^{-1}	/°C	/cP	/ns	
$[Im_{21}][Tf_2N]$	3.6[a]	13	43	25	35	0.14±.02	0.53
$[Im_{41}][BF_4]$	5.3[b]	13	45	10	267[d]	0.8±.2	0.50
$[Im_{41}][PF_6]$	4.8[b]	13[d]	46[d]	25	196[d]	1.0±.1[d,e]	0.65
				70	29[d]	0.14±.02[e]	0.45
$[N_{3111}][Tf_2N]$	3.8[c]	14	43	25	82	0.37±.07	0.46
				65	20	0.07±.01	0.58
$[N_{ip311}][Tf_2N]$	3.4[b]	13[d]	43[d]	10	264[d]	1.2±.2[f]	0.50
				25	113[d]	0.51±.08[d]	0.57
				65	23[d]	0.09±.03[d]	~0.4
$[Pr_{31}][Tf_2N]$	3.4[b]	13[d]	43[d]	25	54[d]	0.28±.04[d]	0.52
$[Pr_{41}][Tf_2N]$	3.3[b]	13[d]	42[d]	21	93[d]	0.46±.07	0.50
$[P_{14,666}][T_2fN]$	1.4[a]	10[d]	43[d]	10	900	~18[f]	
				45	125	2.5±.3	1.0

Table 4-1 Some Characteristics of the Ionic Liquids Studied. [IP] denotes the concentration of ion pairs (formula units), λ_{C153} (±1 kJ/mol) and ΔG_{C153} (± 2 kJ/mol) are the solvent reorganization energy and free energy change associated with the S0↔S1 transition of C153[17] at 25 °C. η is the solvent viscosity (±10%) and $<\tau_{solv}>$ the integral solvation time measured with C153 using TCSPC at the temperatures listed (Eq. 1). f_{obs} is the estimated fraction of the total solvation response observed with the ~25 ps resolution of the TCSPC experiment. Data are from (a) Ref.92, (b) Ref.89, (c) Ref.93, (d) Ref.17, and (e) Ref.94, or from the present study. (f) denotes a value estimated based on data at other temperatures.

provided by λ_{C153} and ΔG_{C153} are only weakly correlated to this bulk ion concentration. These latter measures indicate that solvation energetics should be reasonably constant among this collection of ionic liquids, except in the case of $[P_{14,666}][Tf_2N]$. This constancy is important because barrier heights and therefore rates of electron transfer reactions are expected to vary significantly with solvent polarity. The similar values of λ_{C153} and ΔG_{C153} measured in all but the $[P_{14,666}][Tf_2N]$ solvent suggest that the primary determinant of variable reaction rates measured here will be variations solvent dynamics rather than energetic differences.

As a measure of solvation dynamics we use the integral time associated with the dynamic Stokes shift of C153

$$< \tau_{solv} >= \int_0^\infty \{\nu(t) - \nu(\infty)\} dt / \{\nu(0) - \nu(\infty)\} \qquad 4.1$$

where the $\nu(t)$ are frequencies directly measured using TCSPC. Due to time resolution limitations these solvation times are an upper limit to the true integral Stokes shift or solvation times. The final column of Table 4-1 lists estimates for the fraction of the Stokes shift observed using TCSPC.[17] With the exception of $[P_{14,666}][Tf_2N]$ only about one half of the solvation response is represented by these values of $<\tau_{solv}>$. When comparing reaction and solvation times in the following section, we recognize the uncertainty caused by the missing fast components of solvation by plotting as the lower uncertainty limits of $<\tau_{solv}>$ the values $(1 - f_{obs}) < \tau_{solv} >$.

4.3.1 Biphenyl Acridinium ($BPAc^+$):

Representative steady-state spectra of $BPAc^+$ in conventional solvents and in the ionic liquid $[Im_{21}][Tf_2N]$ are shown in Figure 4-2. In the weakly polar solvent tetrahydrofuran (THF) the S_1 absorption of $BPAc^+$ shows clear vibronic structure and the emission spectrum is approximately the mirror image of the absorption. Emission in THF is mainly from the LE state localized on the acridinium ring. In more polar solvents such as acetonitrile and in ionic liquids the absorption spectrum broadens but does not shift appreciably and dual emission is observed. LE emission occurs at approximately the same frequency as in THF (~19,000 cm^{-1}) and a new emission appears near 15,000 cm^{-1} attributed to a CT state reached by electron transfer from the biphenyl donor to the acridinium acceptor.[87]

To decompose steady-state and time-resolved emission into LE and CT contributions we use the spectrum of the reference compound 9-phenyl-10-methylacridinium (PAc^+, bottom panel of Figure 4-2), which does not undergo charge transfer. Specifically, we assume that the lineshape ($\chi(\nu) \propto F(\nu)/\nu^3$ where $F(\nu)$ is the emission spectrum) of the LE emission of $BPAc^+$ in a given solvent is a slightly broadened and shifted version of the lineshape of PAc^+. We further assume that the CT emission lineshape is Gaussian and fit fluorescence spectra to the function

$$F(\nu) \propto \nu^3 \left\{ (1-f_{CT}) \int \chi_{LE}(\nu-\delta) g_{LE}(\delta) d\delta + f_{CT} \chi_{CT}(\nu) \right\} \qquad 4.2$$

where

$$g_{LE}(\delta) = \frac{1}{\sqrt{2\pi\sigma_{LE}^2}} \exp\left\{ -\frac{(\delta-\delta_{LE})}{2\sigma_{LE}^2} \right\} \qquad 4.3$$

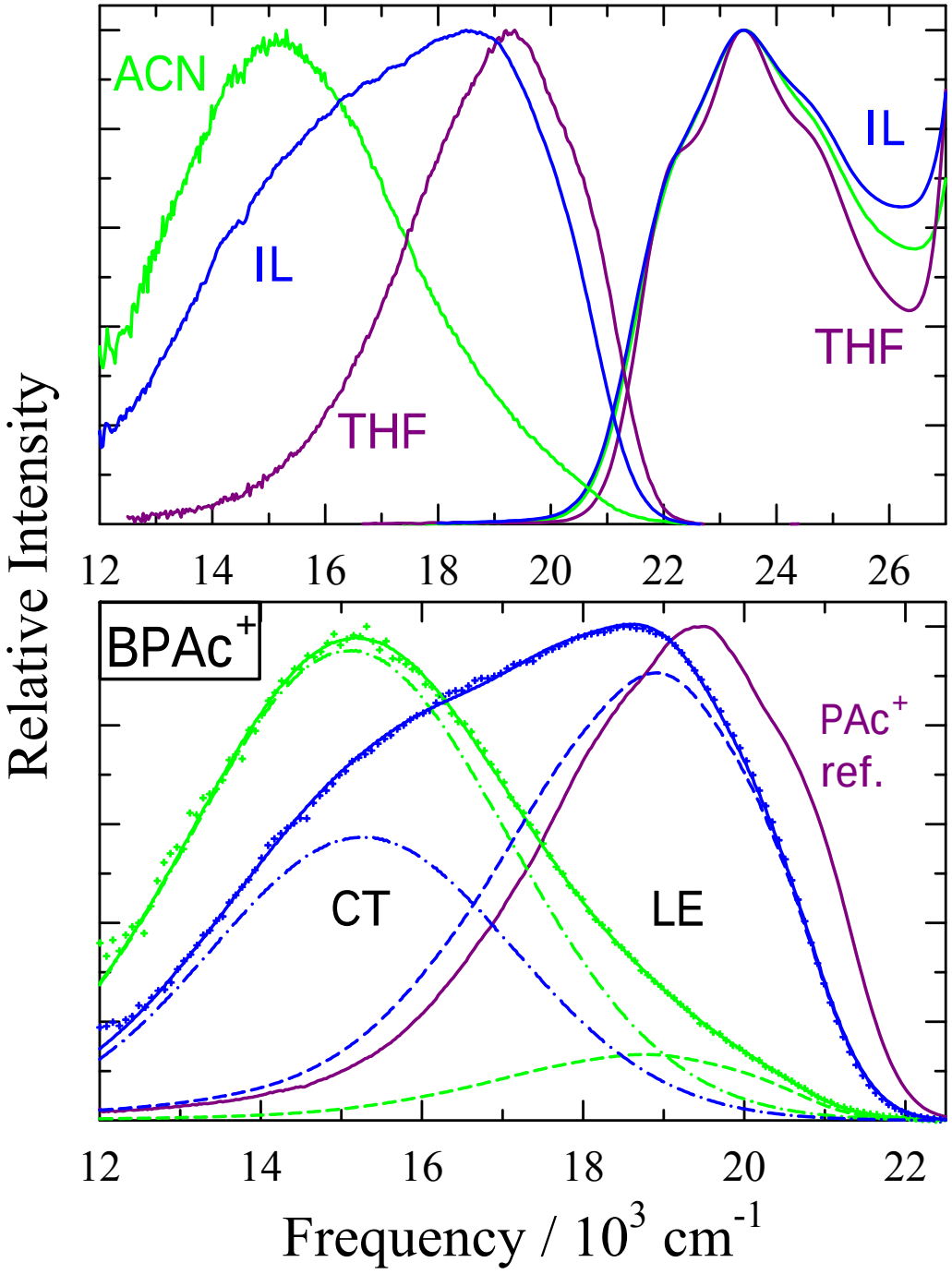

Figure 4-2 Top panel: Absorption and emission spectra of $BPAc^+$ in tetrahydrofuran (THF), acetonitrile (ACN) and $[Im_{21}][Tf_2N]$ (IL). Bottom panel: Reference emission spectrum of 9-phenyl-1-methylacridinium (PAc^+) in acetonitrile and fits of the emission of $BPAc^+$ in acetonitrile and $[Im_{21}][Tf_2N]$ showing decompositions into LE (dashed) and CT (dash-dot) components as described in the text.

and

$$\chi_{CT}(\nu) = \frac{1}{\sqrt{2\pi\sigma_{CT}^2}} \exp\left\{ -\frac{(\nu - \nu_{CT})^2}{2\sigma_{CT}^2} \right\} \qquad 4.4$$

The parameter f_{CT} is the relative population of the CT state, which is of most interest for understanding the kinetics of the LE→CT reaction. The bottom panel of Figure 4-2 illustrates the LE (dashed) and CT (dash-dot) component spectra obtained from such fitting. There are a total of 5 parameters in this model, δ_{LE}, Γ_{LE}, f_{CT}, ν_{CT}, and Γ_{CT} where the $\Gamma_i = \sqrt{8\ln 2}\sigma_i$ are full widths. In many cases, especially the low-spectral resolution TCSPC data, the spectra do not uniquely determine all five parameters. A survey of the steady-state spectra in high polarity conventional solvents and ionic liquids shows the width parameters can be fixed at average values Γ_{LE} = 770 cm^{-1} and Γ_{CT} = 4300 cm^{-1} without degrading the quality of the fits significantly. From fits constrained in this way we find that the LE and CT frequencies in ionic liquids are only slightly red shifted relative to those in high-polarity conventional solvents such as acetonitrile, dimethylformamide, and methanol. The frequency of the LE band is 200 ± 100 cm^{-1} and the CT band 650 ± 300 cm^{-1} lower in the case of ionic liquids, indicating that BPAc$^+$ feels an effective polarity just slightly higher than the polarities of these conventional solvents. A much more obvious distinction between conventional solvents like acetonitrile and ionic liquids illustrated by Figure 4-2 is the fact that the relative contribution of CT emission is much smaller in ionic liquids, f_{CT} = .48 ± .09 compared 0.89 ± .02 in high polarity conventional solvents. This difference is a kinetic effect. In conventional solvents the LE ↔ CT reaction is much faster than S_1 depopulation so that, apart from a

radiative rate factor, f_{CT} indicates the fractional population of the CT state in equilibrium.[58] In ionic liquids on the other hand, S_1 decay is competitive with charge transfer, which means that the steady-state spectra do not reflect equilibrium excited-state populations.

Representative time-resolved emission spectra of PAc^+ and $BPAc^+$ in the ionic liquid $[N_{ip311}][Tf_2N]$ are shown in Figure 4-3. As illustrated by the top panel, the LE-state surrogate PAc^+ undergoes a small (~200 cm^{-1}) dynamic Stokes shift in ionic liquids. In the cases we have examined, the Stokes shift times of PAc^+ are within uncertainties of those measured using probe C153. We expect similar Stokes shifts of the LE band of $BPAc^+$, which means that emission decays measured at individual wavelengths will reflect both the LE $\leftrightarrow$ CT interconversion and the solvation of the LE and possibly CT bands. For this reason we analyzed kinetics by fitting the time-resolved spectra as described above. Typical fits are shown in the bottom panel of Figure 4-3. In all cases we found that satisfactory fits to the time-evolving spectra could be obtained by fixing the frequency of the CT band to the frequency observed in the steady-state spectrum (ν_{CT} ~ 14,700 cm^{-1}) and allowing the LE band position, as specified by δ_{LE}, to vary by a few hundred wavenumbers. From such fits we derived the time-dependent relative intensities of the LE and CT bands, free of the effect of Stokes shifting, for kinetic analysis. Three examples of intensity decay data are shown in Figure 4-4. All of the band intensity data generated in this manner could be well represented by bi-exponential functions of time, and parameters obtained from unconstrained bi-exponential fits are listed in Table 4-2.

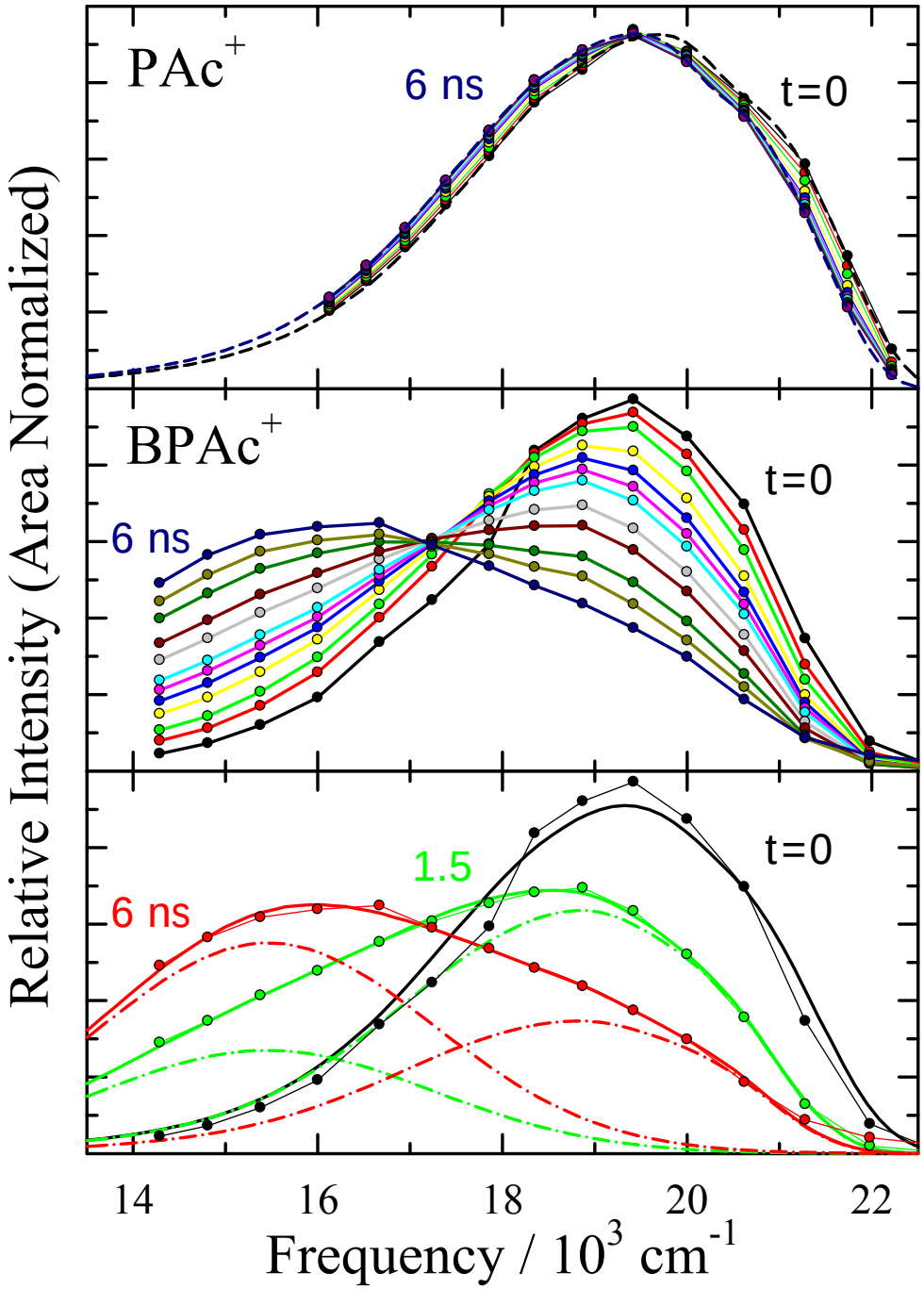

Figure 4-3 Time-resolved emission spectra of PAc^+ (top panel) and $BPAc^+$ in $[N_{ip311}][Tf_2N]$ at 25 °C. The points are reconstructed spectra at times of 0, 0.1, 0.2, 0.4, 0.6, 0.8, 1, 1.5, 2, 3, 4, and 6 ns. The dashed curves in the top panel and the thick curves in the bottom panel show representative fits and decompositions into LE (dashed) and CT (dash-dot) components.

Ionic Liquid	T /°C	Biexponential Fits[a]						2-State Fits[b]				τ_{rxn}[c]
			a_1	τ_1	a_2	τ_2	$<\tau>$	k_{LE}	k_{CT}	k_f	K_{eq}	
$[Im_{21}][Tf_2N]$	25	LE	0.93	0.31	0.07	1.09	0.36	2.8	11.9	27.1	24	0.32±.07
		CT	-0.52	0.25	0.48	1.01						
$[Im_{41}][PF_6]$	25	LE	0.61	0.17	0.39	0.57	0.32	1.4	4.5	6.6	3.1	1.6±.4
		CT	-0.49	0.18	0.51	0.84						
$[Im_{41}][PF_6]$	70	LE	0.24	0.72	0.76	2.08	1.75	5.0	13.3	39.8	5.2	0.24±.07
		CT	-0.48	0.70	0.52	2.98						
$[N_{3111}][Tf_2N]$	25	LE	0.65	0.76	0.35	1.48	1.01	2[d]	6.6	10.2	6.3	1.0±.2
		CT	-0.50	0.50	0.50	1.97						
$[N_{3111}][Tf_2N]$	65	LE	0.87	0.20	0.13	0.77	0.27	5[d]	13.3	48.4	7.3	0.20±.07
		CT	-0.46	0.18	0.54	0.79						
$[N_{ip311}][Tf_2N]$	25	LE	0.80	0.87	0.20	1.76	1.05	1.9	7.5	8.1	16	1.1±.2
		CT	-0.51	0.69	0.49	1.77						
$[N_{ip311}][Tf_2N]$	65	LE	0.83	0.19	0.17	0.67	0.27	5.0	15.1	39.7	10	0.22±.05
		CT	0.51	0.17	0.49	0.81						
$[P_{14,666}][Tf_2N]$	45	LE	1.00	1.13	--	--	1.13	3.1	3.4	5.3	>50	1.6±.2
		CT	-0.52	1.14	0.48	3.38						

Table 4-2 Kinetic Parameters of the LE→CT Reaction of $BPAc^+$ in Various Ionic Liquids. All times are in units of ns and rate constants in units of 10^8 s^{-1}. (a) Parameters of unconstrained fits of LE and CT band intensities to $I(t)/I(0) = a_1 \exp(-t/\tau_1) + a_2 \exp(-t/\tau_2)$. $<\tau>$ is the average decay time $a_1\tau_1 + a_2\tau_2$ (b) Parameters of fits to Eqs. 5-7 with $r_{rad} = 0.55$. Values of k_A are fixed at the values $k_A = 1/\tau_{PAc}$ where τ_{PAc} is the lifetime observed for PAc^+. (c) τ_{rxn} is the best estimate of the reaction time constant (see text). (d) estimated values.

In conventional solvents a 2-state description of the LE→CT reaction was found to be appropriate[58] and we therefore analyzed band intensities using this kinetic model, which is defined in Scheme 4-1. Assuming that excitation occurs to only the LE state, the time-dependent band intensities of this model are given by:

$$I_{LE}(t)/I_{LE}(0)=\left(\frac{1}{\lambda_+-\lambda_-}\right)\left\{(Y-\lambda_-)e^{-\lambda_- t}+(\lambda_+-Y)e^{-\lambda_+ t}\right\} \quad 4.5$$

and

$$I_{CT}(t)/I_{LE}(0)=\left(\frac{k_{rad}^{CT}}{k_{rad}^{LE}}\right)\frac{k_f}{(\lambda_+-\lambda_-)}\left\{e^{-\lambda_- t}-e^{-\lambda_+ t}\right\} \quad 4.6$$

where

$$\lambda_\pm=\frac{1}{2}\left\{(X+Y)\pm\sqrt{(X-Y)^2+4k_f k_r}\right\}, \quad 4.7$$

$X=k_{LE}+k_f$, $Y=k_{CT}+k_r$, and where k_{rad}^I is the radiative rate constant of state *I*. In comparing the measured intensities to this model we fixed the rate constant k_{LE} to the intensity decay rates of PAc^+, which are listed in Table 4-2. The parameters k_f, k_{CT}, and $K_{eq}=k_f/k_r$, and $r_{rad}=k_{rad}^{CT}/k_{rad}^{LE}$ were allowed to vary. Examples of such fits are shown in Figure 4-4 and parameters derived from them listed in Table 4-2. As illustrated in Figure 4-4, the kinetics of the LE and CT band intensities are reasonably represented by this 2-state description. Based on quantum yield data in conventional high-polarity solvents a value of $r_{rad}=k_{rad}^{CT}/k_{rad}^{LE}$~0.3 is expected for $BPAc^+$. Somewhat larger values are obtained when this parameter is allowed to vary freely (solid curves in Figure 4-4). The parameters in Table 4-2 are those derived using an average value of r_{rad} = 0.55 (dash-dot

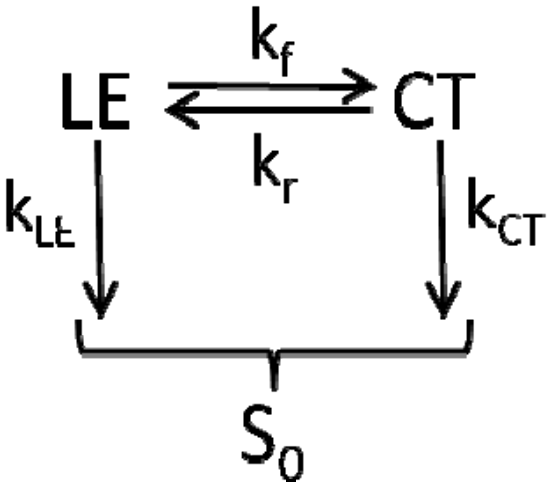

Scheme 4-1:

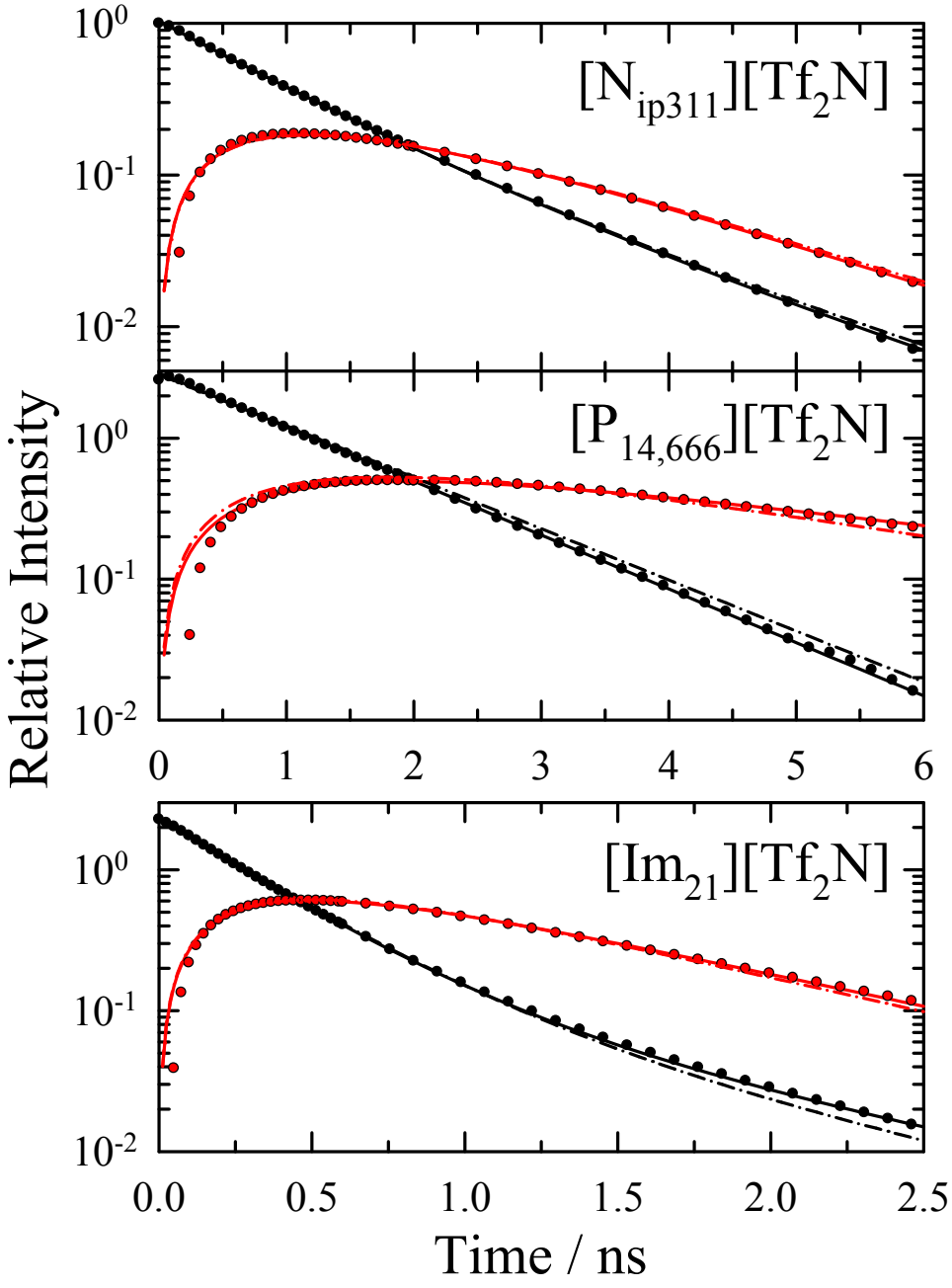

Figure 4-4 Representative decays of LE (black) and CT (red) band intensities in three ionic liquids. The $[P_{14,666}][Tf_2N]$ data were recorded at 45 °C and the other two data sets at 25 °C. Points indicate observed relative intensities and the curves indicate unconstrained (solid) and constrained (dash-dot) fits to Eqs. 5-7 ($r_{rad} = 0.55$).

curves) which fit the ionic liquid data much better than does $r_{rad} = 0.3$. The values of K_{eq} obtained using either choice of r_{rad} are typically much larger than unity as values of K_{eq} obtained using either choice of r_{rad} are typically much larger than unity as expected based on values observed in high-polarity conventional solvents. The variation in K_{eq} among the different ionic liquids does not appear to be sensibly related to their relative polarities and these variations probably only reflect uncertainties in the data. As a final measure of the time constant for the LE→CT reaction, τ_{rxn}, which is listed in the final column of Table 4-2, we use the average of the times (k_f^{-1}) determined from the k_f values obtained from unconstrained fits and from fits in which $r_{rad} = 0.3$ is used. The difference between the two k_f^{-1} values provides an estimate of the uncertainty in τ_{rxn}.

Figure 4-5 compares the times for the LE→CT reaction of $BPAc^+$ to average solvation times measured using the C153 probe. Data in both conventional polar solvents (small circles from Ref.[58]) and ionic liquids (large symbols) are shown. With the possible exception of $[P_{14,666}][Tf_2N]$, the reaction times in ionic liquids appear to follow the same correlation with solvation times observed in conventional solvents. The ionic liquid data overlap the data in the long-chain alcohols n-pentanol and n-decanol, which have the slowest solvation times (100 and 260 ps[54]). Thus, with respect to its effect on charge transfer in $BPAc^+$, there appears to be nothing distinctive about the environment presented by most of the ionic liquids studied beyond the fact that solvation is slow. As already discussed, the energetics of reaction are likely to be somewhat different in the case of $[P_{14,666}][Tf_2N]$ (Table 4-1), which could be the reason for its lack of correlation

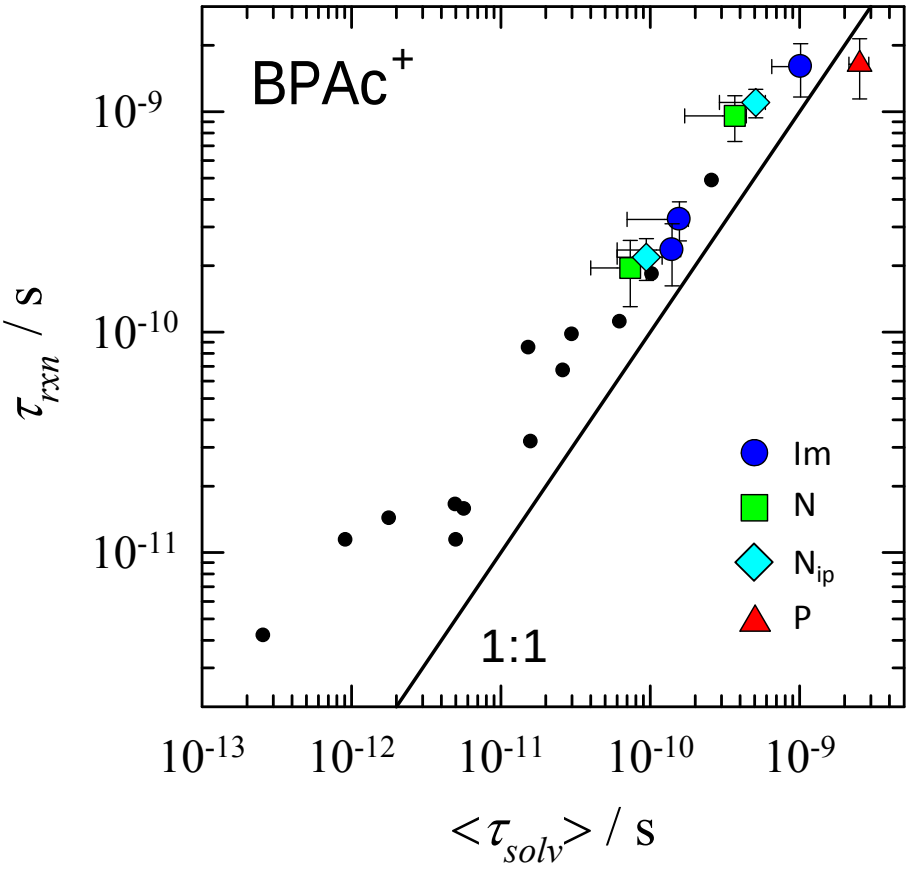

Figure 4-5 Time constants τ_{rxn} of the LE $\rightarrow$ CT reaction of $BPAc^+$ in conventional solvents (small symbols from Ref.[58]) and ionic liquids (large colored symbols) plotted versus integral solvation times $<\tau_{solv}>$ (Eq. 1) measured with C153.

with the remaining data. Alternatively, we note that the heterogeneous structure created by the high alkyl content of the $P_{14,666}^+$ cation[95] appears to markedly influence the solvation times of C153.[17] In this solvent, the reaction time of $BPAc^+$ is comparable to the times observed in other ionic liquids of comparable viscosity, but the solvation time is roughly 5-fold slower.[17] This latter effect could also account for the deviation $[P_{14,666}][Tf_2N]$ displays compared to the other ionic liquid data.

4.3.2 Crystal Violet Lactone (CVL):

Steady-state spectra of CVL are shown in 4-6. In contrast to $BPAc^+$ (and BA) the frequency of the $S_0 \rightarrow S_1$ (LE) absorption of CVL varies significantly with solvent polarity. The 1200-1400 cm^{-1} red shifts observed between the absorption in n-hexane and high-polarity solvents like acetonitrile indicate that the LE state of CVL is substantially more polar than the ground state. For this reason the LE emission of CVL depends much more on solvent polarity than in the case of the other two solutes studied. As in $BPAc^+$, both the LE and CT bands contribute to the emission in solvents of moderate to high polarity, and in CVL these peaks are typically better separated than in $BPAc^+$. To determine characteristics of the LE and CT emission bands, we employ the same procedure for fitting the spectra as described for $BPAc^+$. The only difference is that the emission of CVL in n-hexane, where the CT contribution is assumed negligible, is used to obtain the LE lineshape. Representative decompositions into LE and CT components are shown in the bottom panel of Figure 4-6. Once again, the much larger contribution

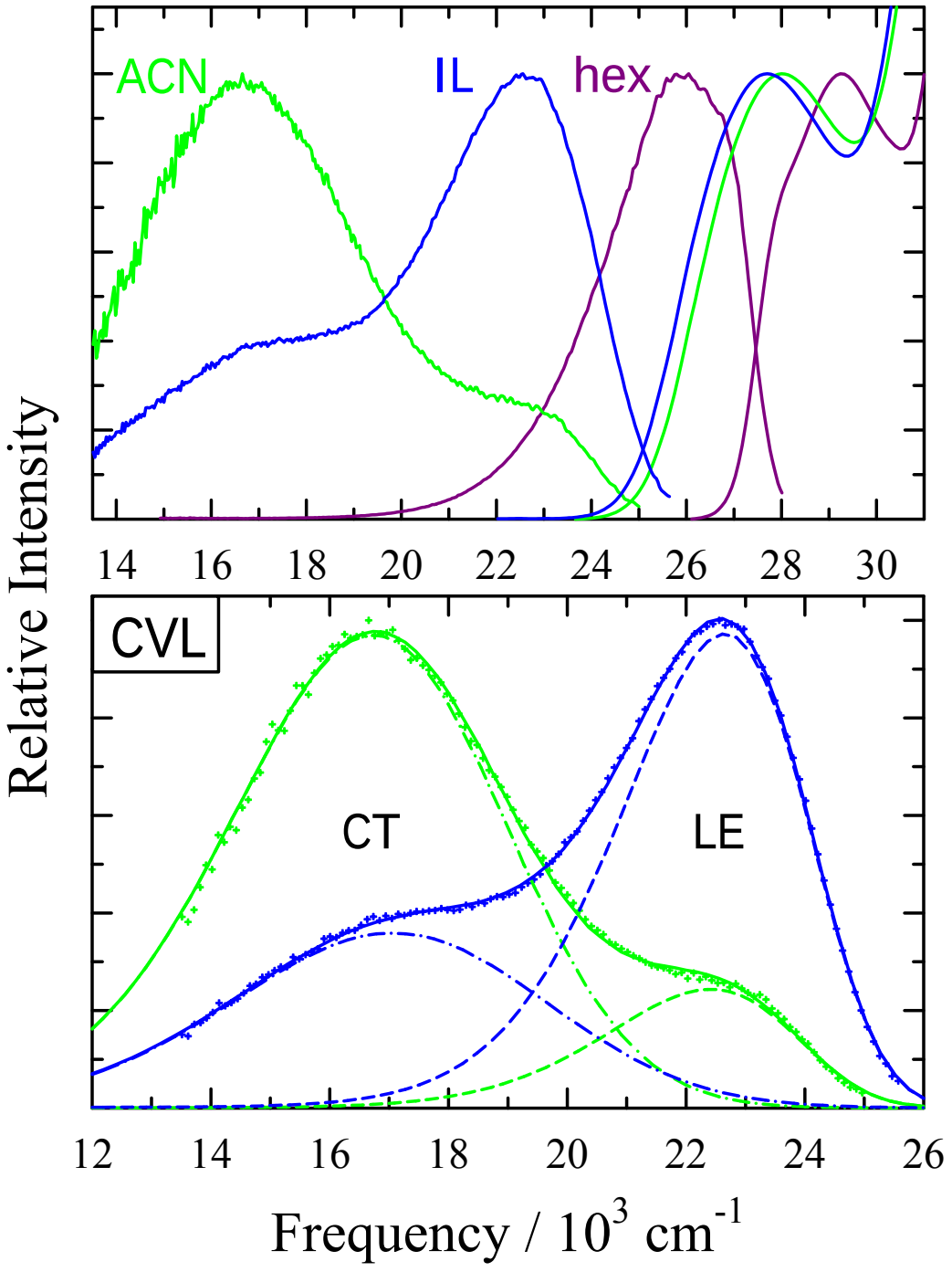

Figure 4-6 Top panel: Steady state absorption and emission spectra of CVL in n-hexane (hex), acetonitrile (ACN) and $[N_{3111}][Tf_2N]$ (IL). Bottom panel: Decomposition of the acetonitrile and $[N_{3111}][Tf_2N]$ spectra into LE (dashed) and CT (dash-dot) components as described in the text.

of CT emission in the spectrum of acetonitrile compared to that in $[N_{3111}][Tf_2N]$ is due to the fact that emission of CVL is not equilibrated in ionic liquids whereas it is in most conventional solvents.[62]

Examples of time-resolved emission spectra of CVL in ionic liquids are provided in Figure 4-7. The features of these spectra are similar to those observed in the $BPAc^+$ reaction, but in CVL the difference in polarity between the S_0 and LE states leads to a much larger (~2000 cm^{-1}) dynamic Stokes shift of the LE band occurring simultaneously with the LE→CT reaction. This Stokes shift tends to blur any isoemissive points in the area-normalized spectra,[96] but the 2-state character of the spectral dynamics is still evident. As in the case of $BPAc^+$, we fit the time-resolved spectra (Eqs. 2-4) in order to obtain information about the reaction kinetics free from contamination by this spectral shifting. To within uncertainties, the reconstructed spectra (points in Figure 4-7) could be fit by constraining the width parameters Γ_{LE} (~1900 cm^{-1}) and Γ_{CT} (~5000 cm^{-1}) as well as the frequency of the CT emission ($\nu_{CT} \cong 17000$ cm^{-1}) to values obtained from steady-state spectra and only allowing δ_{LE} and f_{CT} to vary with time. The smooth curves in Figure 4-7 are the results of such fits.

Representative LE and CT band intensities derived from this analysis are shown in Figure 4-8. These intensities are not as cleanly represented by the simple kinetic model applied to the $BPAc^+$ data. For one thing, the CVL band intensities are not as well represented as bi-exponential functions of time. As can be seen from Figure 4-8, although bi-exponential fits (smooth curves) provide reasonable characterizations of the data (points) the fit is not as accurate as in the $BPAc^+$ case. Because the quantum yield of

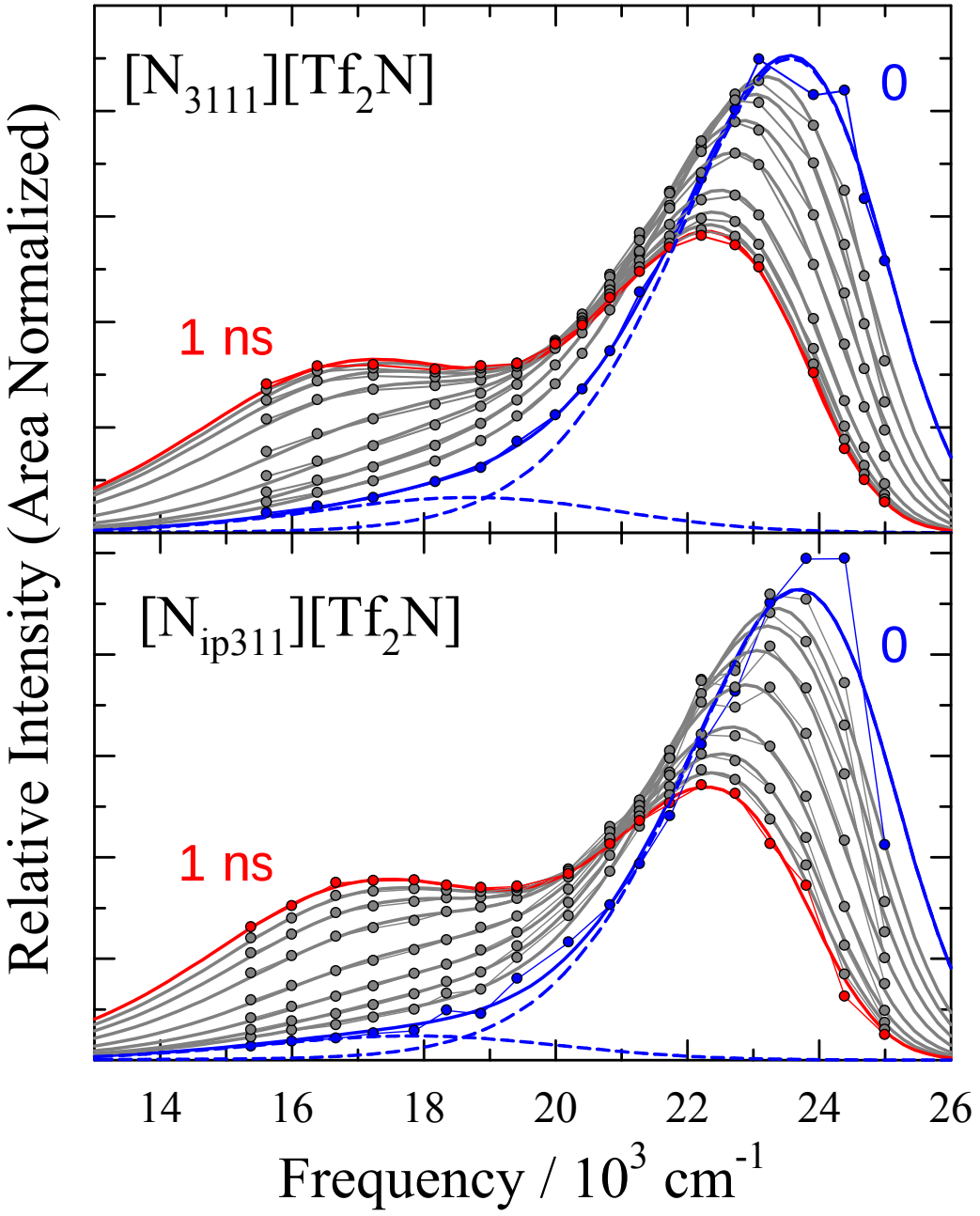

Figure 4-7 Time-resolved emission spectra of CVL in two ionic liquids. The connected points are the reconstructed spectra and the heavy smooth curves are fits to these data as described in the text. Times shown are 0, 25, 50, 100, 200, 400, 600, 800, and 1000 ps. The blue dashed lines show the LE and CT components at t=0.

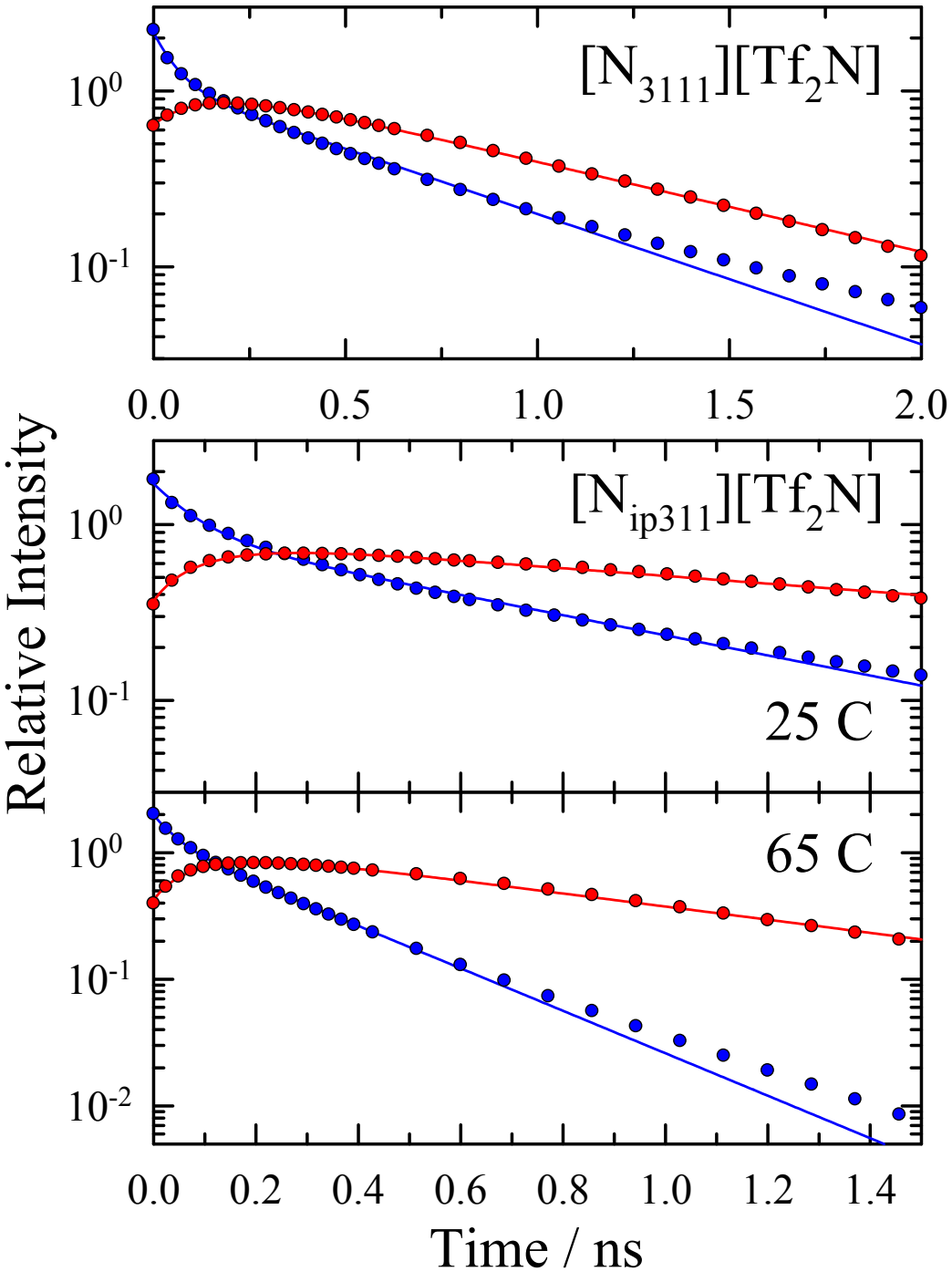

Figure 4-8 Time-dependence of the LE (blue) and CT (red) band intensities obtained from fits of CVL emission spectra. Points are the intensity data and curves are unconstrained biexponential fits to these data.

CVL emission is low ($<10^{-2}$ in highly polar solvents[61] and even lower in some ionic liquids[51]), it seems reasonable to ascribe the lack of perfect fit bi-exponential fits to impurity fluorescence from the ionic liquid solvents that is not completely removed by solvent subtraction. A more serious departure from simple 2-state kinetics is that, with the exception of $[P_{14,666}][Tf_2N]$, the reconstructed spectra show significant CT intensity (f_{CT}~0.2) at the earliest times. (See Figure 4-7.) This prompt CT emission might also result from residual impurity emission or from fast components of the reaction not adequately captured in the present experiments.[62] Whatever the source, the presence of this prompt CT emission means that the CVL data cannot be fit accurately using Eqs. 4-6. For this reason we can only make rough estimates of the times associated with the LE $\rightarrow$ CT reaction. We do so using the data summarized in Table 4-3. The columns labeled "Biexponential Fits" are the parameters obtained from independent fits of the LE and CT intensities. From these fits, as well as from constrained fits in which the CT intensity is required to be zero at t=0, we obtain average values of the fast time constant associated with decay of LE and rise of CT intensity, labeled τ_{fast}. This time should provide an approximate lower limit for the reaction time. The integral decay time of the LE intensity, $<\tau_{LE}>$, is an approximate upper limit for the reaction time. This measure would be appropriate if the reaction was irreversible and non-exponential. Finally, the inverse of the forward reaction rate constant obtained from the best simultaneous fit of the LE and CT intensities to Eq. 5-7, k_f^{-1} provides a third estimate of the reaction time. As a practical, albeit crude, measure of the LE $\rightarrow$ CT reaction time we take the average of these three estimates, and as a measure of uncertainty use the spread in these times.

IL	T/°C	Biexponential Fits[a]					Time Estimates[b]			τ_{rxn}[c]
			a_1	τ_1	a_2	τ_2	τ_{fast}	$<\tau_{LE}>$	k_f^{-1}	
$[Im_{21}][Tf_2N]$	25	LE	0.42	.043	0.58	.24	.059	.17	.091	.10±.05
		CT	-0.40	.11	0.60	.34				
$[N_{3111}][Tf_2N]$	25	LE	0.49	.055	0.51	.59	.076	.35	.12	.18±.13
		CT	-0.33	.15	0.67	.85				
$[N_{ip311}][Tf_2N]$	25	LE	0.49	.082	0.51	.76	.10	.48	.21	.26±.19
		CT	-0.36	.12	0.64	2.0				
$[N_{ip311}][Tf_2N]$	65	LE	0.38	.044	0.62	.26	.068	.18	.14	.13±.06
		CT	-0.40	.11	0.60	.84				
$[Pr_{31}][Tf_2N]$	25	LE	0.40	.059	0.60	.51	.087	.35	.059	.17±.15
		CT	-0.40	.12	0.60	1.4				
$[P_{14,666}][Tf_2N]$	45	LE	0.22	.67	0.78	5.9	1.1	4.9	5.3	3.7±2.0
		CT	0.49	1.3	0.51	10.0				

Table 4-3 Parameters Characterizing the Emission Dynamics of CVL. All times are in units of ns. (a) Parameters of unconstrained fits of LE and CT band intensities to $I(t)/I(0) = a_1 \exp(-t/\tau_1) + a_2 \exp(-t/\tau_2)$. (b) Three possible measures of reaction time: $<\tau_{fast}>$ is the average short component of the LE decay and CT rise, $<\tau_{LE}>$ is the integral decay time of the LE band, and k_f^{-1} is the inverse of the forward rate constant obtained from unconstrained fits to the 2-state model described by Eqs. 5-7. (c) Best estimate of reaction rate obtained from the average of the previous time estimates and uncertainties given by one half of the spread of these values.

These reaction times are compared to solvation times of C153 in Figure 4-9. Also shown are reaction times observed in high-polarity conventional solvents (small filled circles), where determination of the reaction time is straightforward.[62] In the ionic liquids studied, the estimated reaction times are within a factor of 2 of the integral solvation times, with most reaction times being somewhat less than solvation times. In contrast, in conventional solvents of low viscosity, reaction times are considerably greater than solvation times. But an extrapolation of the relationship between τ_{rxn} and $<\tau_{solv}>$ in conventional solvents to the regime found in ionic liquids (dashed-line, $\tau_{rxn} \propto <\tau_{solv}>^{0.6}$) suggests that the behavior in ionic liquids is probably not qualitatively different from that in conventional solvents. Unfortunately, unlike the other two reactions studied here, side reactions[61] prevent measuring the charge transfer of CVL in n-alcohol solvents in order to extend the conventional solvent data to the ionic liquid regime. The most that can be concluded from the present data is that the CVL reaction is probably controlled by solvation dynamics in both conventional solvents and ionic liquids and the nature of this solvent control is probably similar in the two classes of solvent.

4.3.3 Bianthryl (BA):

Steady-state spectra of bianthryl are shown in Figure 4-10. The room-temperature spectra in the top panel illustrate the relative solvent insensitivity of the anthracene-like absorption spectra of bianthryl. This weak solvatochromism indicates that the S_0 and LE states of bianthryl have similar polarities. In nonpolar solvents like 2-methylbutane, the

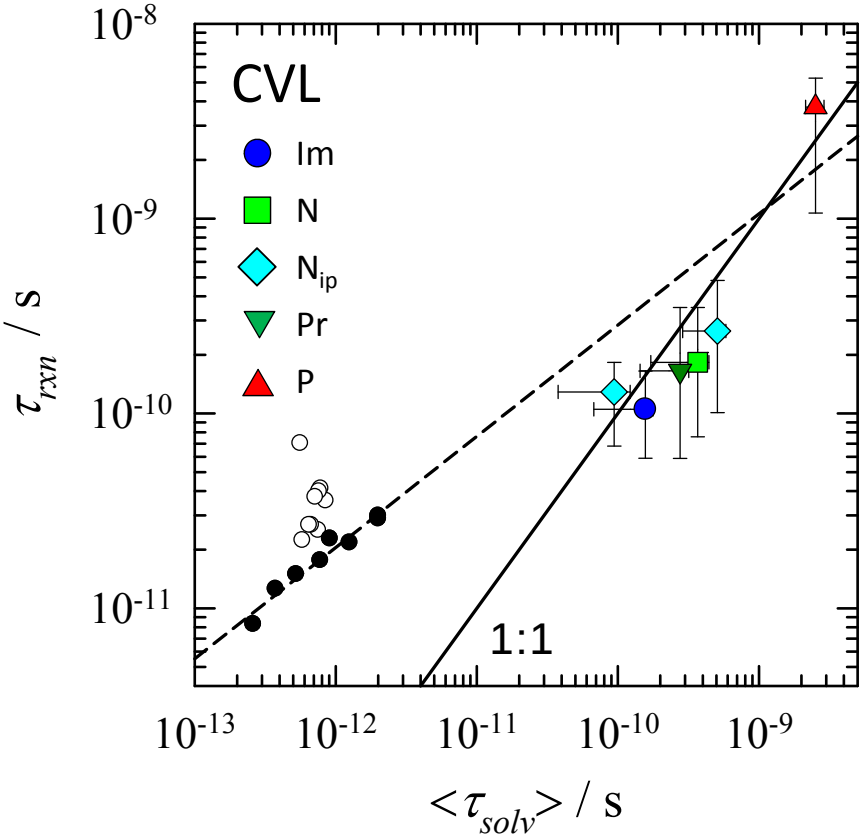

Figure 4-9 Time constants of the LE → CT reaction of CVL in conventional solvents at 25 °C (small symbols) from Ref.[62] and ionic liquids (large colored symbols) plotted versus integral solvation times $<\tau_{solv}>$ measured with C153. Among the conventional solvents, open symbols indicate low to moderate polarity and filled symbols high-polarity solvents ($\varepsilon > 25$). The dashed line is a fit to the latter data.

structured emission of bianthryl is characteristic of the LE state. In highly polar solvents like acetonitrile and ionic liquids, the broad, red-shifted emission of the CT state dominates the spectrum, with the only indication of some LE population being the residual structure on the blue side of the emission band. In contrast to the previous two cases, the CT emission of bianthryl accounts for a larger proportion of the emission and is red-shifted in the ionic liquid $[Im_{21}][Tf_2N]$ compared to acetonitrile. The reason for this distinction is that the S_1 lifetime of bianthryl (20-30 ns) is sufficiently large that the steady-state emission reflects an equilibrium between the LE and CT states. The greater CT fraction and red shift indicate that bianthryl senses a more polar environment in $[Im_{21}][Tf_2N]$ than it does in acetonitrile. The bottom panel of Figure 4-10 shows the temperature dependence of the steady-state emission spectra of bianthryl in $[P_{14,666}][Tf_2N]$. This ionic liquid readily forms a glass upon cooling (T_g = 197 K[97]) which allows easy access to a rigid solvent environment. Under such conditions, exemplified by the 166 K data in Figure 4-10, the LE→CT reaction is inhibited and only the structured emission of the LE state is observed. CT emission becomes evident above the glass transition, even at temperatures as low as 220 K where extrapolated viscosities exceed 10^6 cP. At room temperature, where reaction equilibrium is expected, CT emission accounts for about 75% of the spectrum. Both the smaller CT fraction and the lower frequency of the CT emission indicate that bianthryl sees $[P_{14,666}][Tf_2N]$ as substantially less polar than $[Im_{21}][Tf_2N]$ or the other ionic liquids studied here.

Time-resolved spectra of bianthryl in two ionic liquids are provided in Figure 4-11. These spectra do not display clear signatures of a 2-state reaction as did the spectra

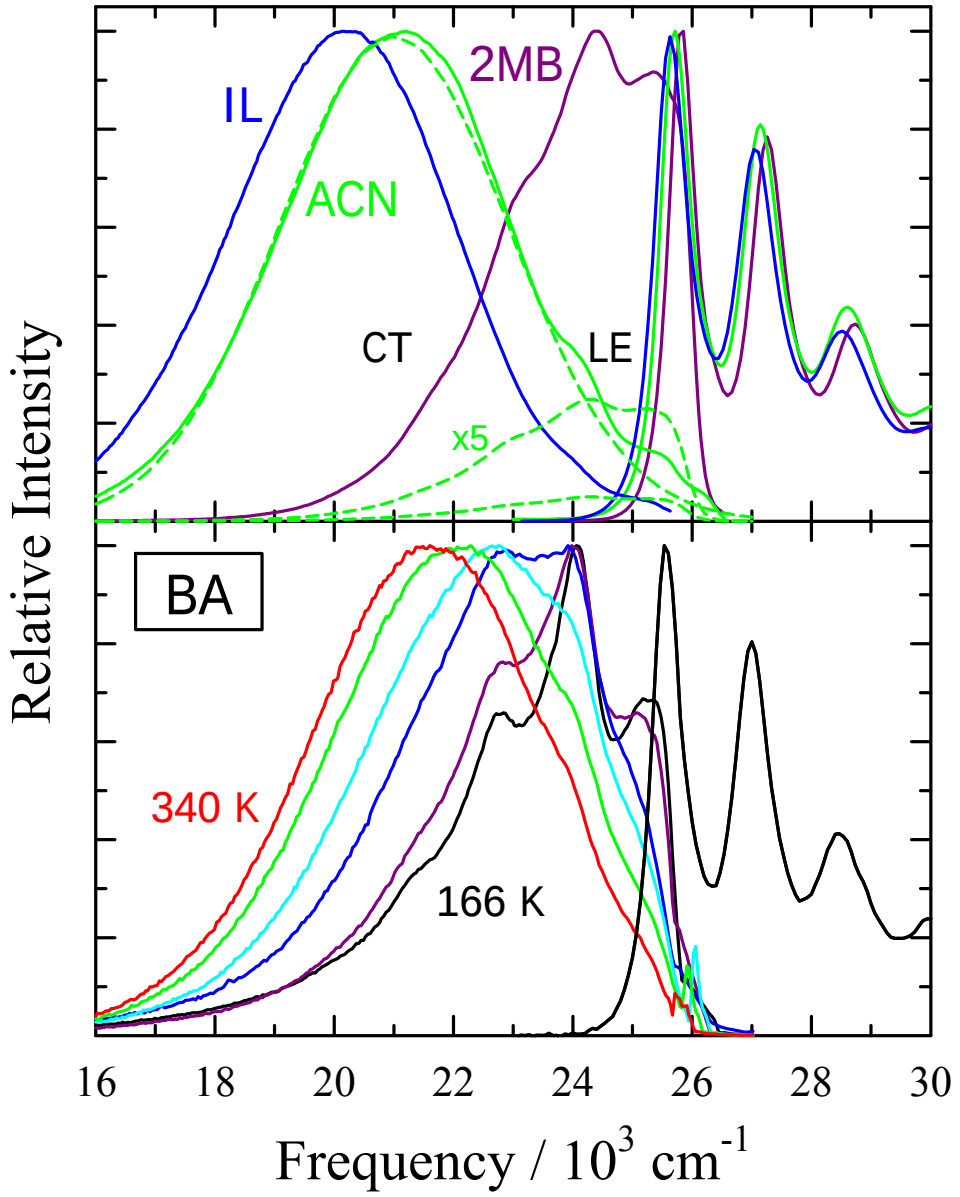

Figure 4-10 Steady-state spectra of bianthryl. Top panel: Absorption and emission spectra of BA in 2-methylbutane (2MB), acetonitrile (ACN) and $[Im_{21}][Tf_2N]$ (IL) at 25 °C (in order of decreasing frequency). Dashed green curves show approximate decomposition of the acetonitrile spectrum into LE and CT components. Bottom panel: Room-temperature absorption and temperature-dependent emission spectra of BA in $[P_{14,666}][Tf_2N]$. The temperatures shown are 166, 204, 222, 260, 281, and 340 K in order of decreasing frequency. (Note that the highest energy peak in the LE emission at low temperature is distorted by the inner filter caused by a high OD (.35) of this sample.)

of $BPAc^+$ and CVL. To within the time and spectral resolution employed here, it is difficult to discern any genuine structure in the time-resolved spectra or approximate isoemissive points in area-normalized spectra as were present in Figures. 4-3 and 4-6. Instead, as shown in Figure 4-11, the reconstructed spectra are reasonably represented by single log-normal lineshape functions. In this sense, the time-dependent spectra of bianthryl resemble those of a non-reactive probe such as C153 whose emission shifts in time due to solvation dynamics. The lack of obvious dual emission and resemblance to the dynamics observed for a pure solvation process result from the fact that the LE→CT reaction in bianthryl entails essentially barrierless motion along an adiabatic reaction coordinate comprised mainly of solvent polarization modes. The existence of a change of electronic state is nevertheless clearly signaled by the large drop in intensity as the spectrum shifts. In nonpolar solvents, where the LE state is primarily responsible for emission, the radiative rate of bianthryl is $\sim 10^8$ s^{-1} whereas in highly polar solvents like acetonitrile, where most emission is from the CT state, k_{rad} is about 10-fold smaller.[80] The loss of intensity in the time-dependent emission therefore reports on the evolution from the LE-like Franck Condon state to a CT-like state at long times, and we will use this intensity change to measure reaction times.

The dashed curves in Figure 4-11 show the time-zero spectra[98] predicted for the LE state immediately after excitation. Although the peak frequency and perhaps even the structure in the earliest measured spectrum of bianthryl in $[Pr_{41}][Tf_2N]$ are similar to that in the predicted LE spectrum, upconversion experiments discussed later indicate that a

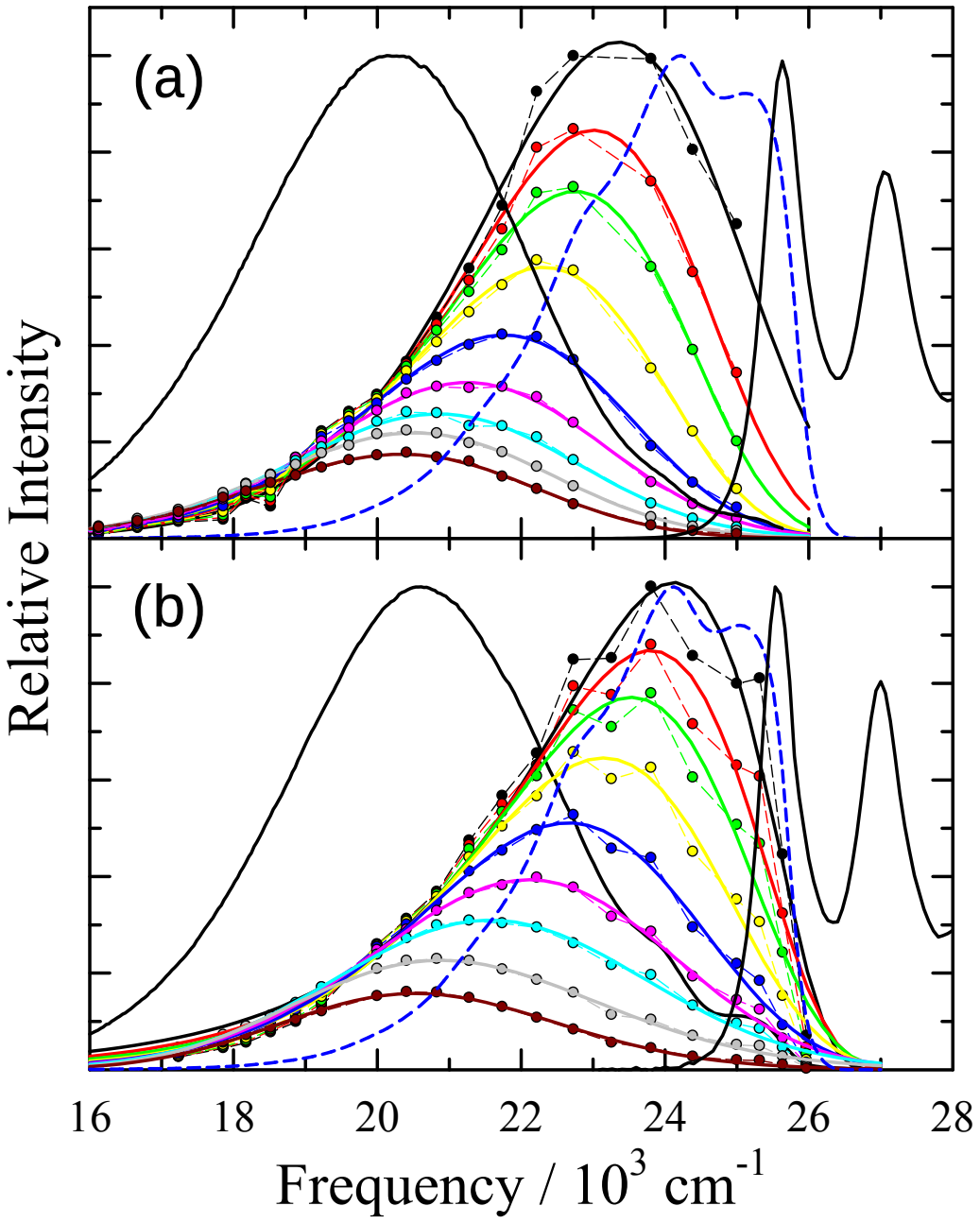

Figure 4-11 Time-resolved emission spectra (connected points) of bianthryl in (a) $[Im_{21}][Tf_2N]$ at 25 °C and (b) $[Pr_{41}][Tf_2N]$ at 21 °C and fits of these data to log-normal lineshape functions (smooth curves). Spectra in panel (a) are at times of 0, 10, 20, 40, 80, 160, 320, 640, 4000 ps and (b) at 0, 20, 40, 80, 160, 320, 640, 2000, and 10000 ps. Also shown (black curves) are absorption and steady-state emission spectra and estimated time-zero spectra (dashed blue curves).

substantial loss of intensity in the LE region occurs too rapidly to be measured in these TCSPC experiments. This observation is consistent with the fact that roughly half of the solvation dynamics in [Pr_{41}][Tf_2N] and most of the other ionic liquids studied is missed by such experiments[17,20,99]. (See f_{obs} in Table 4-1.) The fact that we only observe the later portions of both solvation and reaction in bianthryl should be kept in mind when viewing the data derived from such spectra.

Figure 4-12 illustrates the time-dependence the integrated intensities as well as the peak frequencies derived from log-normal fits of the spectra in Figure 4-11. (Prior to analysis, the emission spectra were divided by ν^3 to remove the intensity effect caused by the dependence of radiative rate upon frequency, but similar results are obtained using the emission spectra directly.) Both the frequency shifts and intensity decays of bianthryl in ionic liquids are highly non-exponential. We first consider the frequency shifts. The dynamic Stokes shifts observed here for bianthryl are similar to those of C153 in ionic liquids. Using the ~25 ps time resolution afforded by TCSPC, the frequencies of both C153[17] and bianthryl can be fit to within uncertainties using a stretched exponential time dependence,

$$\nu(t) = \nu(\infty) + \Delta\nu \exp\{-(t/\tau_0)^{\beta}\}. \qquad 4.8$$

The solid curves in the top panel of Figure 4-12 are fits to this functional form, with some fit parameters provided. Table 4-4 summarizes the magnitudes Δν and the integral times $\tau_{\Delta\nu}$, calculated as $\tau_{\Delta\nu} = (\tau/\beta)\Gamma(1/\beta)$, for all of the systems studied. (Γ in this expression is the gamma function.) The magnitudes of the observed Stokes shifts of bianthryl are all near 3000 cm^{-1}, much larger than the shifts measured with C153, due to

the larger polarity change in bianthryl. The values of β typically fall within the range 0.6-0.7, similar to what was previously reported for C153 in a wide variety of ionic liquids.[17] Finally, as illustrated in Figure 4-13, the integral Stokes shift times measured with bianthryl ($\tau_{\Delta\nu}$) and C153 ($<\tau_{solv}>$) are also nearly equal. In all cases the bianthryl shifts are slightly slower than those of C153 but in most cases the differences are within the anticipated uncertainties of the data. Thus, it seems clear that the observed Stokes shift dynamics of bianthryl faithfully reflect at least the slower portions of the solvation response that can be measured with the present experiments. Previous studies have come to this same conclusion and have provided Stokes shift times of bianthryl in several imidazolium ionic liquids.[45-47] In the two cases which overlap with the present data, the agreement with the integral times reported here is relatively poor. Detailed comparisons and discussion of the discrepancy are provided in the Supporting Material. Here we simply remark that we believe the $\tau_{\Delta\nu}$ (and the intensity decay times discussed next) reported here to be accurate to within their stated uncertainties for the particular time resolution employed. Both times represent only upper bounds to what would be observed with perfect time resolution, as do the solvation times of C153 used for comparison

To estimate reaction times we make use of the conclusions of Barbara and coworkers based on detailed modeling of the time-evolving emission spectra of bianthryl in several solvents.[72,73] They found that the progress of the LE→CT reaction, which they equated with the survival probability of LE state content in the mixed LE/CT wavefunction, can be tracked by monitoring either the integrated emission intensity or the

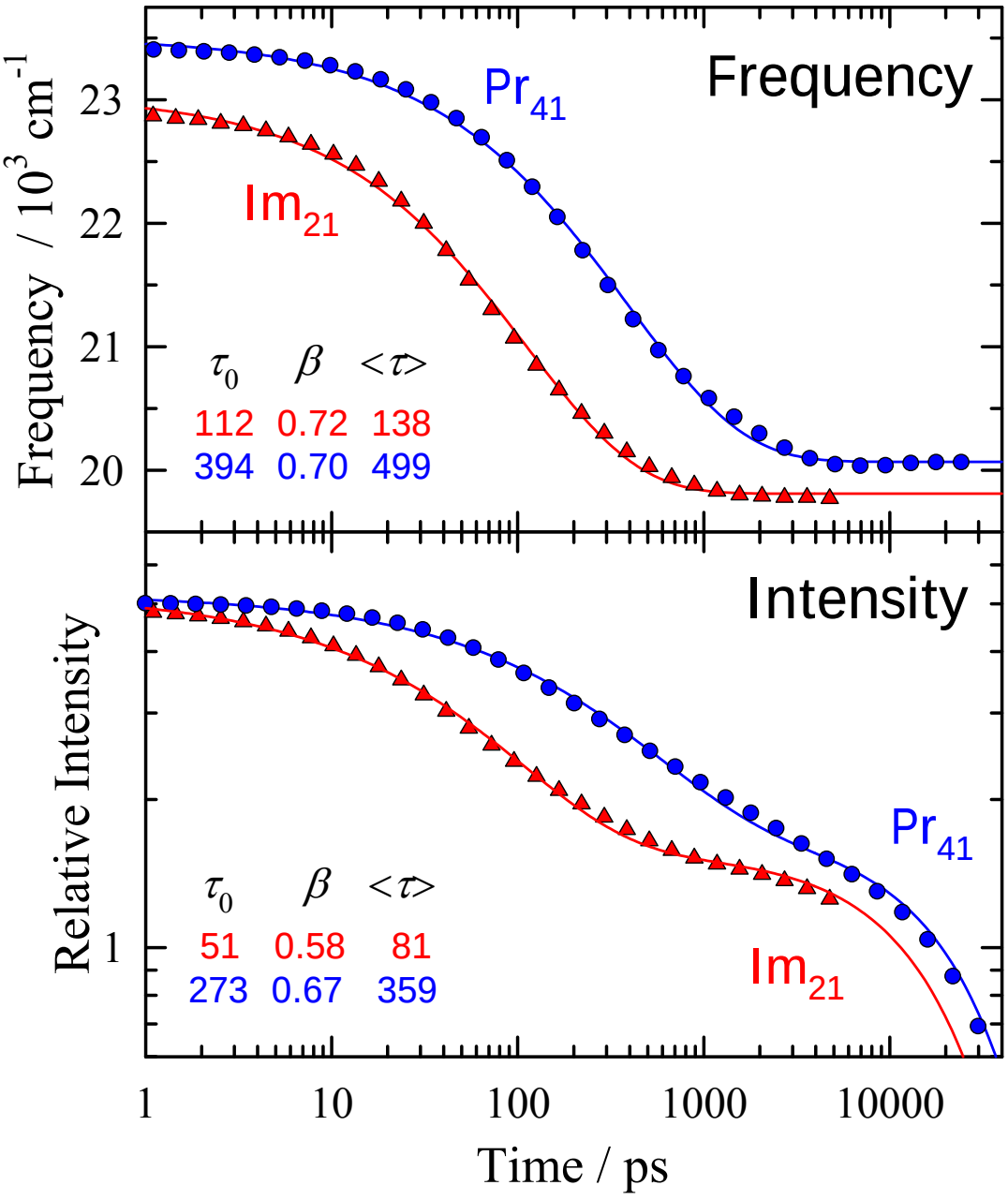

Figure 4-12 Characteristics of bianthryl emission obtained from log-normal fits of the (ν^3 normalized) time-evolving spectra in Figure 4-11. The top panel shows the peak frequencies and the bottom panel integral intensities in $[Im_{21}][Tf_2N]$ at 25 °C (red triangles) and $[Pr_{41}][Tf_2N]$ at 21 °C (blue circles). The smooth curves are fits to these data according to Eqs. 8 and 9 and the inset tables provide selected parameters from these fits.

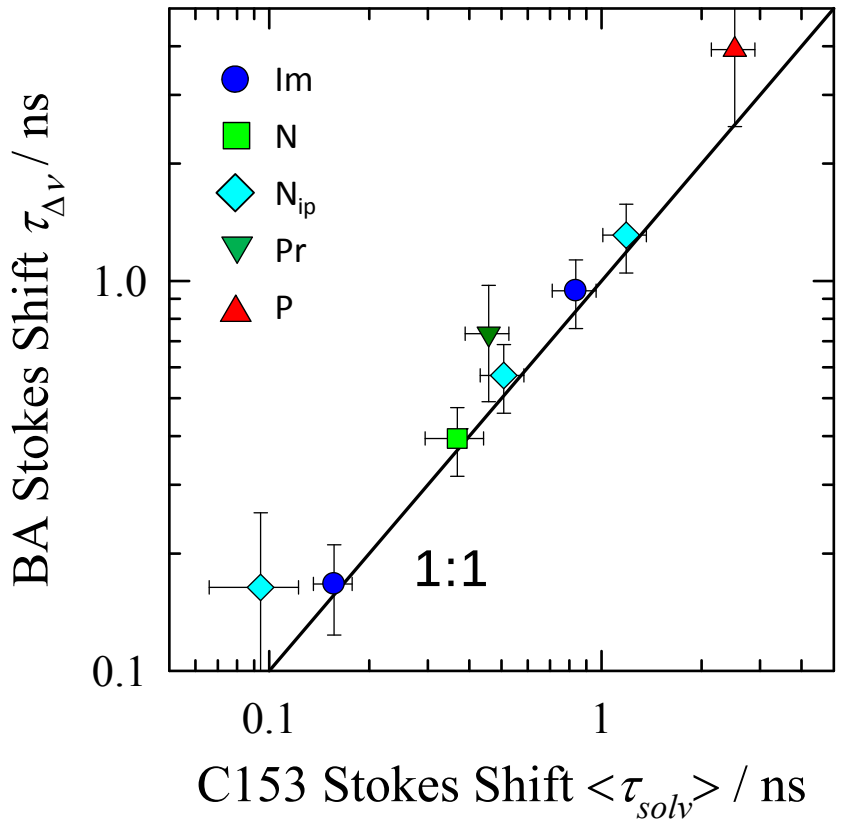

Figure 4-13 Comparison of the integral times associated with the Stokes shifts of C153 and bianthryl.

intensity decays observed at wavelengths on the blue edge of the emission spectrum (λ<420 nm) where CT contributions are small. We employ both intensity measures to derive reaction times here. Examples of total intensity decay data are shown in the bottom panel of Figure 4-12. Such data were characterized by fitting to the function

$$I_{tot}(t)/I_{tot}(0) = f_{str}\exp\{-(t/\tau_0)^{\beta}\} + (1-f_{str})\exp(-t/\tau_{dec}) \qquad 4.9$$

The parameter τ_{dec} is the decay time of the equilibrated S_1 population, which is well separated from other time constants of the emission decays. Example fits are the shown as the continuous curves in Figure 4-11 and selected parameters listed in the inset table. For the ionic liquids studied values of f_{str} and β fall in the range 0.7 ± .1 and 0.6±.1. Values of τ_{dec}, and the integral intensity decay time, $\tau_{II} = (\tau_0/\beta)\Gamma(1/\beta)$, used as one measure of the reaction time, are compiled in Table 4-4. As an alternative measure of reaction time, we also determined the average of the decay times measured at individual wavelengths between 390-420 nm. Decay data were fit to a multi-exponential form

$$I_{\lambda}(t)/I_{\lambda}(0) = \sum_{i=1}^{n} a_i \exp(-t/\tau_i) + a_{dec}\exp(-t/\tau_{dec}) \qquad 4.10$$

with *n* typically between 2-3 and the decay time determined from $<\tau_{\lambda}> = \Sigma_i a_i\tau_i / \Sigma_i a_i$. The averages of $<\tau_{\lambda}>$ over wavelengths $\lambda \leq 420$ nm are listed as $\tau_{\leq 420}$ in Table 4-4. As seen in this table, the two measures of reaction time, τ_{II} and $\tau_{\leq 420}$, agree only to about 33% on average. As a final estimate of reaction times, τ_{rxn}, we therefore take the mean of these two values and use their difference to estimate uncertainties.

		Frequency Shift[(a)]		Intensity Decay[(b)]			τ_{rxn}[(c)]
Ionic Liquid	T/°C	$\Delta\nu$	$\tau_{\Delta\nu}$	τ_{dec}	τ_{II}	$\tau_{\leq 420}$	
$[Im_{21}][Tf_2N]$	25	3.1	0.17±.04	26.1	0.076	0.046	0.06±.03
$[Im_{41}][BF_4]$	10	2.9	0.9±.2	31.3	0.41	0.45	0.43±.09
$[N_{3111}][Tf_2N]$	25	3.4	0.39±.08	30.8	0.17	0.32	0.25±.12
$[N_{ip311}][Tf_2N]$	10	3.4	1.3±.3	36.2	0.65	0.51	0.58±.12
	25	2.7	0.53±.11	35.6	0.33	0.29	0.31±.06
	65	3.0	0.16±.09	31.2	0.16	0.19	0.18±.04
$[Pr_{41}][Tf_2N]$	21	3.2	0.7±.2	35.7	0.41	0.57	0.49±.11
$[P_{14,666}][Tf_2N]$	10	--	--	32.7	4.8	2.6	4±2
	45	3.3	4±1	31.8	2.1	1.1	1.6±1.0

Table 4-4 Parameters Characterizing the Emission Dynamics of Bianthryl. Δν is in units of 10^3 cm^{-1} and all times in units of ns. (a) Stokes shift parameters obtained from log-normal fits of the time-resolved emission spectra to Eq. 8. The values listed are 2:1 weighted averages obtained from peak and first moment measures of frequency. (b) Intensity decay parameters: τ_{dec} is the longest component of the emission decays, τ_{II} is the integrated intensity decay time (Eq. 9) as described in the text, and $\tau_{\leq 420}$ is the average decay time obtained from fitting individual wavelengths on the blue edge of the spectrum (Eq. 10 and text). (c) τ_{rxn} is the best estimate for the reaction time obtained as the average of τ_{II} and $\tau_{\leq 420}$.

Reaction times are plotted versus C153 solvation times in Figure 4-14. Included in this Figure are data in conventional solvents (small symbols) from the early measurements of Barbara and coworkers[71,72] as well as the more recent data of Kovalenko *et al*.[82] Although most of the ionic liquid data fall slightly below the 1:1 line, there is no obvious distinction between the ionic liquid and conventional solvent data. As in the case of $BPAc^+$ and probably CVL, it appears that the same relationship between charge transfer and solvation dynamics holds in both dipolar and ionic environments.

This result requires further discussion as it contradicts the conclusion reached by the two other groups who have recently studied bianthryl in ionic liquids. As described in the Introduction, both Nagasawa and coworkers[45,46] and Khara *et al*.[47] concluded that, in contrast to the case in conventional dipolar solvents, charge transfer in bianthryl occurs much more rapidly than solvation. The primary evidence for this contrary perspective comes from femtosecond transient absorption (TA) data in the visible region by the Nagasawa group.[45] Nagasawa *et al*. measured integral rise times of an excited-state absorption attributed to the CT state to be in the range 53-100 ps in the three imidazolium ionic liquids, $[Im_{41}][Tf_2N]$, $[Im_{41}][BF_4]$, and $[Im_{41}][PF_6]$, whereas they measured integral Stokes shift times of the emission ($\tau_{\Delta\nu}$) using TCSPC to be in the range 650-2400 ps. In addition, Nagasawa *et al*. found that 30-50% of the rise of the CT transient absorption band occurs with an ultrafast time constant of 0.4-0.5 ps. Superficially, this comparison suggests that the charge transfer reaction is at least an order of magnitude faster than solvation in these ionic liquids. But it is difficult to directly compare the results of experiments with such different time resolutions: 200 fs in the TA experiments versus 30 ps in the TCSPC experiments. It is clear that Stokes shift components as fast as 0.5 ps

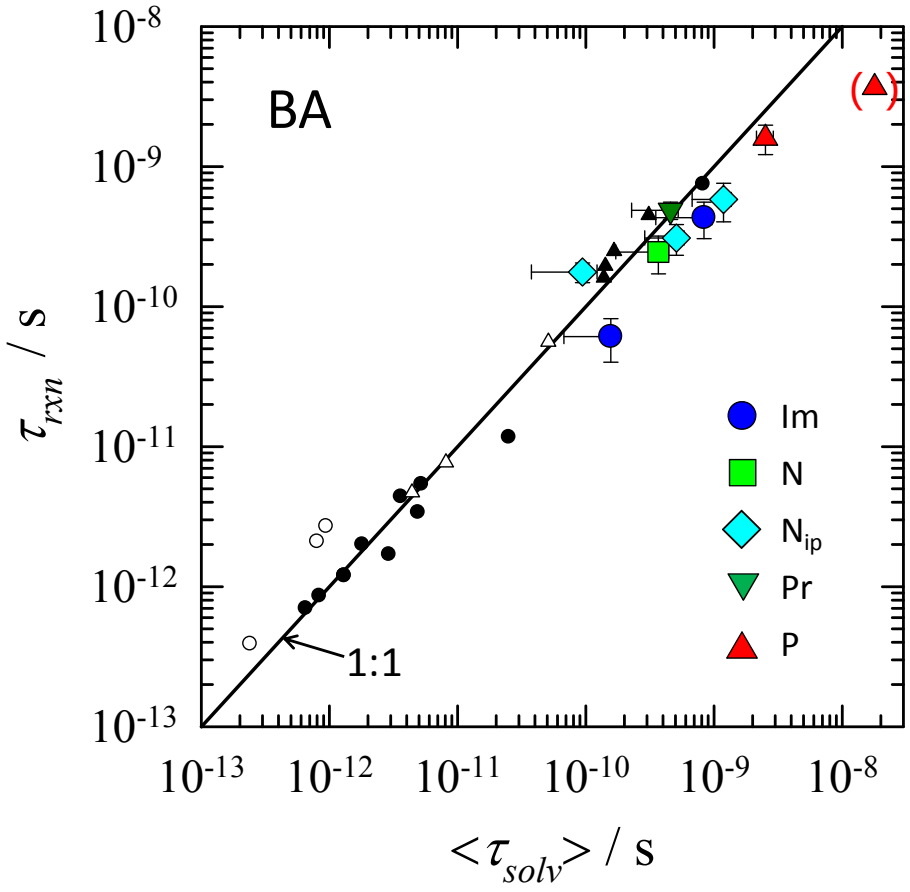

Figure 4-14 Estimated charge transfer times of bianthryl versus integral solvation times measured with C153. Large symbols indicate data in ionic liquids. Small symbols indicate data in conventional solvents from Refs.[71,72] (filled symbols) and [82] (open symbols). Dipolar aprotic solvents are shown as small circles and n-alcohols as small triangles.

would not be registered by the TCSPC experiments, and as already mentioned, TCSPC experiments only capture the longer time components of the dynamics. Conversely, it might be that the lower sensitivity of absorption relative to the emission experiments makes the TA data less sensitive to the relatively small long-time components detected in the TCSPC data.

Ideally, one would measure both the BA reaction dynamics and the solvation response with a technique that accurately captures both phenomena over the entire time range of relevance. We have not yet done so, but preliminary fluorescence upconversion data in $[Pr_{41}][Tf_2N]$ provide some perspective on the TA results of Nagaswa *et al*.[45] Figure 4-15 shows a comparison of the decays measured on the blue edge of the emission spectrum, 410 and 420 nm, recorded using fluorescence upconversion with ~300 fs time resolution (noisy data) and using TCSPC (smooth fit curves). The decays at these two wavelengths are very similar. Multi-exponential fits to the upconversion transients (to 500 ps) yield time constants of 6 ps (44%), 90 ps (40%), ~550 ps (12%), and >5 ns (4%). We do not detect any prominent sub-picosecond components in these emission data. The two fastest times we observe are similar to the longer two CT rise components reported by Nagasawa *et al*.,[45] which ranged between 7-14 ps and 140-330 ps, respectively. The origins of the subpicosecond component present in the TA data but absent in emission experiments is unclear. But the data in Figure 4-15 suggest that by using TCSPC to examine this reaction we are missing approximately 50% of the intensity decay indicative of the reaction progress. As indicated in Table 4-1 (f_{obs} = 0.50) about 50% of the solvation response measured with C153 is also missed in TCSPC experiments. This comparison helps justify the use of TCSPC data to explore the

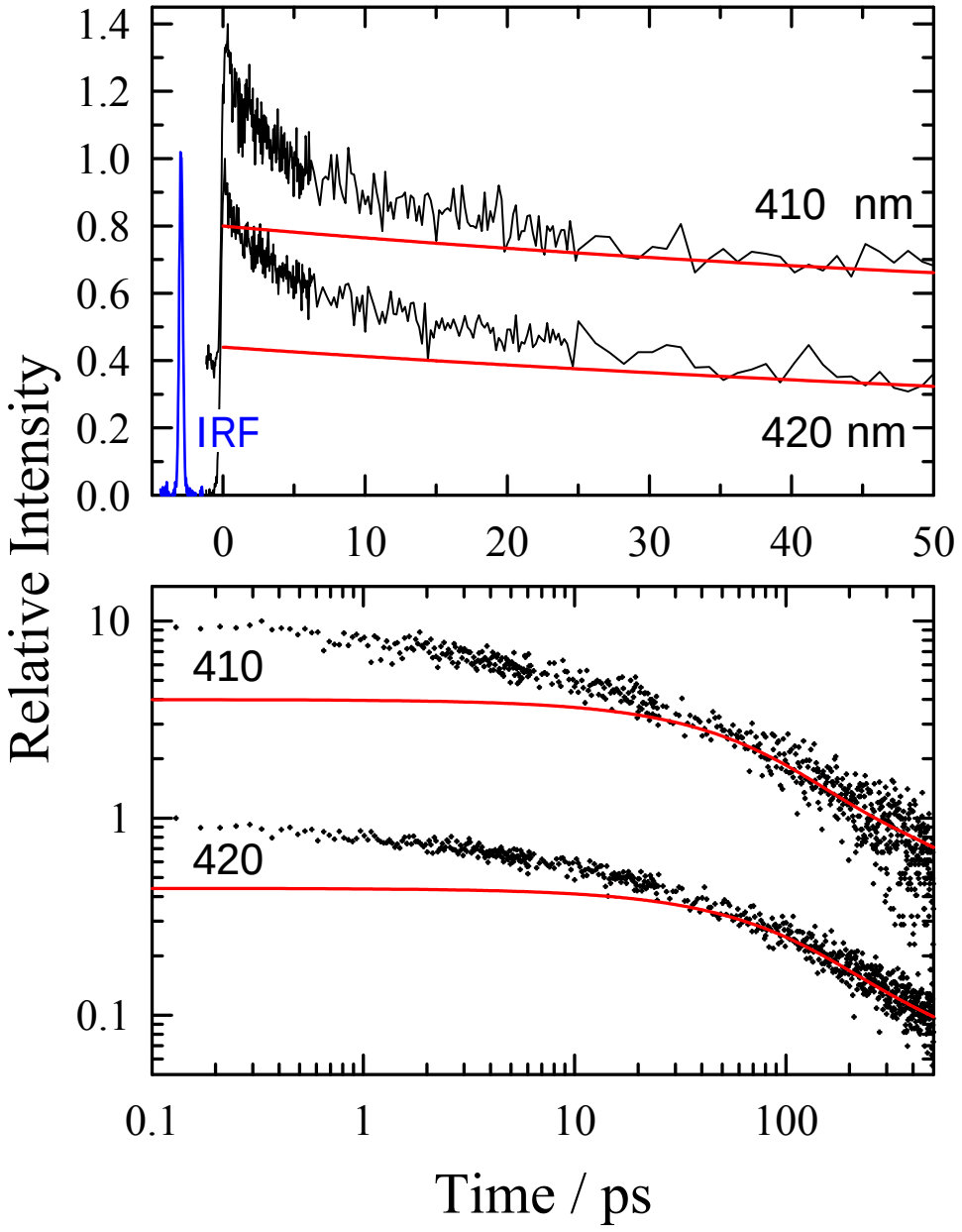

Figure 4-15 Comparison of normalized decays on the blue edge of the emission of bianthryl in $[Pr_{41}][Tf_2N]$ recorded using TCSPC (smooth red curves) and fluorescence upconversion (points and noisy curves). The blue curve labeled IRF is the response function of the upconversion data (FWHM=320 fs). The peak counts in these data sets were 130 and 200 at 410 and 420 nm, respectively. The TCSPC curves are multi-exponential fits to the data. For clarity both sets of 410 nm data have been shifted upward, by adding 0.4 in the top panel and by multiplying by 10 in the bottom panel.

connection between charge-transfer and solvation in the bianthryl system, despite the fact that a large portion of the reaction is faster than can be detected.

4.4 Summary & Conclusions

In this study we have used time-correlated single photon counting to measure the rates of three excited-state intramolecular electron transfer reactions in an assortment of room temperature ionic liquids. The solutes $BPAc^+$, CVL, and bianthryl were chosen because their excited state reactions had already been well characterized as being solvent controlled in conventional solvents. The goal here was to determine whether the same relationship between solvation and reaction previously established for these reactions in dipolar solvents also holds in ionic liquids.

The simplest behavior was observed in the $BPAc^+$ reaction. In this case, emission from the LE state undergoes only a small dynamic Stokes shift, and time-evolving spectra closely resemble those expected for 2-state kinetics between the LE and CT states. The lifetime of $BPAc^+$ is also sufficiently long (1-3 ns at 25 °C) that the reaction could be followed to equilibrium and relatively accurate values of the LE $\rightarrow$ CT rate constant k_f obtained. With the exception of $[P_{14,666}][Tf_2N]$, reaction times, $\tau_{rxn} = k_f^{-1}$, were found to be strongly correlated to solvation times $<\tau_{solv}>$ measured using the C153 and the correlation pertains to both ionic and dipolar solvents.

The situation is less straightforward in the case of the CVL reaction. Although the time-resolved spectra are clearly those of a 2-state process, the integrated intensities of the LE and CT bands do not conform to a 2-state kinetic scheme. It could be that

heterogeneity of the ionic liquid environment leads to distributed kinetics in the CVL reaction,[66] thereby spoiling the fit to a simple kinetic scheme. But this seemingly more complex kinetics compared to $BPAc^+$ could also be caused by solvent emission, impossible to eliminate ionic liquids, contaminating the weak emission of CVL. Whatever the origin, the departures from a 2-state kinetic scheme meant that reaction times could be only roughly estimated for the CVL reaction. To within the considerable uncertainties in the times deduced, an approximate equality $\tau_{rxn} \cong < \tau_{solv} >$ was found between reaction and solvation times. An approximate equality of this sort was also noted by Samanta and coworkers in their recent study of CVL in ionic liquids.[51] This relationship differs from what is observed in conventional dipolar solvents of low viscosity, where reaction is much faster than solvation. Nevertheless, extrapolation of the dipolar liquid data to the ionic liquid regime suggests that there is probably no qualitative distinction between the reaction – solvation relationship in these two solvent classes.

Finally, the bianthryl reaction is rather different from the other two reactions. Instead of time-resolved spectra resembling those expected for a 2-state process, they are more similar to spectra of a non-reactive probe undergoing solvation. This difference in character is attributed to the fact that the LE→CT conversion, like solvation, is essentially a barrierless process in bianthryl. In such a case reaction is not governed by simple rate laws and no unique time constant can be assigned. As did Barbara and coworkers[72,73] we define reaction times in terms of the time-dependent intensities of the undifferentiated LE+CT emission band to approximately measure the survival probability of LE character. Doing so, we find that the (integral) times associated with electron

transfer in bianthryl are approximately equal to the (integral) solvation times in ionic liquids. This near equality between reaction and solvation times in ionic liquids agrees nicely with the behavior reported previously in conventional dipolar solvents.[71,72,82] But the finding $\tau_{rxn} \cong < \tau_{solv} >$ obtained here disagrees with conclusions of two prior studies of bianthryl in ionic liquids.[45-47] Comparison of TCSPC and femtosecond transient absorption data led Nagasawa *et al*.[45] to conclude that reaction is much faster than solvation. Preliminary fluorescence upconversion data presented here suggest that difference in time resolution between the TCSPC and TA experiments probably accounts for some, but not all of the disagreement. The substantial subpicosecond component of the reaction observed in transient absorption is not found in fluorescence measurements. Additional femtosecond fluorescence and absorption measurements will be needed to understand the reason for this discrepancy.

To summarize, the results in $BPAc^+$, bianthryl, and with less certainty CVL, suggest that ionic liquids behave as slow-moving versions of high-polarity conventional solvents in their effect on solvent-controlled electron transfer reactions. At least in these low-barrier adiabatic processes, the distinction between solvation in dipolar versus ionic environments appears to be largely irrelevant. The situation might be different in the case of reactions with higher barriers. As shown by the modeling studies of Shim and Kim,[13,23] reactions with higher barriers sample only the faster portions of the solvation response and in such cases the unusually distributed nature of ionic liquid solvation is likely to lead to more distinctive and liquid-specific results.

4.5 Supporting Materials: Comparison of Bianthryl Stokes Shift Times to Literature Data:

Nagasawa and coworkers[45,46] and Samanta and coworkers[100] both reported TCSPC measurements of bianthryl in imidazolium ionic liquids. The integral Stokes shift times $\tau_{\Delta\nu}$ reported here for bianthryl in $[Im_{41}][BF_4]$ and $[Im_{21}][Tf_2N]$ can be compared to the corresponding times from these earlier studies. Interpolating Arrhenius fits to the temperature dependent data of Nagasawa *et al*.[46] provides integral times $\tau_{\Delta\nu} = 2.2$ ns in $[Im_{41}][BF_4]$ at 283 K and $\tau_{\Delta\nu} = 0.78$ ns in $[Im_{21}][Tf_2N]$ at 298 K. These values are respectively 2-fold and 5-fold slower than the values we report in Table 4-4. Such large differences are surprising given that the methods and time resolution employed in the Nagasawa work were very similar to those used here. To better discern possible reasons for these differences, in Figures. S1 and S2 we compare the time evolution of the peak frequencies reported by Nagasawa *et al*.[46] at temperatures closest to our data. In addition to comparing the primary data (read from Figures. 4-7 and 4-8 of Ref.[46]) we fit these data to Eq. 6 and tabulated the results in Table 4-1. Although there are differences between the integral times obtained using the stretched exponential fit function employed here and the multi-exponential form used by Nagasawa *et al*., fitting differences alone do not account for the large differences in $\tau_{\Delta\nu}$. Figures S1-2 and Table 4-5 show that the $\nu(t)$ data reported by Nagasawa *et al*. are more broadly distributed in time (smaller β) than our data. Their data also extrapolate to values of $\nu(\infty)$ which are higher than our values by a significant amount and generally show smaller Stokes shift magnitudes $\Delta\nu$ than our data.

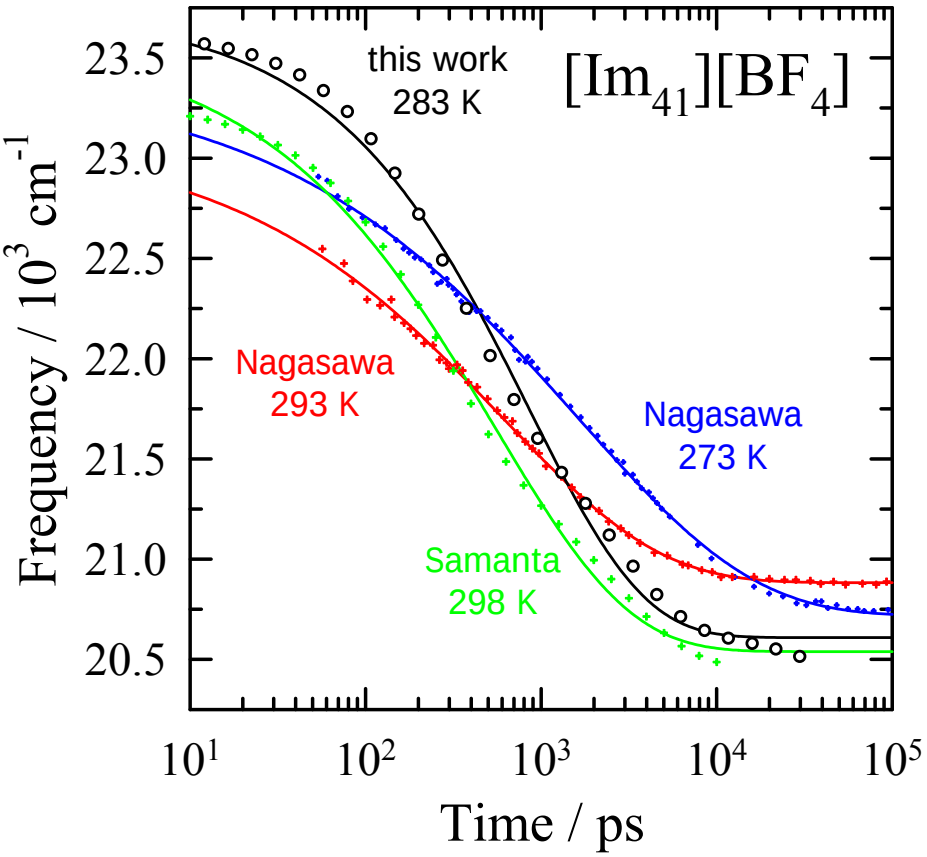

Figure 4-16 Comparison of peak frequencies of bianthryl in $[Im_{41}][BF_4]$ data measured in this work and reported by Nagasawa and coworkers[46] and Khara *et al.*[100]. Points are data and smooth curves are fits of these data according to Eq. 8. Data points were read from Figure 4-7 of the Nagasawa work and generated from the biexponential fit parameters and an estimate of $\nu(\infty) = 20{,}540$ cm^{-1} in the case of the Khara data. Fit parameters are provided in Table 4-5.

Ionic Liquid	T/K	Fits to Equation 8[a]					Reported[b]	Ref
		τ	$\nu(\infty)$	$\Delta\nu$	β	$\tau_{\Delta\nu}$	$\tau_{\Delta\nu}$	
$[Im_{41}][BF_4]$	283	0.85	20.61	3.12	0.66	1.13	.9±.2	this work
	273	1.62	20.72	2.69	0.43	4.41	3.28	[46]
	293	0.61	20.88	2.23	0.48	1.29	1.61	[46]
	298	0.54	20.54	3.06	0.57	0.88	1.22	[100]
$[Im_{21}][Tf_2N]$	298	0.12	20.37	3.13	0.70	0.15	.17±.04	this work
	293	0.15	20.62	2.85	0.48	0.33	0.83	[46]
	313	0.10	20.80	(2.85)[c]	0.59	0.15	0.71	[46]

Table 4-5 Comparison of $\nu(t)$ Fits and Integral Solvation Times. Frequencies are in units of 10^3 cm^{-1} and times in ns. (a) Parameters derived from fits of peak frequency data to Eq. 8 in the main text and the corresponding integral times. (b) The integral times reported. These values differ from the former value because Refs. 2 and 3 used a multi-exponential representation and because we reported a weighted average of peak and first moment frequency data (from ν^3 normalized data). (c) Value fixed to be the same as found for the 293 K data.

The difference is particularly clear in the $[Im_{41}][BF_4]$ data shown in Figure 4-16. It seems likely that these frequency differences are caused by differences in the steady-state spectra used for normalization during the spectral reconstruction process. Nagasawa *et al*. do not state whether their emission spectra are corrected for detection efficiency. The steady-state emission spectra reported in Figure 4-2 of Ref. 1 are systematically blue shifted and narrowed relative to our spectra, suggesting that their spectra are not corrected. Further support for this conjecture is the fact that our ionic liquid spectra are more comparable to the spectra reported by Samanta and coworkers,[100] which were corrected. The latter paper also report Stoke shift magnitudes comparable to ours. It is unclear how the use of uncorrected spectra would influence the dynamics of most interest here. It doesn't seem reasonable to expect it could cause differences as large as we find in $[Im_{21}][Tf_2N]$. We note that the integral Stokes shift times reported by Samanta and coworkers for bianthryl in $[Im_{41}][BF_4]$ as well as $[Im_{41}][PF_6]$ and $[Im_{41}][Tf_2N]$ at 298 K are nicely bracketed by the times reported for these ionic liquids by Nagasawa *et al*.[46] at 273 and 298 K. But Samanta's $\nu(t)$ data in $[Im_{41}][BF_4]$, shown in Figure 4-16, actually resemble our data much more than they do Nagasawa's data, especially if one accounts for the difference in instrumental response times (65 ps in the Samanta work versus 25-30 ps here).

References and Notes:

(1) Wasserscheid, P.; Welton, T.; Editors *Ionic Liquids in Synthesis*, 2nd ed., 2008.

(2) *Ionic Liquids*; Kirchner, B., Ed.; Springer-Verlag: Berlin, 2009; Vol. 290.

(3) Plechkova, N. V.; Seddon, K. R. *Chem. Soc. Rev.* **2008**, *37*, 123.

(4) Wishart, J. F. *Energy & Environmental Science* **2009**, *2*, 956.

(5) Zhou, F.; Liang, Y.; Liu, W. *Chem. Soc. Rev.* **2009**, *38*, 2590.

(6) Sun, P.; Armstrong, D. W. *Anal. Chim. Acta*, *661*, 1.

(7) Parvulescu, V. I.; Hardacre, C. *Chem. Rev.* **2007**, *107*, 2615.

(8) Demchenko, A. P. *Biophys. Chem.* **1982**, *15*, 101.

(9) Moniruzzaman, M.; Nakashima, K.; Kamiya, N.; Goto, M. *Biochem. Eng. J.* **2010**, *48*, 295.

(10) Hapiot, P.; Lagrost, C. *Chemical Reviews (Washington, DC, United States)* **2008**, *108*, 2238.

(11) Tsuda, T.; Hussey, C. L. *Mod. Aspects Electrochem.* **2009**, *45*, 63.

(12) Lynden-Bell, R. M. *Electrochem. Comm.* **2007**, *9*, 1857.

(13) Shim, Y.; Kim, H. J. *J. Phys. Chem. B* **2007**, *111*, 4510.

(14) Poole, C. F. *Journal of Chromatography, A* **2004**, *1037*, 49.

(15) Reichardt, C. *Green Chem.* **2005**, *7*, 339.

(16) Ferrer, B.; Garcia, H.; Schultz, K. P.; Nelsen, S. F. *J. Phys. Chem. B* **2007**, *111*, 13967.

(17) Jin, H.; Baker, G. A.; Arzhantsev, S.; Dong, J.; Maroncelli, M. *J. Phys. Chem. B* **2007**, *117*, 7291.

(18) Heitele, H. *Angew. Chem. Int. Ed. Engl.* **1993**, *32*, 359.

(19) Nemkovich, N. A.; Matseiko, V. I.; Tomin, V. I. *Opt. Spektrosk.* **1980**, *49*, 274.

(20) Arzhantsev, S.; Jin, H.; Baker, G. A.; Maroncelli, M. *J. Phys. Chem. B* **2007**, *111*, 4978.

(21) Shim, Y.; Choi, M. Y.; Kim, H. J. *J. Chem. Phys.* **2005**, *122*, 044511.

(22) Kobrak, M. N. *J. Chem. Phys.* **2006**, *125*.

(23) Shim, Y.; Kim, H. J. *J. Phys. Chem. B* **2009**, *113*, 12964.

(24) Grote, R. F.; Hynes, J. T. *J. Chem. Phys.* **1980**, *73*, 2715.

(25) Gordon, C. M.; McLean, A. J. *Chem. Comm.* **2000**, 1395.

(26) McLean, A. J.; Muldoon, M. J.; Gordon, C. M.; Dunkin, I. R. *Chem. Comm.* **2002**, 1880.

(27) Skrzypczak, A.; Neta, P. *J. Phys. Chem. A* **2003**, *107*, 7800.

(28) Grampp, G.; Kattnig, D.; Mladenova, B. *Spectrochim. Acta A* **2006**, *63A*, 821.

(29) Paul, A.; Samanta, A. *J. Phys. Chem. B* **2007**, *111*, 1957.

(30) Vieira, R. C.; Falvey, D. E. *J. Phys. Chem. B* **2007**, *111*, 5023.

(31) Takahashi, K.; Sakai, S.; Tezuka, H.; Hiejima, Y.; Katsumura, Y.; Watanabe, M. *J. Phys. Chem. B* **2007**, *111*, 4807.

(32) Sarkar, S.; Pramanik, R.; Seth, D.; Setua, P.; Sarkar, N. *Chem. Phys. Lett.* **2009**, *477*, 102.

(33) Castner, E. W., Jr.; Margulis, C. J.; Maroncelli, M.; Wishart James, F. *Ann. Rev. Phys. Chem.* **2011**, *62*, 85.

(34) Liang, M.; Kaintz, A.; Maroncelli, M. **2011**, unpublished results.

(35) Liu, H.; Liu, Y.; Li, J. *Phys. Chem. Chem. Phys.* **2010**, *12*, 1685.

(36) Dolidze, T. D.; Khoshtariya, D. E.; Illner, P.; Kulisiewicz, L.; Delgado, A.; van Eldik, R. *J. Phys. Chem. B* **2008**, *112*, 3085.

(37) Khoshtariya, D. E.; Dolidze, T. D.; van Eldik, R. *Chemistry--A European Journal* **2009**, *15*, 5254.

(38) Endres, F.; Hoefft, O.; Borisenko, N.; Gasparotto, L. H.; Prowald, A.; Al-Salman, R.; Carstens, T.; Atkin, R.; Bund, A.; Zein, E. A. S. *Phys. Chem. Chem. Phys.* **2010**, *12*, 1724.

(39) Hayes, R.; Warr, G. G.; Atkin, R. *Phys. Chem. Chem. Phys.* **2010**, *12*, 1709.

(40) Lockard, J. V.; Wasielewski, M. R. *J. Phys. Chem. B* **2007**, *111*, 11638.

(41) Jin, H.; Li, X.; Maroncelli, M. *J. Phys. Chem. B* **2007**, *111*, 13473.

(42) Jin, H.; Li, X.; Maroncelli, M. *J. Phys. Chem. B* **2010**, *114*, 11370.

(43) Blanco-Rodriguez, A. M.; Ronayne, K. L.; Zalis, S.; Sykora, J.; Hof, M.; Vlcek, A., Jr. *J. Phys. Chem. A* **2008**, *112*, 3506.

(44) Banerji, N.; Angulo, G.; Barabanov, I.; Vauthey, E. *J. Phys. Chem. A* **2008**, *112*, 9665.

(45) Nagasawa, Y.; Itoh, T.; Yasuda, M.; Ishibashi, Y.; Ito, S.; Miyasaka, H. *J. Phys. Chem. B* **2008**, *112*, 15758.

(46) Nagasawa, Y.; Oishi, A.; Itoh, T.; Yasuda, M.; Muramatsu, M.; Ishibashi, Y.; Ito, S.; Miyasaka, H. *J. Phys. Chem. C* **2009**, *113*, 11868.

(47) Khara, D. C.; Paul, A.; Santhosh, K.; Samanta, A. *Journal of Chemical Sciences (Bangalore, India)* **2009**, *121*, 309.

(48) Bose, S.; Wijeratne, A. B.; Thite, A.; Kraus, G. A.; Armstrong, D. W.; Petrich, J. W. *J. Phys. Chem. B* **2009**, *113*, 10825.

(49) Oum, K.; Lohse, P. W.; Ehlers, F.; Scholz, M.; Kopczynski, M.; Lenzer, T. *Angewandte Chemie, International Edition* **2010**, *49*, 2230.

(50) Santhosh, K.; Banerjee, S.; Rangaraj, N.; Samanta, A. *J. Phys. Chem. B* **2010**, *114*, 1967.

(51) Santhosh, K.; Samanta, A. *J. Phys. Chem. B* **2010**, *114*, 9195.

(52) Khurmi, C.; Berg, M. A. *J. Phys. Chem. Lett.* **2010**, *1*, 161.

(53) Wu, H.; Wang, H.; Xue, L.; Shi, Y.; Li, X. *J. Phys. Chem. B* **2010**, *114*, 14420.

(54) Horng, M. L.; Gardecki, J. A.; Papazyan, A.; Maroncelli, M. *J. Phys. Chem.* **1995**, *99*, 17311.

(55) 0000.

(56) Jones, G., II; Farahat, M. S.; Greenfield, S. R.; Gosztola, D. J.; Wasielewski, M. R. *Chem. Phys. Lett.* **1994**, *229*, 40.

(57) van Willigen, H.; Jones, G., II; Farahat, M. S. *J. Phys. Chem.* **1996**, *100*, 3312.

(58) Horng, M. L.; Dahl, K.; Jones, G.; Maroncelli, M. *Chem. Phys. Lett.* **1999**, *315*, 363.

(59) Lappe, J.; Cave, R. J.; Newton, M. D.; Rostov, I. V. *J. Phys. Chem. B* **2005**, *109*, 6610.

(60) Jones, G., II; Yan, D.; Hu, J.; Wan, J.; Xia, B.; Vullev, V. I. *J. Phys. Chem. B* **2007**, *111*, 6921.

(61) Karpiuk, J. *J. Phys. Chem. A* **2004**, *108*, 11183.

(62) Li, X.; Maroncelli, M. *J. Phys. Chem. A* **2010**, *ASAP*, DOI: 10.1021/jp106240x.

(63) Karpiuk, J. *Phys. Chem. Chem. Phys.* **2003**, *5*, 1078.

(64) Karpiuk, J. *Phys. Chem. Chem. Phys.* **2005**, *7*, 4070.

(65) Schmidhammer, U.; Megerle, U.; Lochbrunner, S.; Riedle, E.; Karpiuk, J. *J. Phys. Chem. A* **2008**, *112*, 8487.

(66) Annapureddy, H. V. R.; Margulis, C. J. *J. Phys. Chem. B* **2009**, *113*, 12005.

(67) Hu, Z.; Margulis, C. J. *Proc. Natl. Acad. Sci.* **2006**, *103*, 831.

(68) Hurley, M. M.; Harrowell, P. *Phys. Rev. E* **1995**, *52*, 1694.

(69) Schneider, F.; Lippert, E. *Ber. Bunsenges. Phys. Chem.* **1968**, *72*, 1155.

(70) Kahlow, M. A.; Kang, T. J.; Barbara, P. F. *J. Phys. Chem.* **1987**, *91*, 6452.

(71) Kang, T. J.; Kahlow, M. A.; Giser, D.; Swallen, S.; Nagarajan, V.; Jarzeba, W.; Barbara, P. F. *J. Phys. Chem.* **1988**, *92*, 6800.

(72) Kang, T. J.; Jarzeba, W.; Barbara, P. F.; Fonseca, T. *Chem. Phys.* **1990**, *149*, 81.

(73) Tominaga, K.; Walker, G. C.; Kang, T. J.; Barbara, P. F.; Fonseca, T. *J. Phys. Chem.* **1991**, *95*, 10485.

(74) Wortmann, R.; Elich, K.; Lebus, S.; Liptay, W. *J. Chem. Phys.* **1991**, *95*, 6371.

(75) Elich, K.; Kitazawa, M.; Okada, T.; Wortmann, R. *J. Phys. Chem. A* **1997**, *101*, 2010.

(76) Baumann, W.; Spohr, E.; Bischof, H.; Liptay, W. *J. Lumin.* **1987**, *37*, 227.

(77) Toublanc, D. B.; Fessenden, R. W.; Hitachi, A. *J. Phys. Chem.* **1989**, *93*, 2893.

(78) Piet, J. J.; Schuddeboom, W.; Wegewijs, B. R.; Grozema, F. C.; Warman, J. M. *J. Am. Chem. Soc.* **2001**, *123*, 5337.

(79) Schutz, M.; Schmidt, R. *J. Phys. Chem.* **1996**, *100*, 2012.

(80) Grabner, G.; Rechthaler, K.; Kohler, G. *J. Phys. Chem. A* **1998**, *102*, 689.

(81) Jurczok, M.; Plaza, P.; Martin, M.; Meyer, Y.; Rettig, W. *Chem. Phys.* **2000**, *253*, 339.

(82) Kovalenko, S. A.; Lustres, J. L. P.; Ernsting, N. P.; Rettig, W. *J. Phys. Chem. A* **2003**, *107*, 10228.

(83) Takaya, T.; Hamaguchi, H.-o.; Iwata, K. *J. Chem. Phys.* **2009**, *130*, 014501/1.

(84) Asami, N.; Takaya, T.; Yabumoto, S.; Shigeto, S.; Hamaguchi, H.-o.; Iwata, K. *J. Phys. Chem. A* **2010**, *114*, 6351.

(85) Subaric-Eitis, A.; Monte, C.; Roggan, A.; Rettig, W.; Zimmerman, P.; Heinze, J. *J. Chem. Phys.* **1990**, *93*, 4543.

(86) Tanaka, K.; Honma, K. *J. Phys. Chem. A* **2002**, *106*, 1926.

(87) Jones, G.; Farahat, M. S.; Greenfield, S. R.; Gosztola, D. J.; Wasielewski, M. R. *Chem. Phys. Lett.* **1994**, *229*, 40.

(88) Bell, F.; Waring, D. H. *J. Chem. Soc.* **1949**, 267.

(89) Jin, H.; O'Hare, B.; Dong, J.; Arzhantsev, S.; Baker, G. A.; Wishart, J. F.; Benesi, A.; Maroncelli, M. *J. Phys. Chem. B* **2008**, *112*, 81.

(90) Heitz, M. P.; Maroncelli, M. *J. Phys. Chem. A* **1997**, *101*, 5852.

(91) Maroncelli, M.; Fleming, G. R. *J. Chem. Phys.* **1987**, *86*, 6221.

(92) Tariq, M.; Forte, P. A. S.; Gomes, M. F. C.; Lopes, J. N. C.; Rebelo, L. P. N. *J. Chem. Thermodyn.* **2009**, *41*, 790.

(93) Matsumoto, H.; Kageyama, H.; Miyazaki, Y. *Chem. Comm.* **2002**, 1726.

(94) Ito, N.; Arzhantsev, S.; Maroncelli, M. *Chem. Phys. Lett.* **2004**, *396*, 83.

(95) Shimizu, K.; Costa, G. M. F.; Padua, A. A. H.; Rebelo, L. P. N.; Canongia, L. J. N. *J. Mol. Struct.: THEOCHEM* **2010**, *946*, 70.

(96) Koti, A. S. R.; Krishna, M. M. G.; Periasamy, N. *J. Phys. Chem. A* **2001**, *105*, 1767.

(97) Del Sesto, R. E.; Corley, C.; Robertson, A.; Wilkes, J. S. *J. Organomet. Chem.* **2005**, *690*, 2536.

(98) Fee, R. S.; Maroncelli, M. *Chem. Phys.* **1994**, *183*, 235.

(99) Zhang, X.; Liang, M.; Ernsting, N. P.; Maroncelli, M. *J. Phys. Chem. B* **2011**, manuscript in preparation.

(100) Khara, D. C.; Paul, A.; Santhosh, K.; Samanta, A. *J. Chem. Soc. (Bangalor)* **2009**, *121*, 309.

Chapter 5

Exploring Heterogeneity with Red-Edge Excitation Spectroscopy

5.1 Introduction

A number of recent studies have suggested[1-7] that dispersive kinetics is present in room temperature ionic liquids and is similar to what is observed in glasses and super-cooled liquids. By dynamic heterogeneity, we mean that there exists a distribution of local micro-environments having different relaxation rates. We have observed that in typical ionic liquids the solvation response[3,8] is broadly distributed in time, requiring stretched exponential functions with a stretching factor below 0.5 or multi-exponential functions with 3-4 components for proper fits. This distributed response might be due to the presence of dynamic heterogeneity. The connection between distributed kinetics and dynamic heterogeneity is illustrated in figure 5-1. This figure shows two different origins for dispersive kinetics: homogenous dynamics with same (complex) decay function across the whole system or an average over subensembles having different and simpler decays with a distribution of times. The latter case is what we refer to as "dynamic heterogeneity".

Since the 1970s, red edge excitation spectroscopy (REES) has been primarily used as a structural tool to study various systems including proteins,[9,10] micelles, and membranes.[13,14] REES is rarely used in simple liquids and most studies have focused on "static" or "energetic" heterogeneity[15-17] – the fact that different local

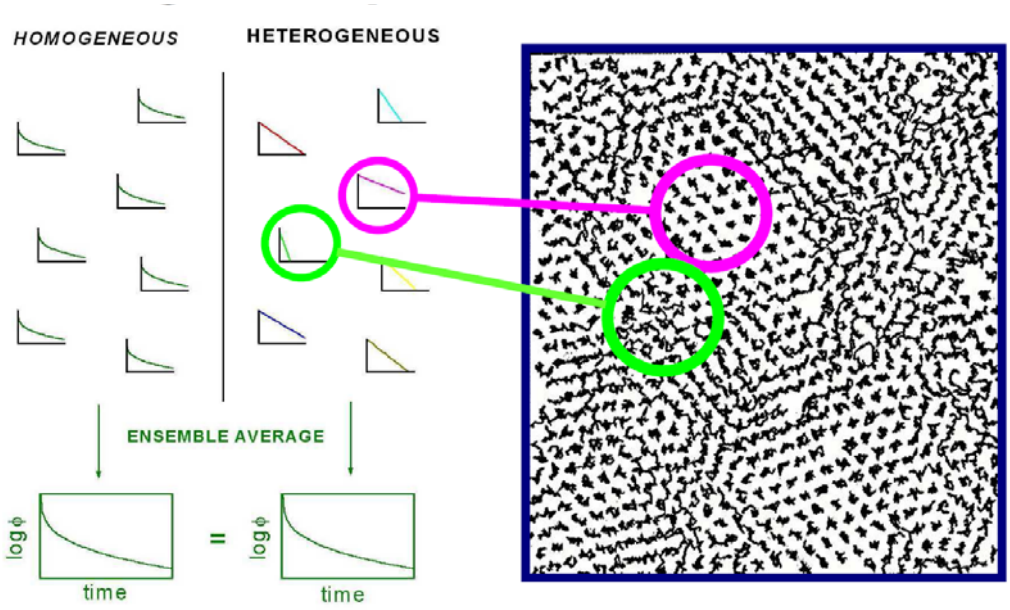

Figure 5-1 A scheme that represents different sources of non-exponential decays in homogenous solvation dynamics scenario while the right side[12] shows heterogeneous dynamics. In the left panel, red and green decays correspond to the two different solvation environments from a 2d simulation picture of both crystallized and amorphous regimes in the right panel.

solute environments produce different absorption or emission frequencies as a result of different solvation energies [18-20]. Because of the asymmetric nature of vibronic structure, excitation on the red-edge of an absorption band tends to select a narrowed and red-shifted subset of the overall solvation energy distribution. In contrast, excitation near to the peak or on the blue side of an electronic absorption tends to excite a broad distribution of energetically different solute-solvent environments. As a result, steady state spectra are expected to be red-shifted and narrower when excitation is made at longer wavelengths. This obvious violation to Kasha's rule only happens in a system where the solvent reorganization time is comparable to or greater than the lifetime of the probe. Both experiments[21-24] and computational[18,19,25,26] studies have demonstrated the presence of such energetic heterogeneity in ionic liquids. One example for such observations is using Coumarin153 (C153) and 4-Aminophthalimide (4-AP) as probe (Scheme 1), a work[27] from the Maroncelli group has shown that the static heterogeneity property of 1-proponol at below glass transition temperature (88K) by red-edge excitation spectroscopy. Significant red shift of fluorescence emission spectra were observed when exciting wavelength move towards redder frequencies.

Dynamic heterogeneity can also be sensed by red-edge excitation spectroscopy. In the presence of dynamic heterogeneity , time-resolved spectra collected at different time delays should have different widths[28,29] while the overall averaged solvation times are expected to depend on excitation wavelength. Therefore, red-edge spectroscopy can serve as a useful means of exploring dynamic heterogeneity in ionic liquids. Moreover, compared with conventional dipolar solvents, the average solvation times of ionic liquids

Structure of C153 and [N_{ip311}^{+}][Tf2N^{-}]

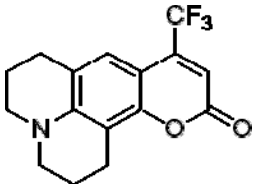

Coumarin 153

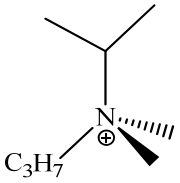

[N_{ip311}^{+}]

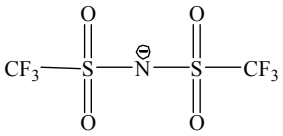

[Tf2N^{-}]

Structure of 4-AP and [$P_{14,6,6,6}$+][Tf_2N^{-}]

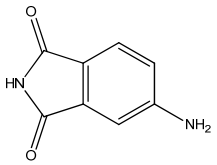

4-AP

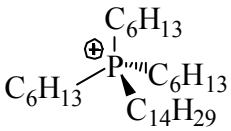

[$P_{14,6,6,6}^{+}$]

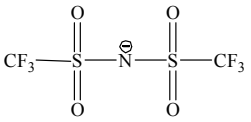

[Tf2N^{-}]

Scheme 5-1

are much longer (on the nanosecond scale[3]) and this fact makes TCSPC a suitable tool for measuring changes in solvation times in ionic liquids. However, experimental evidence for "dynamic heterogeneity" in the solvation response is scant[5,30]. One published result is a report from our group, using C153 as probe in the ionic liquid $[N_{ip311}{}^{+}][Tf_2N^{-}]$ as shown in (scheme 1). In that study, despite the fact that we were not able to excite very far on the red edge of the absorption band, detectable differences were observed in the solvation time. We and other groups have been looking for suitable systems for additional and more definitive evidence of dynamic heterogeneity in ionic liquids.

From preliminary studies, we find that it is important to choose the proper ionic liquid and probe for this kind of study. Some of the major considerations when probing solvation times using red-edge excitation are the following. First, one needs to choose an ionic liquid where significant heterogeneity is expected to exist, for example in liquids containing cations possessing long alkyl side chains. Previous studies using X-ray scattering and simulation techniques[31,32] have shown that such ionic liquids tend to form large non-polar domains and these domains might be expected to give rise to dynamic heterogeneity. Second, a probe should be selected considering the excitation range available, in the present case 370 nm to 430 nm from the Ti:sapphire laser. Furthermore, in order to be able to accurately measure the entire solvation process, the ionic liquid chosen must have a relatively slow solvation time so that short components of the relaxation are not missed due to inadequate time resolution. In a previous survey of solvation times in ionic liquids, we noticed that it is common to miss the first 30%-50% of the solvation time of ionic liquids when using TCSPC[33]. In addition, the lifetime of

the probe needs to be at least 2-3 times longer than the solvation time in order to observe of all of the dynamics. Finally, the magnitude of the probe's Stokes shift is important. When exciting at the far red edge of a probe's absorption spectrum, the Stokes shift will be much smaller than when exciting at the peak. Use of a probe with the largest Stokes shift possible is desirable in order to maintain accuracy for red-edge excitation. To choose a probe and ionic liquid combination to satisfy all the criteria listed above requires effort.

We made several attempt including using 4-AP in $[P_{14,6,6,6}^{+}][Tf_2N^{-}]$ (trihexyl(tetradecyl)phosphonium *bis*(trifluoromethylsulfonyl)imide). Figure 5-2 shows the time-evolving peak and average frequencies observed upon excitation at three different wavelengths. The limited magnitude of the shift when excited at the red edge (excited at 410 nm) was a major drawback in this system because it leads to inaccurate time estimates

In this chapter we report the most successful set of experiments, made using Coumarin102 (C102) in $[N_{4,4,4,1}^{+}][Tf_2N^{-}]$ (Scheme 5-1) for detailed study of dynamic heterogeneity by red edge spectroscopy. Choice of this ionic liquid was motivated by the fact that Castner and co workers[7] previously showed using C153 as a probe and a TCSPC system similar to ours, that the complete solvation response of this liquid could be measured near to room temperature. We choose C102 as probe instead of C153 in order to be able to excite to the far red edge of the absorption spectrum. Detailed study of this system will serve to provide more information about dynamic heterogeneity in ionic liquids.

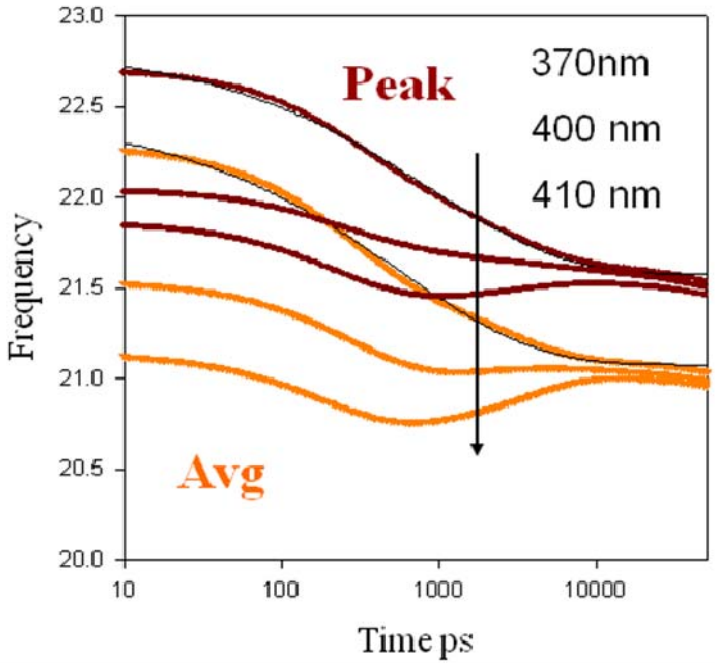

Figure 5-2 Shifts of frequency versus time for 4-AP/[$P_{14,6,6,6}^{+}$][$Tf2N^{-}$]. The brown curves are peak frequencies and orange lines are average (first moment) frequencies calculated from time-resolved spectra collected using TCSPC. The three different curves in each color represent the different excitation wavelength (370 nm, 400 nm and 410 nm) of the sample as indicated by the arrow. Black lines are the fits of each curve.

5.2 Materials and Methods

The ionic liquid chosen for the present study is N-methyl-tri-N-butylammonium *bis*(trifluoromethylsulfonyl)imide, $[N_{4,4,4,1}^{+}][Tf_2N^{-}]$. It was synthesized using a modified literature procedure[34]. $[N_{4,4,4,1}^{+}][Cl^{-}]$ was purchased from IoLiTech, dissolved in dichloromethane (HPLC grade >99% from Sigma-Aldrich) and stirred with activated charcoal overnight. The charcoal was then filtered through syringe filters and the solvent was then removed by rotaryevaporation. Conversion of the chloride to the bis(trifluoromethylsulfonyl)imide salt was performed by mixing equimolar quantities of the chloride salt and $[Li^{+}][Tf_2N^{-}]$ (>99%, purchased from Sigma Aldrich) in aqueous solution. The aqueous layer was removed and the liquid washed with aliquots of water until no chloride was detectable in the washings using a silver nitrite test. The ammonium bis(trifluoromethylsulfonyl)imide ionic liquid was further purified by stirring with activated charcoal overnight and the carbon removed by passing through a syringe filter three times. The dichloromethane solvent was removed by rotary evaporation and the resulting ionic liquid was dried at reduced pressure at 313 K for at least 24 h prior to use.

The melting point of $[N_{4,4,4,1}^{+}][Tf_2N^{-}]$ is 300 K,[7] and it tends to crystallize at room temperature. We found that addition of C102 as probe in the ionic liquid was sufficient to prevent crystallization and maintain the sample in the form of a viscous liquid at room temperature. Such samples did crystallize at temperatures below 273 K.

In the experiments reported here we employ both steady state absorption and emission spectroscopy and time-correlated single photon counting (TCSPC) measurements as described in Chapter 2.2.1.

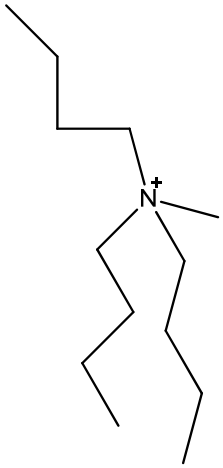

$[N_{4,4,4,1}^{+}]$

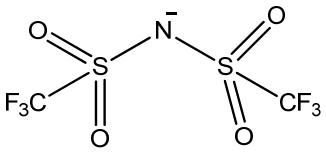

$[Tf_2N^{-}]$

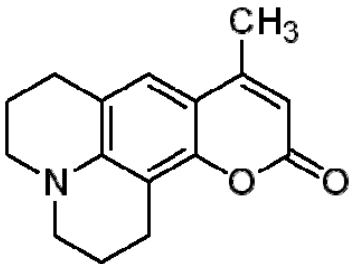

Coumarin 102

Scheme 5-2

5.3 Results and Discussion

Figure 5-3 shows the absorption and steady state emission spectra of C102 in $[N_{4,4,4,1}^{+}][Tf_2N^{-}]$. The colored arrows in this figure indicate the different excitation wavelengths employed. The range of wavelengths shown here represents the range readily accessed by the TCSPC laser system. As illustrated, C102 is well matched to this laser system, much more so than the C153 probe used previously[5]. Also shown in Fig. 5-3 is the fact that the emission spectrum is red-shifted for excitation on the red edge of the absorption, as expected, but this red shift is small (less than 10 nm from excitation at 390 nm to 430 nm). Even when the absorption spectrum is significantly broadened by static heterogeneity, large excitation dependence to the emission frequency is only expected when the fluorescence lifetime is comparable to or shorter than the solvation time. In the present case the requirement that we observe all of the solvation response necessarily means that this condition is not met and we thus observe only a small shift despite the presence of significant heterogeneity of solvation environments.

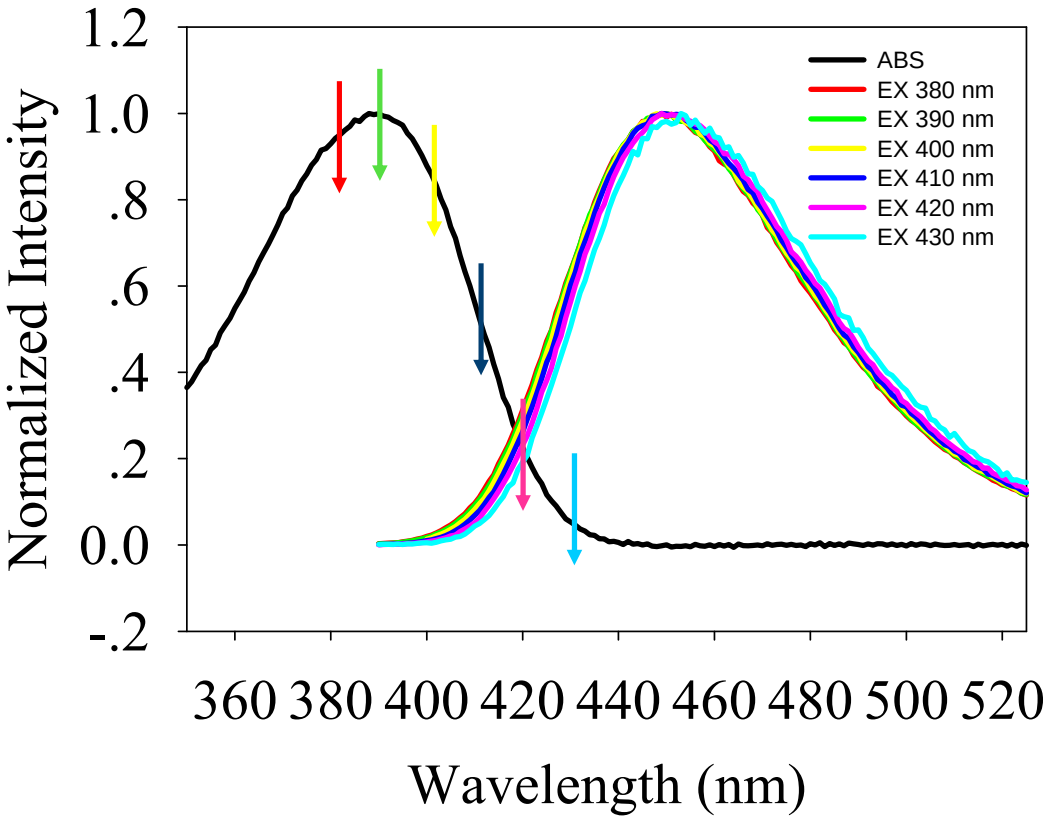

Figure 5-3 Steady-state and absorption an emission spectra of C102 in $[N_{4,4,4,1}^{+}][Tf_2N^{-}]$. Arrows indicate excitation wavelengths employed here. The spectra have been normalized to constant peak height.

5.3.1 Temperature Tependence

A temperature dependence study was first conducted in order to determine the best temperature for measuring the solvation response. Use of too high a temperature will result in a solvation time that is too fast for TCSPC to measure completely and use of too low a temperature will make the process too slow to be followed to completion with the 4 ns lifetime of C102. For this purpose samples of C102 in $[N_{4,4,4,1}^{+}][Tf_2N^{-}]$ were prepared and excited at the absorption peak (390nm) at five different temperatures over the range 10-70 °C. Figure 5-4 shows the time-resolved spectra at 10 °C and 50 °C as well as estimated time-zero spectra (details on how to estimate time-zero spectra are provided in Chapter 2.3.4). The peak frequency of the time-zero spectrum at 10 °C is nearly the same as the measured spectrum at zero time, showing that not much of the initial dynamics are missing at this temperature. The data at 50 °C show a more significant difference from the measured spectrum. Figure 5-5 shows the average and peak frequencies obtained by fitting reconstructed time-resolved spectra versus time at all temperatures. Given the relatively short lifetime of C102 in $[N_{4,4,4,1}^{+}][Tf_2N^{-}]$ (~4 ns in ionic liquids at room temperature), time resolved spectra can only be measured reliably up to about 20 ns. At 10 °C and 25 °C (red and blue lines in figure 5-5), equilibrium is not yet reached at 20 ns. Fitting these data with a stretched exponential function[3] helps to determine the equilibrium (infinite time) frequency ν_∞, but the values so obtained are not accurate enough for our purposes. At 50 °C, 60 °C and 70 °C, the system reaches

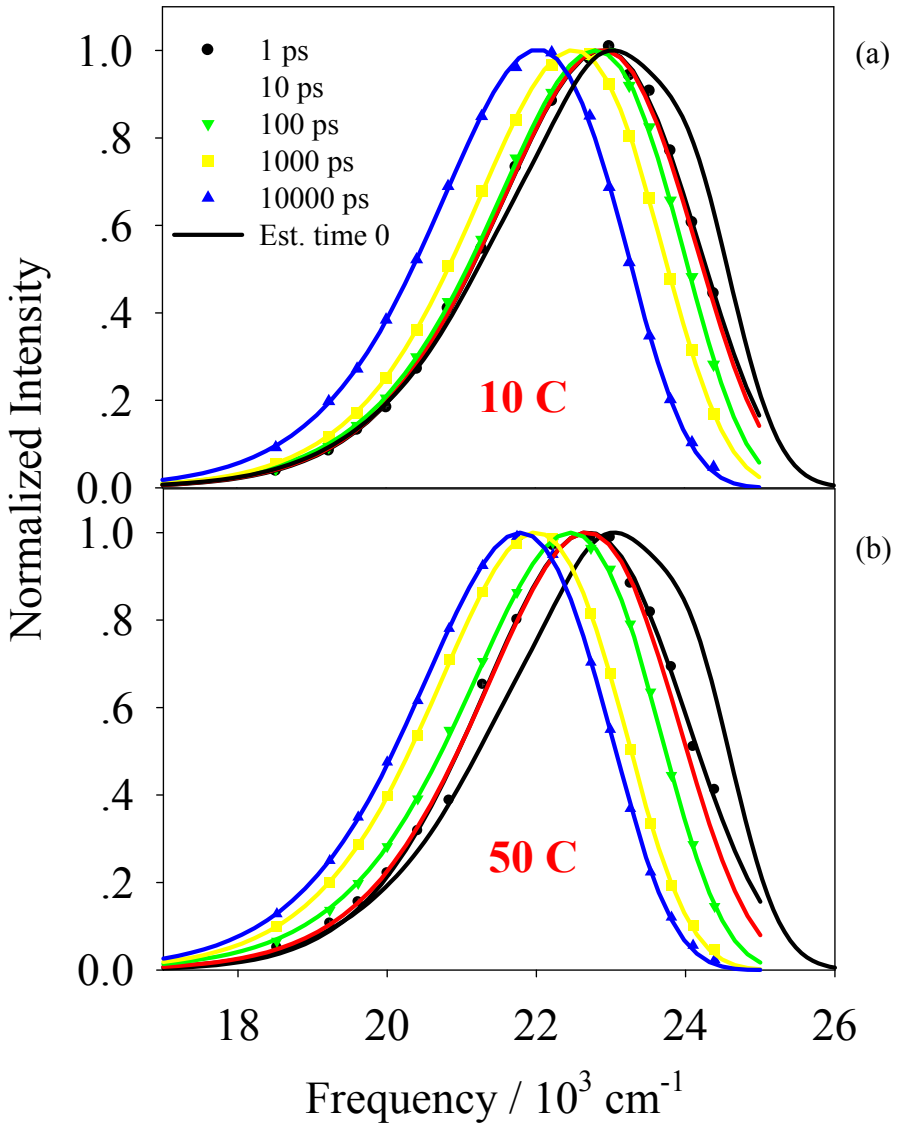

Figure 5-4 Time resolved spectra of C102 in $[N_{4,4,4,1}^{+}][Tf_2N^{-}]$ at 10 °C (panel a) and 50 °C (panel b). Black curve shows the estimated time-zero. Colored symbols correspond to the data points and lines show fitting curves. All spectra have been normalized to peak height equals one.

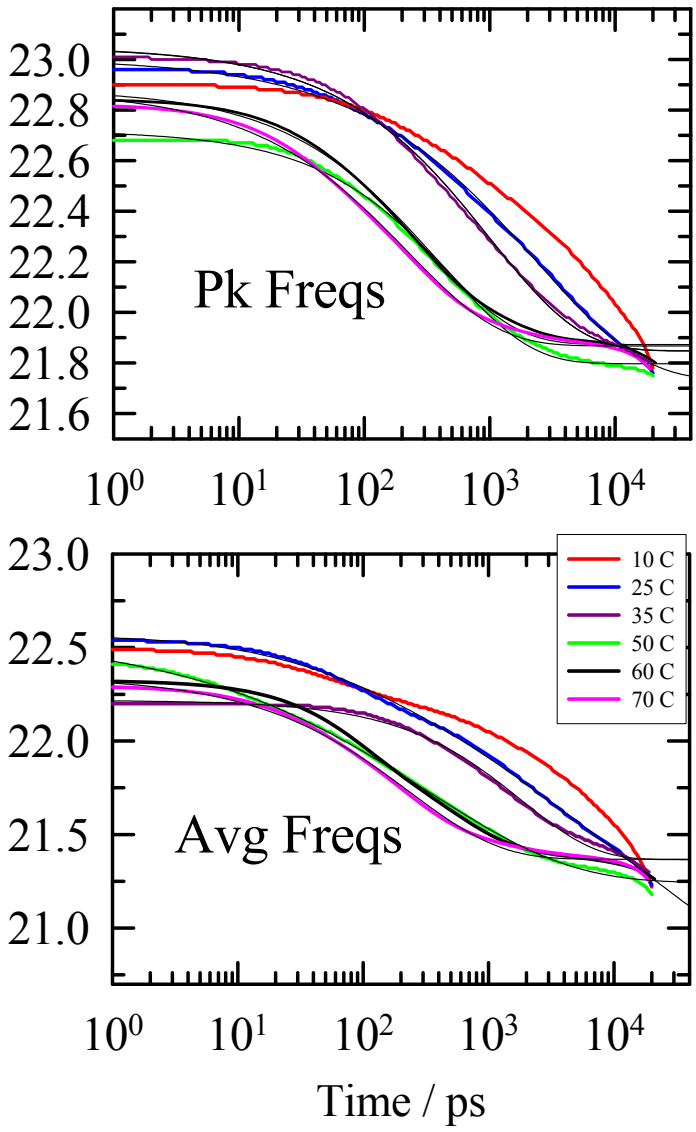

Figure 5-5 Temperature dependence of the Stokes shift dynamics of C102 in $[N_{4,4,4,1}^{+}][Tf_2N^{-}]$ at different temperatures. The top panel shows peak frequencies vs. time and bottom panel the average frequencies vs. time derived from log-normal fits to the time-resolved spectra. The lighter black curves show fits to these data using stretched exponential functions.

equilibrium at 20 ns (i.e. the frequency does not change after 20 ns). However, if T ≥ 50 °C is chosen as the experimental condition, we miss about 20% of the initial relaxation due to insufficient time resolution, as indicated by the difference between the estimated and measured time zero spectra (Figure 5-4). An intermediate temperature of 35 °C is therefore chosen for red-edge excitation measurements. We also notice that ν_∞ varies with temperature. In contrast, previous measurements of C153 in $[N_{4,4,4,1}^+][Tf_2N^-]$ by Castner and coworkers[34] showed a constant value of ν_∞ over a comparable temperature range. The difference might be caused by fitting errors, due to the shorter lifetime of C102 or it might reflect a real difference between C102 and C153. It is reasonable to expect ν_∞ to vary with temperatures because solvent polarity changes with temperature and such variations have been reported in other ionic liquids.[35]

5.3.2 Best estimation of time-resolved spectra

Time resolved spectra can be obtained from the methods described in Chapter 2. Several different experimental conditions and fitting methods were used here in order to determine the best time- resolved spectra for solvation time calculations. The results obtained are general and will be relevant to other measurements of solvation times in ionic liquids which might be undertaken in the future. The first condition examined was the emission polarization angle. We examined the effect of changing the polarization angle detected from magic to perpendicular. Usually, excitation light is polarized vertically excite samples and time-resolved decays are collected at the "magic angle" (as discussed in chapter 2.2.1). This angle eliminates the effect of reorientational dynamics

of the probe on the fluorescence decay. The disadvantage of collecting fluorescence at the magic angle is that Rayleigh scattering of the excitation light is so intense that the signal around the excitation wavelength is distorted, such that a region of ±10 nm around excitation wavelength must be omitted from the reconstructed spectra. An example of this effect is shown in figure 5-6(a). Collecting decays at perpendicular polarization was proposed to solve this problem since Rayleigh scattering is vertically eliminated when the collection polarization is orthogonal to the excitation as shown in Figure 5-6 (b). But in order to not distort the solvation data, which only rely on the position and not the intensity of the spectrum, the effect of probe rotation must be constant across the emission spectrum. Defining the signals collected at perpendicular and parallel polarizations $I_{\perp}(t,\lambda)$ and $I_{\parallel}(t,\lambda)$, the population decay measured at magic angle $m(t,\lambda)$ is related to the anisotropy change $r(t,\lambda)$ in the following way[36]:

$$I_{\parallel}(t,\lambda) = m(t,\lambda)\{1 + 2r(t,\lambda)\}; \qquad I_{\perp}(t,\lambda) = m(t,\lambda)\{1 - r(t,\lambda)\} \tag{5.1}$$

or

$$m(t,\lambda) = \frac{1}{3}\{I_{\parallel}(t,\lambda) + 2I_{\perp}(t,\lambda)\}; \qquad r(t) = \frac{I_{\parallel}(t,\lambda) - I_{\perp}(t,\lambda)}{I_{\parallel}(t,\lambda) + 2I_{\perp}(t,\lambda)} \tag{5.2}$$

From previous experiments using C153 as probe in ionic liquids,[5] it has been shown that the $r(t,\lambda)$ is the same for decays collected at different wavelength. We therefore make the assumption that $r(t,\lambda)$ is independent of wavelength and represent it as $r(t)$. The shape of the spectra reconstructed using $I_{\perp}(t,\lambda)$ data is determined by $m(t,\lambda)$ only $\{1 - r(t,)\}$ will only change the intensity of the whole spectrum at a given time but won't introduce any distortion in wavelength. By normalizing the reconstructed spectra to unit peak intensity one, the effect of rotation dynamics will be totally erased.

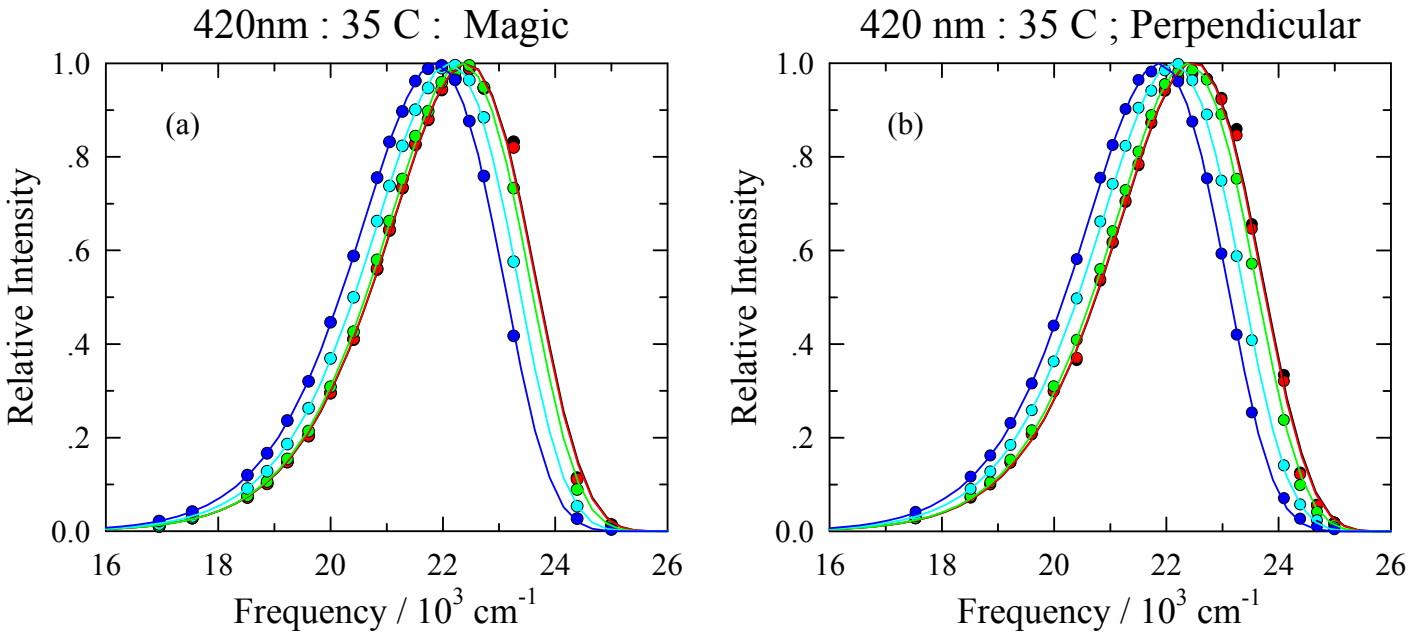

Figure 5-6 Time-resolved spectra of C102 in $[N_{4,4,4,1}^{+}][Tf_2N^{-}]$ (35 °C) excited at 420 nm. Panel (a) shows data collected using magic angle detection and panel (b) perpendicular detection. All spectra are fitted with log-normal line shapes and normalized to unit peak height. The color coding from red, green, cyan to blue represent time 1 ps, 100 ps, 1000 ps, and 10000 ps respectively.

To support this assumption in the system (C102 in $[N_{4,4,4,1}^{+}][Tf_2N^{-}]$) studied here, normalized time-resolved spectra obtained using both polarizations are compared in Figure 5-7. Compared with magic angle spectra in Figure 5-6 (a), spectra constructed using data from perpendicular angle allow more data points on the blue side, which gives more accurate spectra without distortion from solute reorientation effects.

In addition to using perpendicular detection angle, constraining fitting parameters also gives more consistent results due to the moderate number of data points used in constructing time resolved spectra. Spectra are first fit to a log-normal line shape function[37].

$$g(\nu) = \begin{cases} g_0 \exp\left\{ -\ln(2) \left(\frac{\ln\left[1+2\delta\left(\frac{\nu-\nu_p}{\Delta}\right)\right]}{\delta} \right)^2 \right\}, \alpha > 1 \\ 0, \ \alpha \leq 1, \end{cases}$$

$$\alpha = 2\delta(\nu - \nu_p)/\Delta \qquad 5.3$$

When $\delta = 0$, this function reduces into a Gaussian function. The parameters g_0,ν_p and δ correspond to the peak height, peak frequency, and asymmetry factor, respectively. The FWHM (full width half maximum) Γ is related to the width parameter Δ by

$$\Gamma = \Delta\left(\frac{\sinh(\delta)}{\delta}\right) \qquad 5.4$$

Example parameters obtained from log-normal fits to steady-state spectra of C102 excited at different wavelengths in $[N_{4,4,4,1}^{+}][Tf_2N^{-}]$ and in several polar solvents are shown in table 5-1. The shape of the spectra is defined by both Γ and δ. The δ parameter varies around an average of -0.29 for all these spectra that we think this is from the uncertainties of insufficient data points and experimental error: The δ value is determined by the underlying vibronic structure of the spectrum and should not change with time or

solvent polarity environment. We therefore fixed the asymmetry parameter to -0.29 and refit the magic angle spectra. The difference between the use of free and constrained fits is shown in figure 5-8 (b). Compared with the free fits in (a), time-resolved spectra at blue edge and early times are much better defined when δ is fixed (figure 5-8 (b)). Thus fixing the δ parameter is useful in getting the sensible spectra with limited number of data points. At the same time, the FWHM does not show significant change as a result of fixing the δ parameter (Figure 5-9) which supports our assumption that δ should be constant at different time delays.

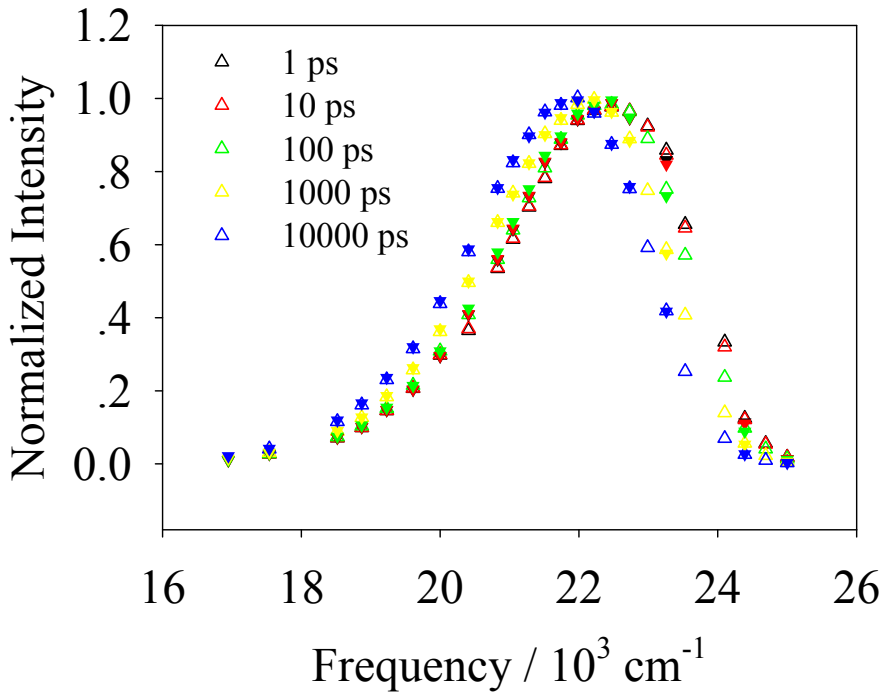

Figure 5-7 Overlapping of the two sets of spectra in Figure 5-6. Magic angle experiments data are in up triangle shape while the perpendicular angle data are in down triangle shape. Most of the data points collected at the same wavelength are overlapping with each other. The overall shapes of the spectra are also unchanged.

SS	**390**	**410**	**420**	**430**	**ACN**	**DMSO**	**ACE**	**MEOH**	**Mean**	**Standev**
FWHM	3.02	2.99	2.99	3.03	2.98	2.96	2.99	3.02	2.99	0.02
δ	-0.26	-0.28	-0.28	-0.28	-0.28	-0.29	-0.3	-0.29	**-0.29**	0.01

Table 5-1 Summary of log-normal parameters determined from fits of steady state emission spectra of C102 in $[N_{4,4,4,1}^{+}][Tf_2N^{-}]$ excited at different wavelengths and in four conventional solvents (ACN-acetonitrile, DMSO-dimethyl sulfoxide, ACE-acetone, MEOH-methanol). The mean value of the asymmetry factor δ is calculated here and is used to fit time-resolved spectra.

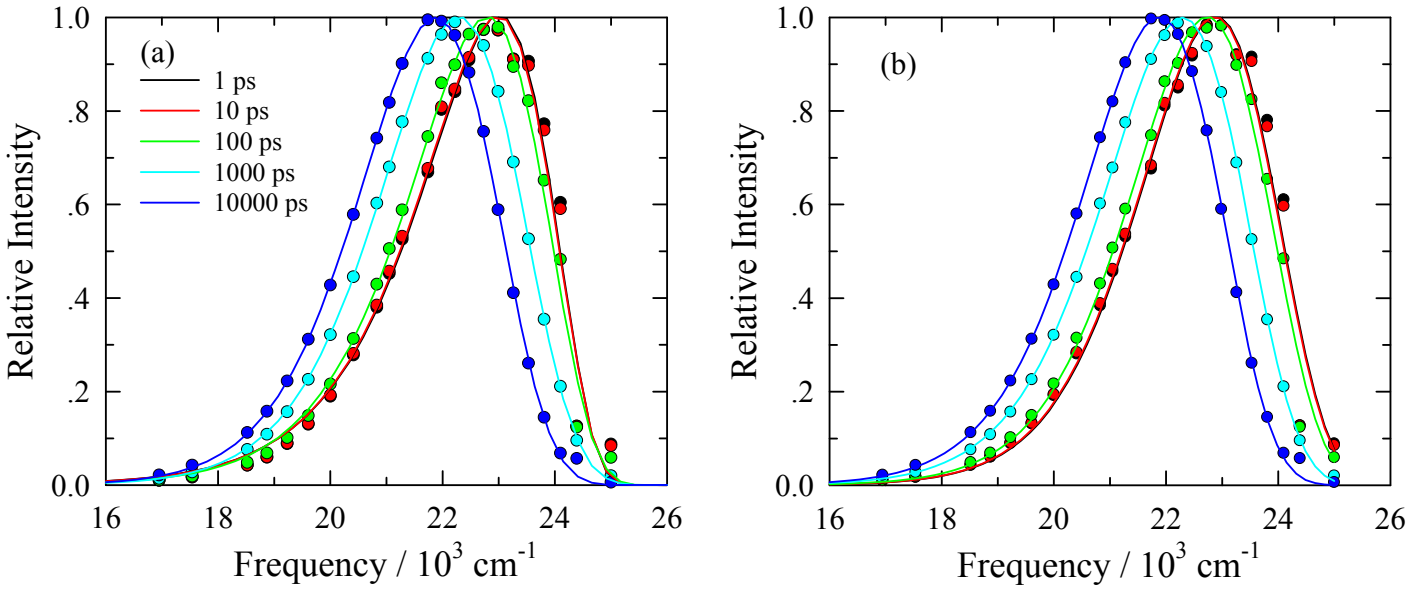

Figure 5-8 Time-resolved spectra of C102 in $[N_{4,4,4,1}^{+}][Tf_2N^{-}]$ (35 °C) excited at 390 nm. All spectra are fitted with log-normal functions. Panel (a) shows fits in which all four parameters of Equation 5-4 are allowed to vary and (b) shows fits using a fixed value of the asymmetry parameter δ=-.29 determined from steady state spectra.

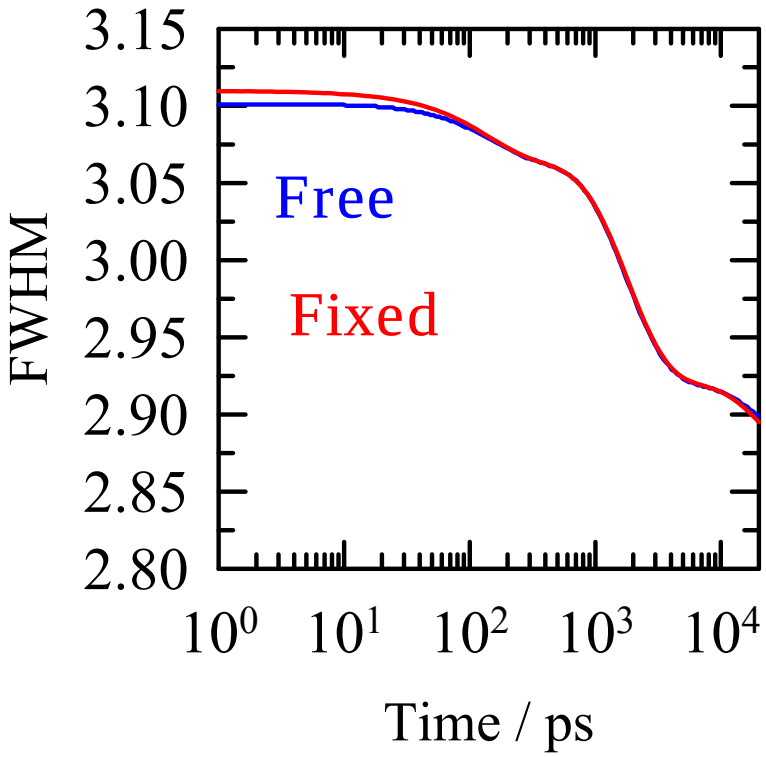

Figure 5-9 Widths (FWHM) of time-resolved spectra versus time. The blue line shows the result from free fitting and red line shows the result from fixed asymmetry fits.

5.3.3 Excitation Dependence of Solvation

Figure 5-10 (a) shows frequency shift vs. time data at different excitation wavelengths collected at perpendicular polarization. These frequency shifts obtained from time-resolved spectra were fit to stretched exponential functions[4] as described in Section 2.3.3:

$$\nu(t) = \nu_\infty + \Delta\nu \exp\{-(t/\tau_0)^\beta\} \quad 5.5$$

Multi-exponential fitting, preferred by some other authors[7,38,39], does fit some data sets more accurately, but it does so by introducing many additional fitting parameters. Moreover, a stretched exponential function represents the presence of a distribution of subensembles with various solvation environments while a multi-exponential function artificially divides the effect into a number of discrete components (usually 2-4 in ionic liquids). Fitting to a stretched exponential function adequately captures the dynamics of ν(t) as confirmed with Figure 5-10 (a). It is also shown in this figure that the Stokes shift decreases with increasing ν_{exc} as one selectively excites more solvated subensembles. However, at the longest times observed (20 ns) the frequencies do not appear to have properly converged to a limiting value of ν_∞. Similar systems which we have previously studied, for example 4AP in $[Im_{41}^+][PF_6^-]$[40], C153 in $[N_{4441}^+][Tf_2N^-]$[35] and $[Im_{41}^+][PF_6^-]$[41], and DCS in a variety of ILs[3] all show a sensible approach to a constant ν_∞ value. The difference might be due to the smaller Stokes shift of C102 which prevents us from measuring to times longer than 20 ns. For all of the temperatures collected, no

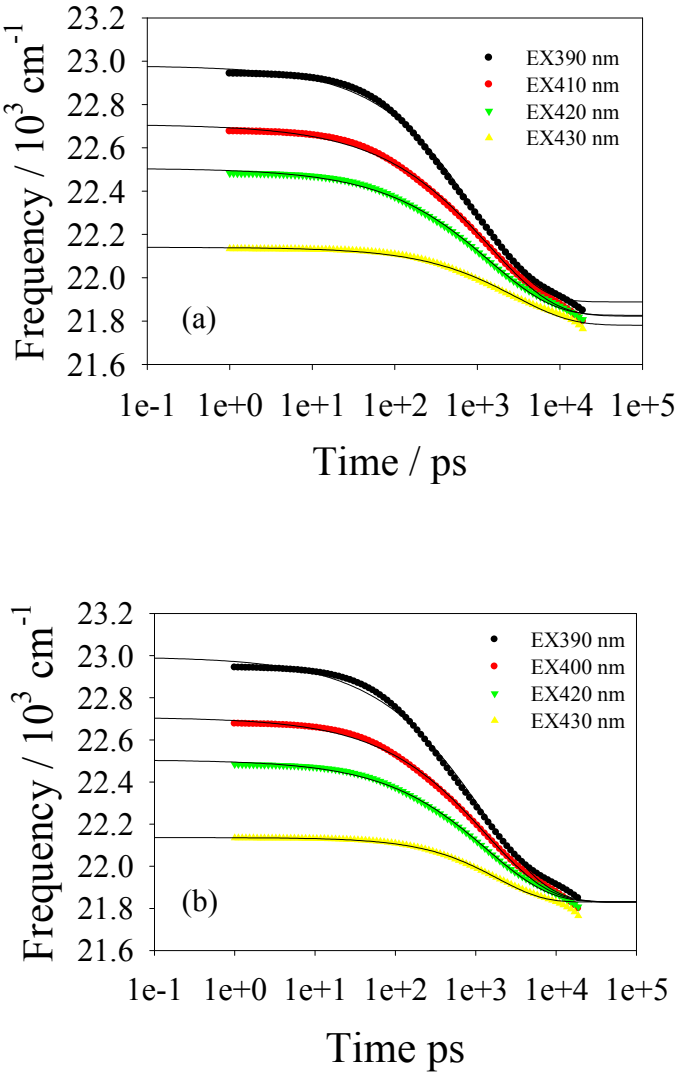

Figure 5-10 Peak frequency data obtained from log-normal fits of the time-resolved spectra for C102 in $[N_{4,4,4,1}^{+}][Tf_2N^{-}]$ excited at 390 nm, 410 nm, 420 nm and 430 nm respectively. All experiments were conducted at 35 °C. The colored lines are the actual data and the black lines are stretched exponential fits (e.q 5.5). Fits in panel (a) have no constraint on ν_∞ while the fits in panel (b) use $\nu_\infty = 21.83$.

equilibrium is reached in our experimental time window and tend to systematically decrease after 20 ns. A stretched exponential function here really helps to determine ν_∞. The value of ν_∞ fluctuates with different excitation wavelength (ν_∞ = 21.89, 21.82, 21.83 and 21.78 for 390 nm, 410 nm, 420 nm and 430 nm, respectively). We did a series of fits to evaluate the effect of ν_∞ on $< \tau_{sol} >$and the results are summarized in table 5-2: The value of ν_∞ was first set free and then fixed to the averaged value of (21.83) for all wavelengths. Average solvation times were calculated using a equation previously reported[35]:

$$< \tau_{sol} >= \frac{1}{\Delta\nu}\int_0^\infty \{\nu_t - \nu_\infty\}dt = \frac{\tau_0}{\beta}\Gamma(\beta^{-1}) \qquad 5.6$$

where $\Gamma(x)$ is the gamma function and β is the stretching factor obtained from fitting with e.q 5.5. All of the solvation times are summarized in table 5-2 too. ν_∞ obtained from free fitting varies significantly upon excitation wavelength. To see what effect ν_∞ has on the average solvation times, the largest value (21.89) and the smallest value (21.78) observed were used as fixed parameters. Note that fitting with fixed infinity frequency stills gives reasonable fitting as shown in Figure 5-10(b). As shown in table 5-2, except for column one, no pronounced increase of $< \tau_{sol} >$ with excitation wavelength was observed. For each row, the calculated $< \tau_{sol} >$ changes significantly upon changing the value of ν_∞. Such results suggest that $< \tau_{sol} >$ is very sensitive to ν_∞. When the lifetime of the probe is long enough to measure the ν_∞, free fitting to stretched exponential function gives much better results and thus more trustable ν_∞. Assuming the absorbing and emitting transitions are identical, one can expect that changing the excitation wavelength will change the initial position of the relaxing spectrum and

therefore the total extent of the Stokes shift observed will also change[5,27,42]. There is indeed an expected change shown in both panels of figure 5-10. The pronounced dependence of $< \tau_{sol} >$ and Stokes shift with excitation wavelength agree with what had been reported in the C153/[N_{ip311}^{+}][$Tf2N^{-}$] [5] case, however, in this combination, ν_{∞} was found to have a common value for all $\nu_{exc.}$

Considering the effect of the missing components of the dynamics, in order to compare the solvation response, we also calculated the normalized solvation response function:

$$S(t) = \{\nu(t) - \nu(\infty)\}/\{\nu(0) - \nu(\infty)\} \quad 5.7$$

the value of $\nu(0)$ can be obtained from estimates of time-zero spectra[43] , as described in section 2.3.2. As shown in figure 5-11, the estimated time-zero values are about 20% from the measured time-zero in the case of the peak frequency shift. Although the average frequency shift shows less missing dynamics at the initial time, this estimation is less trustable than the peak frequency since the estimated time-zero spectrum sometime show an artifact broadening effect than measured. This 20% loss is caused by the time-resolution of TCSPC system (~25 ps[3]). The blue data is from another more concentrated sample that is also excited at 430 nm. When the emission wavelength is moved to the edge of the absorption, 430 nm in our case, the optical density becomes much lower (less than 0.01) compared to exciting at the peak (0.1 abs). Therefore, I increased the concentration of the sample to make the optical density to be 0.06 at 430 nm and repeated the experiments to estimated the uncertainty of the $< \tau_{sol} >$. From figure 5-11, the solvation response function of the more concentrated sample indeed differs from the

λ_{ex} / ν_∞	**Free fits**	**21.89**	**21.83**	**21.78**	average
390nm	15.1	14.9	21.0	28.4	**19.8**
410nm	23.3	15.0	22.2	31.7	**23.1**
420nm	23.3	13.9	22.6	35.6	**23.8**
430nm	39.5	11.3	21.7	40.1	**28.2**

Table 5-2 The effect of ν_∞ on the estimation of the solvation time $< \tau_{sol} >$ The first column gives the excitation wavelength and the second column is $< \tau_{sol} >$. From free fits. The third, fourth and fifth columns are $< \tau_{sol} >$ calculated using fixed values of ν_∞ = 21.89, 21.83 and 21.87 ($\times 10^3$ cm^{-1}) respectively. The last column is the average of the times in each row. All times are in units of nanoseconds.

original sample and is closer to the other excitation wavelengths. This observation suggests that the concentration is other excitation wavelengths. This observation suggests that the concentration is important for this kind of red-edge excitation experiment. Because the solvation time should not depend on the concentration of the probe, we think the difference is from the background emission of ionic liquids. Even though C102 fluoresces strongly, when the probe absorption gets extremely low on the far red edge, impurity fluorescence from the ionic liquid might distort the spectra. We also found that most of the discrepancy comes in the first 100 ps. From 100 ps to 10 ns, which is the best time window for TCSPC measurements[3], the difference is much less. The normalized $S(t)$ were again fitted with equation 5.5 and $< \tau_{sol} >$ calculated from equation 5-6. A common value of ν_∞ for all wavelengths was determined by averaging the ν_∞ from free fits. The fitted curves are plotted in figure 5-11 in black lines and fitting parameters and change of FWHM show a similar curvature for all excitation wavelengths except a small change at around 1 ns which may come from the uncertainties of the fitting since the movement is less than 50 cm^{-1}. Therefore, we conclude that no significant observations of dynamic heterogeneity using FWHM as indicator. All fitting values are summarized in Table 5-3. After normalization, there is no systematic trend in the frequency versus time curves. Most of the differences happened before 100ps. Given the greater uncertainties in this time region and the fact that less than 10% of the total shift were observed in difference makes it hard to determine the real variations of the response function vs. $\nu_{exc.}$ The final $< \tau'_{sol} >$ was determined by a weighted average of solvation times calculated from peak and average frequency shifts and is shown in table 5-3. It does not show a systematic dependence on excitation wavelength as well.

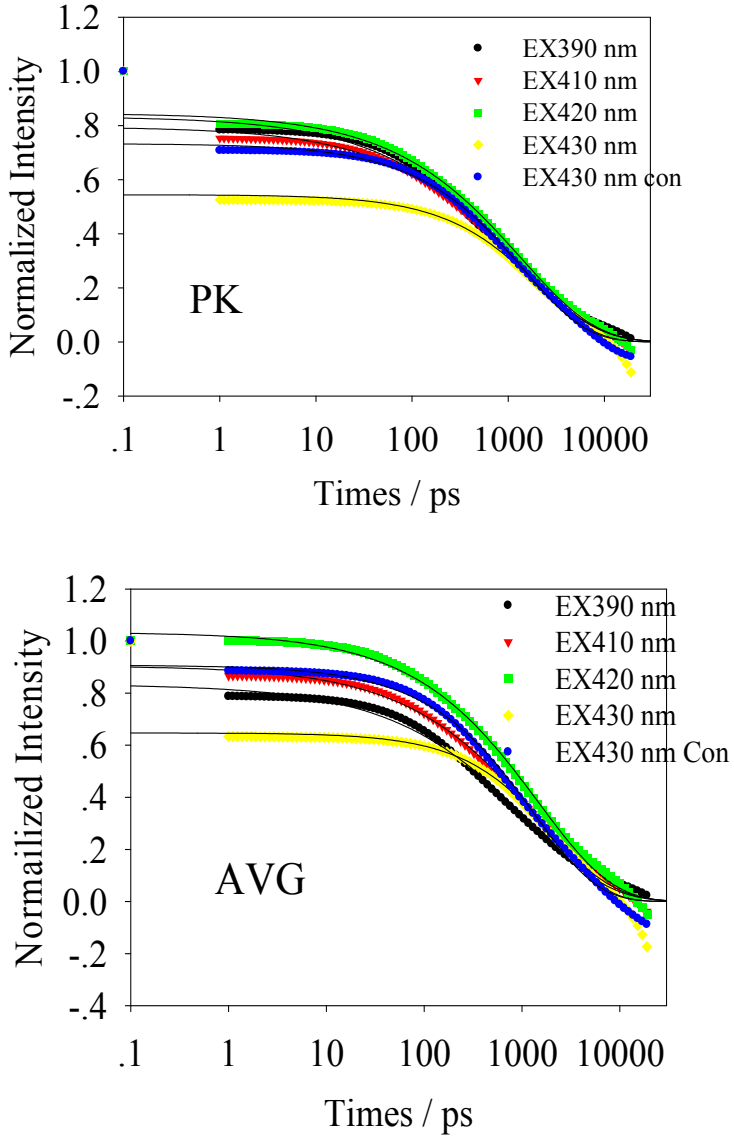

Figure 5-11 $S(t)$ response functions of C102 in $[N_{4,4,4,1}^{+}][Tf_2N^{-}]$ (35 °C) excited at 390, 410, 420 and 430 nm. A more concentrated sample was used to repeat the experiments for uncertainty measurements. Left panel are data from peak frequencies and the right are average frequencies. The initial points on the y axis are the estimated time=0 values. Colored curves represent experimental data and fine black lines are fits.

	ex390		ex410		ex420		ex430		ex430-con	
	ν_{pk}	ν_{av}	ν_{pk}	ν_{av}	ν_{pk}	ν_{av}	ν_{pk}	ν_{av}	ν_{pk}	ν_{av}
R^2	0.993	0.993	0.992	0.997	0.995	0.998	0.935	0.964	0.986	0.995
τ	1.18	1.21	1.28	1.36	1.35	1.48	2.17	2.22	1.43	1.35
$\Delta\nu$	0.83	0.84	0.80	0.91	0.85	1.03	0.54	0.65	0.73	0.91
β	0.53	0.51	0.54	0.56	0.55	0.58	0.75	0.81	0.66	0.67
$< \tau_{sol} >$	2.14	2.31	2.28	2.28	2.28	2.34	2.58	2.49	1.92	1.78
$< \tau_{sol} >$		**2.2**		**2.28**		**2.3**		**2.55**		**1.87**

Table 5-3 Summary of the final fit results and $< \tau_{sol} >$ values in the C102 / $[N_{4,4,4,1}^{+}][Tf_2N^{-}]$ system in this chapter. All data are collected at perpendicular angle, asymmetry factor is fixed to be -0.287, $\nu(\infty)$ of peak shift is fixed to be 21.831 while $\nu(\infty)$ of average shift is fixed to be 21.347. $< \tau_{sol} >$ are calculated from stretched exponential function. $< \tau'_{sol} >$ are final values for solvation time and is calculated by (2:1) averages of the times obtained from peak and average frequency changes with ns as unit

The FWHM was used as an indicator for dynamic heterogeneity in super cooled liquids and other systems by Richert and co-workers[11,44-46]. The linewidths Γ of time-resolved spectra were related[46] to the solvation response function[47] C(t):erived for homogenous (e.q 5.8) and heterogeneous (e.q 5.9) dynamics.

$$\Gamma_{hom}^2(t) = \Gamma_\infty^2 + (\Gamma_0^2 - \Gamma_\infty^2)C^2(t) \qquad 5.8$$

which states that the linewidth changes from $\Gamma_0 = \Gamma$ (t=0) to $\Gamma_\infty = \Gamma$ (t=∞) with solvation coordinate in a monotonic way. While

$$\Gamma_{het}^2(t) = \Gamma_\infty^2 + (\Gamma_0^2 - \Gamma_\infty^2)C\left(2^{\frac{1}{\beta}}t\right) + \Delta^2[C\left(2^{\frac{1}{\beta}}t\right) - C^2(t)] \qquad 5.9$$

in which β (stretch factor in the exponential fitting for solvation response function) controls and leads to peak in the line width as a function of time. Blanco-Rodrı´guez and co-workers also observed this effect in [BMIM$^+$][PF6$^-$] (1-Butyl-3-methylimidazolium hexafluorophosphate) ionic liquid. We did not observe the change of FWHM in this system except a small change at around 1 ns which probably only reflects the uncertainties in the measurement since the movement is less than 50 cm^{-1}. (Figure 5-12)

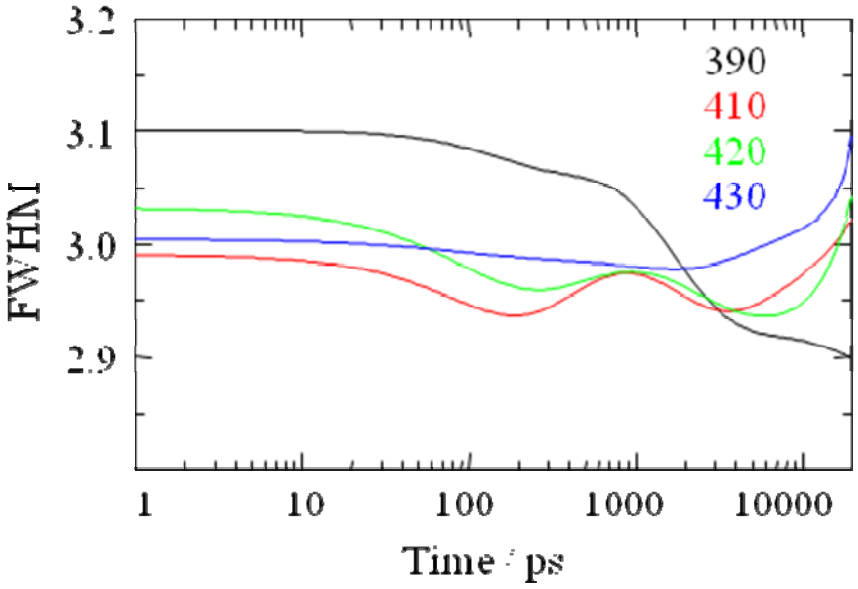

Figure 5-12 FWHM for all excitations plotted vs. time for different excitation wavelength.

5.4 Summary and Conclusion

In this chapter, we have used red edge excitation spectroscopy (REES) to look for the presence of dynamic heterogeneity in the solvation of C102 in $[N_{4,4,4,1}^{+}][Tf_2N^{-}]$. We discussed some details concerning the criteria used for choosing a proper system for this kind of experiment. Despite the fact that there has been a good deal of study of the solvation response in ionic liquids[3,8,33,35], the use of REES and time-resolved measurements to determine dynamic heterogeneity is very limited[5]. In this chapter, the best conditions for reconstructing time-resolved spectra and the proper experimental temperature and data analysis methods are described. As a summary, the data was collected at 35 °C and perpendicular angle and the asymmetry factor was fixed when fitting the time-resolved spectra with log-normal function. The FWHM was then examined as an indicator for dynamic heterogeneity but no substantial trend was observed. For the solvation response function, frequency at time infinity ν_∞ was found to be an important factor in determining integral solvation times. A common average value of ν_∞ was used in stretched exponential fitting and $< \tau'_{sol} >$ was determined from this fitting. This is the first study to carefully examine the effect of each parameter in order to evaluate the solvation time estimated. The present work can also serve as a background for choosing additional systems of interest for solvation response investigations in ionic liquids.

Compared with the C153 / $[Nip_{311}^{+}][Tf_2N^{-}]$ system studied previously[5], we did not observe a systematic change in the average solvation time with excitation wavelength

which may be caused by the insufficient time resolution of TCSPC. The nature of dynamic heterogeneity has been studied recently by computer simulation[48-49] and it was shown that the solvation energy relaxes primarily by collective translational motions of the ions near to the solute, and most motion occurs on femtosecond scale before significant structural change occurs. This means the high resolution instrumentations such as pump-probe systems may be more adequate tools for measuring fast response even the technique part is challenging. Also, there has been some recent debate on the existence of dynamic heterogeneity in ionic liquids. Berg and coworkers have used Multiple Population-Period Transient Spectroscopy (MUPPETS)[50] to provide one example in which the dispersive kinetics observed in ionic liquids is not due to dynamic heterogeneity. Further experimental and computational work is needed to define the origins of dynamic heterogeneity and explore its effect on different chemical reactions.

Reference and Notes

(1) Weingartner, H.; Sasisanker, P.; Daguenet, C.; Dyson, P. J.; Krossing, I.; Slattery, J. M.; Schubert, T. *J. Phys. Chem. B* **2007**, *111*, 4775.

(2) Fruchey, K.; Fayer, M. D. *J. Phys. Chem. B* **2010**, *114*, 2840.

(3) Arzhantsev, S.; Jin, H.; Baker, G. A.; Maroncelli, M. *J. Phys. Chem. B* **2007**, *111*, 4978.

(4) Jin, H.; Baker, G. A.; Arzhantsev, S.; Dong, J.; Maroncelli, M. *J. Phys. Chem. B* **2007**, *117*, 7291.

(5) Jin, H.; Li, X.; Maroncelli, M. *J. Phys. Chem. B* **2007**, *111*, 13473.

(6) Ito, N.; Arzhantsev, S.; Maroncelli, M. *Chem. Phys. Lett.* **2004**, *396*, 83.

(7) Funston, A. M.; Fadeeva, T. A.; Wishart, J. F.; Castner, E. W. *J. Phys. Chem. B* **2007**, *111*, 4963.

(8) Arzhantsev, S.; Jin, H.; Ito, N.; Maroncelli, M. *Chem. Phys. Lett.* **2006**, *417*, 524.

(9) Demchenko, A. P. *Biophys. Chem.* **1982**, *15*, 101.

(10) Demchenko, A. P. *Luminescence* **2002**, *17*, 19.

(11) Richert, R. *J. Phys. Chem. B* **1997**, *101*, 6323.

(12) Hurley, M. M.; Harrowell, P. *Phys. Rev. E* **1995**, *52*, 1694.

(13) Chattopadhyay, A. *Chem. Phys. Lipids* **2003**, *122*, 3.

(14) Sen, P.; Satoh, T.; Bhattacharyya, K.; Tominaga, K. *Chem. Phys. Lett.* **2005**, *411*, 339.

(15) Galley, W. C.; Purkey, R. M. *Proc. Natl. Acad. Sci. U. S. A.* **1970**, *67*, 1116.

(16) Rubinov, A. N.; Tomin, V. I. *Optics and Spectroscopy-Ussr* **1970**, *29*, 578.

(17) Itoh, K. I.; Azumi, T. *J. Chem. Phys.* **1975**, *62*, 3431.

(18) Hu, Z.; Margulis, C. J. *J. Phys. Chem. B* **2006**, *110*, 11025.

(19) Hu, Z.; Margulis, C. J. *Proc. Natl. Acad. Sci.* **2006**, *103*, 831.

(20) Hu, Z.; Margulis, C. J. *Acc. Chem. Res.* **2007**, *40*, 1097.

(21) Triolo, A.; Russina, O.; Bleif, H. J.; DiCola, E. *J. Phys. Chem. B* **2007**, *111*, 4641.

(22) Mandal, P. K.; Paul, A.; Samanta, A. *J. Photochem. Photobiol. A* **2006**, *182*, 113.

(23) Mandal, P. K.; Sarkar, N.; Samanta, A. *J. Phys. Chem. A* **2004**, *108*, 9048.

(24) Shigeto, S.; Hamaguchi, H. *Chem. Phys. Lett.* **2006**, *427*, 329.

(25) Lopes, J. N. C.; Padua, A. A. H. *J. Phys. Chem. B* **2006**, *110*, 3330.

(26) Wang, Y.; Voth, G. A. *J. Phys. Chem. B* **2006**, *110*, 18601.

(27) Fee, R. S.; Milsom, J. A.; Maroncelli, M. *J. Phys. Chem.* **1991**, *95*, 5170.

(28) Richert, R. *J. Phys.: Condens. Matter* **2002**, *14*, R703.

(29) Richert, R. *J. Chem. Phys.* **2001**, *114*, 7471.

(30) Gontrani, L.; Russina, O.; Lo Celso, F.; Caminiti, R.; Annat, G.; Triolo, A. *J. Phys. Chem. B* **2009**, *113*, 9235.

(31) Habasaki, J.; Ngai, K. L. *J. Chem. Phys.* **2008**, *129*, 194501/1.

(32) Castner, E. W.; Wishart, J. F.; Shirota, H. *Acc. Chem. Res.* **2007**, *40*, 1217.

(33) Arzhantsev, S.; Ito, N.; Heitz, M.; Maroncelli, M. *Chem. Phys. Lett.* **2003**, *381*, 278.

(34) Heitz, M. P.; Maroncelli, M. *J. Phys. Chem. A* **1997**, *101*, 5852.

(35) Castner, E. W.; Bagchi, B.; Maroncelli, M.; Webb, S. P.; Ruggiero, A. J.; Fleming, G. R. *Ber. Bunsen-Ges. Phys. Chem. Chem. Phys.* **1988**, *92*, 363.

(36) Fee, R. S.; Maroncelli, M. *Chem. Phys.* **1994**, *183*, 235.

(37) Sanders Headley, L.; Mukherjee, P.; Anderson, J. L.; Ding, R.; Halder, M.; Armstrong, D. W.; Song, X.; Petrich, J. W. *J. Phys. Chem. A* **2006**, *110*, 9549.

(38) Samanta, A. *J. Phys. Chem. B* **2006**, *110*, 13704.

(39) Song, W.; Maroncelli, M. *Chem. Phys. Lett.* **2003**, *378*, 410.

(40) Ito, N.; Arzhantsev, S.; Maroncelli, M. *Chem. Phys. Lett.* **2004**, *396*, 83.

(41) Lewis, J. E.; Maroncelli, M. *Chem. Phys. Lett.* **1998**, *282*, 197.

(42) Yang, M.; Richert, R. *J. Chem. Phys.* **2001**, *115*, 2676.

(43) Richert, R. *J. Chem. Phys.* **2001**, *115*, 1429.

(44) Richert, R. *J. Chem. Phys.* **2001**, *114*, 7471.

(45) Maroncelli, M.; Fleming, G. R. *J. Chem. Phys.* **1987**, *86*, 6221.

(46) Arzhantsev, S.; Jin, H.; Baker, G. A.; Ito, N.; Maroncelli, M. Solvation Dynamics in Ionic Liquids, Results from ps and fs Emission Spectroscopy. In *Femtochemistry VII, Ultrafast Processes in Chemistry, Physics, and Biology*; Castleman, A. W., Kimble, M. L., Eds.; Elsevier B.V., 2006; pp 225.

(47) Shim, Y.; Jeong, D.; Manjari, S.; Choi, M. Y.; Kim, H. J. *Acc. Chem. Res.*, ACS ASAP.

(48) Kobrak, M. N. *J. Chem. Phys.* **2006**, *125*.

(49) Hu, Z.; Margulis, C. J. *Acc. Chem. Res.* **2007**, *ASAP*.

(50) Khurmi, C.; Berg, M. A. *J. Phys. Chem. Lett.* **2010**, *1*, 161.

Chapter 6

Solvation Up-Relaxation Using Far-Red Edge Excitation

1.1 Introduction

The previous chapter introduced the idea of studying dynamical heterogeneity in slowly relaxing media such as ionic liquids by red-edge spectroscopy (REES). In this chapter, I will talk about a related topic, what happens when one excites on the extreme red edge of an absorption band.

The major motivation for this project was an experiment reported by Tomin and coworkers in the 1980s[1]. In this early study, the authors showed the time-resolved spectra of 3-AP (s) and 4-AP (AP=aminophthalimide) in 1-propanolpropanol at -90 °C excited by a nanosecond pulsed dye laser. The time evolution of the peak wavelength excited at different wavelengths is shown in Figure 6-1. When exciting sufficiently far on the red edge of the absorption bands of these molecules (485 nm for 4-AP and > 465 nm for 3-AP), the peak frequency of the time-resolved spectra was observed to shift blue rather than red with time. This phenomenon was explained by Tomin and coworkers[1] as "up-relaxation". The idea is illustrated in figure 6-2. The free energy of the excited state S_1 is represented by a parabola which ~~is calculated to~~ has the same curvature as that of the ground state Excitation at the peak of the absorption spectrum (point a) produces the usual time-dependent Stokes shift. Excitation on the red-edge (between point a and

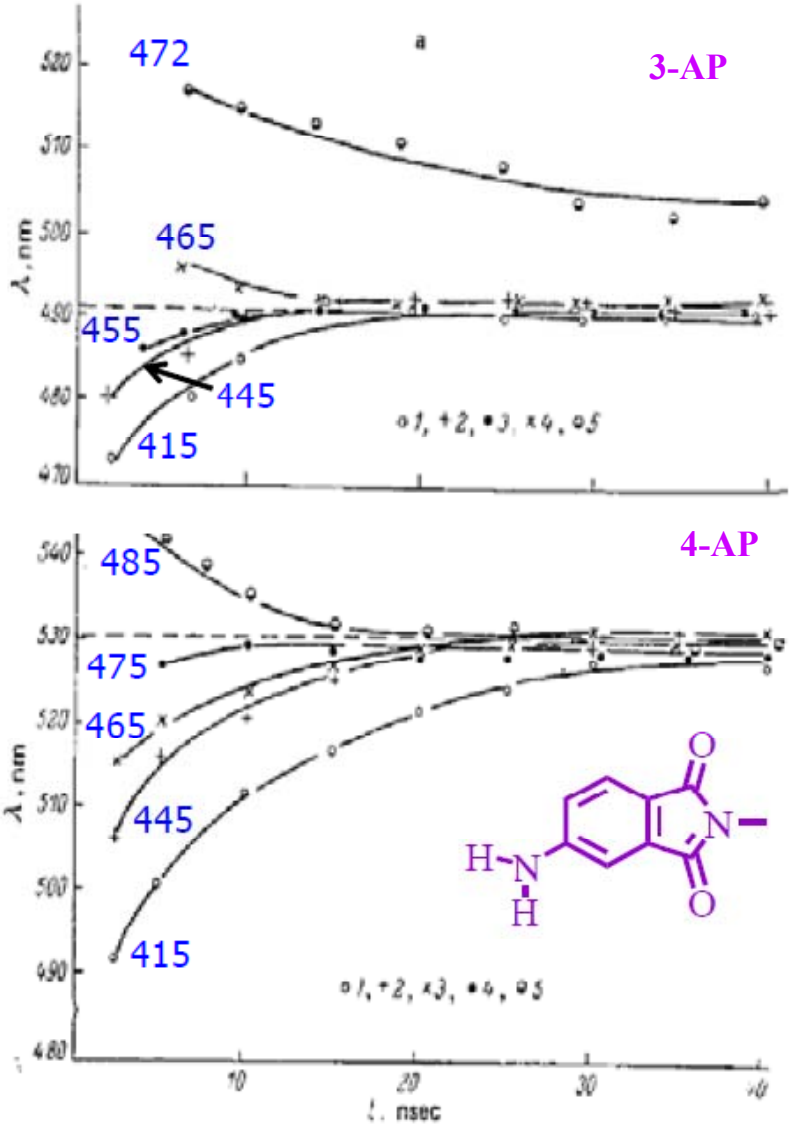

Figure 6-6-1 Peak wavelengths of time resolved emission spectra of 3- and 4-amino-N-methylphthalimide (3,4-AP) recorded after excitation at the wavelengths indicated (nm). Adapted from Ref.2.

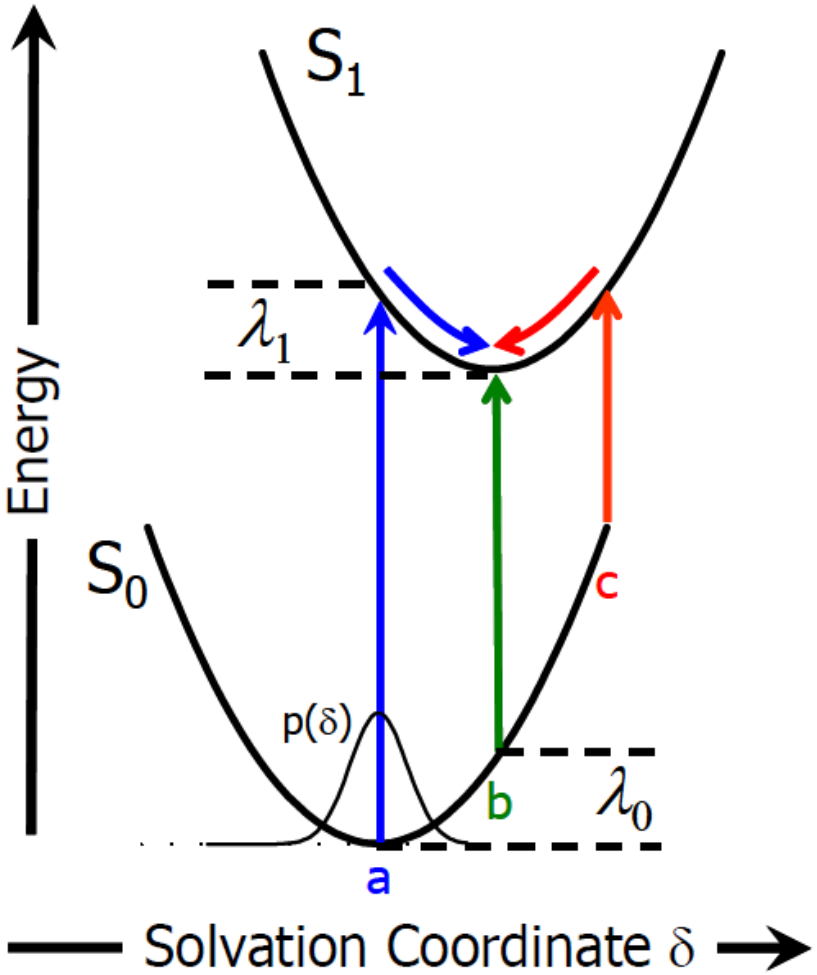

Figure 6-2 Schematic illustrating the energy change along the potential surfaces of both ground state (S0) and excited state (S1) with solvation coordinate δ. p(δ) is the distribution of the molecules in the ground state. When excited at point a, time-resolved spectra will shift red with time, when excited at pint b, no relaxation should be observed and when excited at point c, "up-relaxation" wherein spectra shift to the blue with time are expected.

point b) selects out the better solvated molecules from the ground state solvation distribution $p(\delta)$. Such red-edge excitation leads to red-shifted emission in a frozen solvent. In fluid solvents when solvation time is much faster than than the fluorescence lifetime, this red-shift is small or non-existent in the steady-state measurements, but it is observed in time-resolved emission spectra if sufficient time resolution is available. When excitation reaches point b, where the selected molecules are already solvated to the same extent as the equilibrium excited state, no Finally, when the excitation is moved to even redder wavelengths (point c), molecules will be transferred to the S1 state in an "over solvated" condition and the spectrum will shift to the blue with time, the phenomenon Tomin and coworkers referred to as "up relaxation". As shown in scheme 6-2, the difference between the excitation wavelengths at points a and b is is $\lambda_0+\lambda_1 =\Delta\lambda$. If we use C153 in a highly polar solvent as an example, this $\Delta\lambda$ equals about 2000 cm^{-1}. At such a displacement the absorbance is about 0.5% of the peak absorbance. To reach point c where the spectrum will be dynamically blue shifted by half of $\Delta\lambda$=1000 cm^{-1}, the absorbance is only 0.001% of the peak value which may become a major obstacle for getting reliable ɔ emission spectra.

It is noteworthy that other than the work mentioned above, no other "up-relaxation" results have been reported. This might be due to the fact that the original report was written in Russian and these results are not widely known in other countries. Another reason is the aforemention difficulties associated with observing this phenomenon.

To verify the realty of this interesting and fundamental aspect of solvation dynamics, we wanted to revisit extreme REES experiments in typical solvents and ionic liquids. As a start we sought to reproduce the experiments of Tomin and coworkers[2] on 4-AP in propanol at low temperatures. These first experiments are described in the present chapter.

1.2 Materials and Methods

We recently purchased a nitrogen-pumped dye laser and detection electronics (LaserStrobe™) that interface with an existing steady-state fluorometer from PTI, which could be used to achieve the desired excitation wavelengths and time window for this experiment. Although the TCSPC system has much higher time resolution, the 30 ns lifetime of 4-AP[2] will be better captured by the nanosecond system, which can access times between 2 ns and 50 μs. The excitation wavelengths needed, ___ to 480 nm in the 4-AP case, are also much easier to obtain from the N_2-dye laser system. The N_2 laser generates a one nanosecond (ns) pulse with repetition rate of 10 Hz at 337 nm and is used to pump a dye laser giving a tunable laser output from 360 nm to 900 nm depending on the dye solution used. To study the 4-AP/propanol system, Stilbene 420 (Scheme 6-1) was dissolved in a mixture of ethanol and water with volume? ratio of 1 to 4 to achieve a solution of 2.0×10^{-3} mol. This dye was used to excite samples at 425 nm and 445 nm. A 10^{-2} M coumarin 481(Scheme 6-1) / p-dioxane solution was used to provide excitation wavelengths of 475 and 485 nm. A 1 mM solution of 4-AP in 1-propanol (0.004g in 25 ml of propanolpropanol) was made to reproduce the experimental condition described by

Tomin and coworkers. The ~~four slits' width of PTI fluorometer was~~ set to be 0.2 mm (2nm). For time-resolved spectra, a calibration file was generated using a published method[3] to compensate for the different sensitivity of the detector screen. The delays collected show different delays replying on the length of the fiber, a fluorescence decay is always needed to determine time zero using its peak position when the length of the optical fiber is changed to determine time zero.

new sentence

An Oxford optical cryostat (model LN_2) is used to achieve the temperature of 183 K used for all the steady state and time-resolved measurements. The sample chamber needs to be purged with N_2 gas flow for at least 5 minutes before cooling down. Multiple scanning at the same temperature is always performed until spectra overlapping with the previous one to assure the constant experimental temperature.

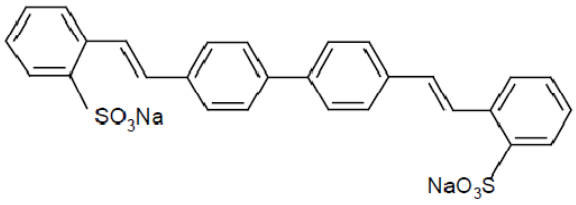

Stilbene 420

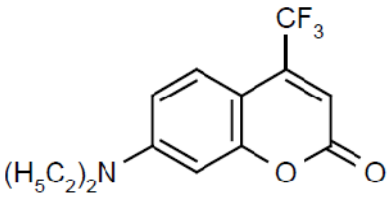

Coumarine 481

Scheme 6-1

1.3 Results and Discussion

1.3.1 Absorption and Steady State Emission

The inset of Figure 6-2 shows the absorption spectrum of 4-AP in 1-propanol (1 mM) at room temperature. The excitation wavelengths used to collect steady state and time-resolved spectra are the same as those employed by Tomin and coworkers[3]: 425 nm, 445 nm, 475 nm and 485 nm. For excitation at 425 nm and 445 nm, which is already on the red-edge of the absorption band, the absorbances are about 0.07 and 0.015. Such absorbance provide relatively noise-free steady-state emission spectra as shown in Figure 6-2. For excitation at 475 nm and 485 nm, the very small absorption (<0.001) yield noisy spectra. .

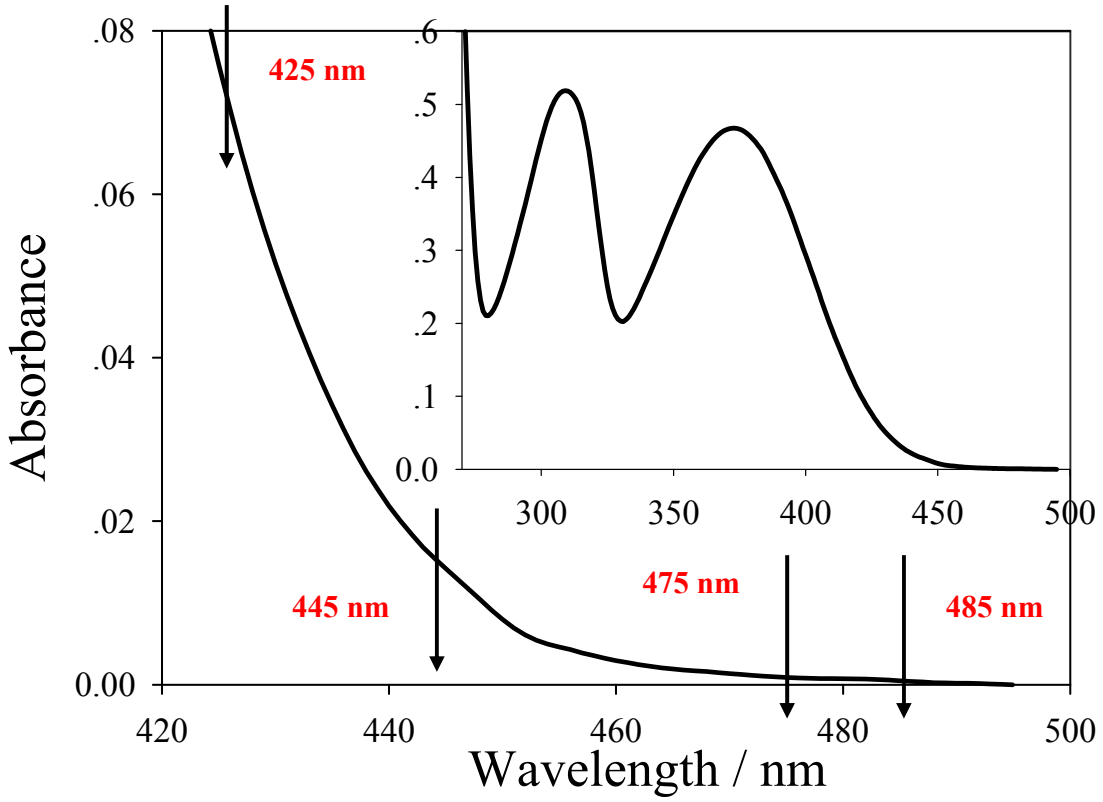

Figure 6-3 Absorption spectra of 4AP in 1-propanol at room temperature. Arrows at different wavelength indicate the excitation wavelengths used for collecting steady state and time-resolved spectra. propanol

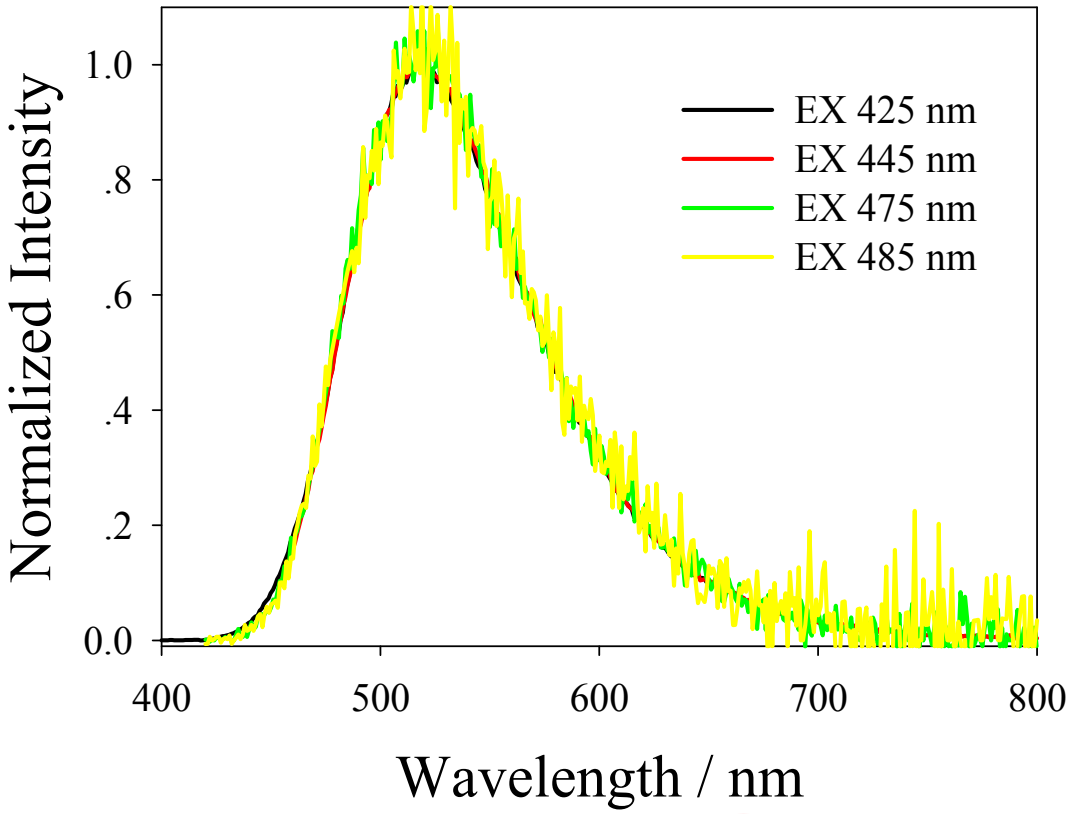

Figure 6-4 Steady state emission spectra of 4-AP in propanolpropanol at 183K excited at different wavelengths on the red-edge of the absorption band. Spectra of 475 nm and 485 nm are noisy due to the small absorbance of the sample at these wavelengths.

1.3.2 Time-resolved spectra and up-relaxation behavior

Figure 6-4 to 6-7 shows the time-resolved spectra of 4-AP in propanolpropanol (183 K) excited at different wavelengths. The large spikes in the 425 nm and 445 nm data come from the excitation light. These spikes were removed from the 475 nm and 485 nm data for clarity and in order to fit the spectra. All time-resolved spectra are fit with log-normal functions, which are shown as the thin black lines in these figures. The emission of propanol is measured by using a blank sample at the same temperature and delay time. This background was subtracted from the 475 nm and 485 nm data. Subtraction was not necessary in the case of the 425 nm and 445 nm data, in which background emission was negligible. Also, for 445 nm data and 485 nm data, the first time-resolved spectrum (in black ~~color~~) shows less intensity indicating a spectrum before time zero.

The time-dependence of the peak wavelengths in these spectra are plotted in 6-8. at long times equal to We do observe the "up-relaxation" behavior with the ~~infinity~~ wavelength ~~equals to~~ about 520 nm which agrees with what was observed by Tomin and co-workers (Figure 6-1). However, the data collected at 485 nm excitation are scattered, due to the poor quality of the spectra at the low absorbance values found at this extreme wavelength. The peak wavelength versus time data are fit to exponential functions and the fit results are shown in Table 6-1. It appears that excitation at 425 nm and 445 nm produces similar relaxation behavior but that but that 475 nm and 485 nm excitation results in different time dependence.

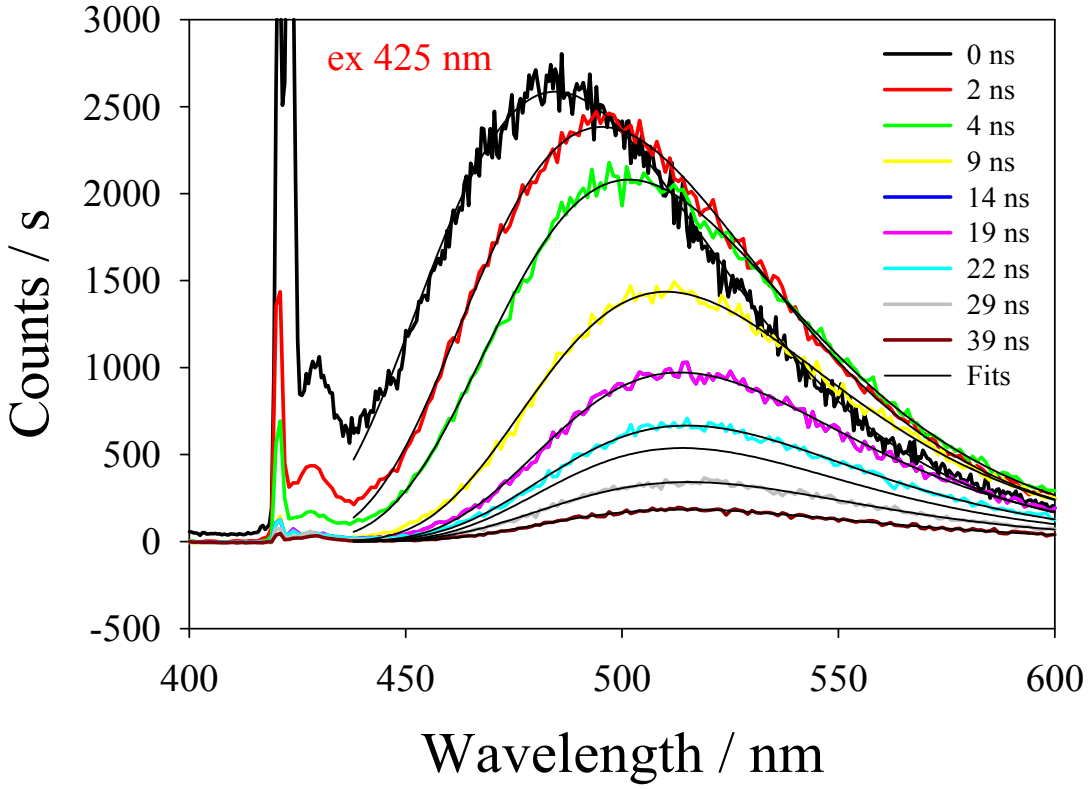

Figure 6-5 Time-resolved spectra of 4-AP in propanolpropanol at 183 K excited at 425 nm. Colored lines show measured spectra and the thin black lines are log-normal fits to these data.

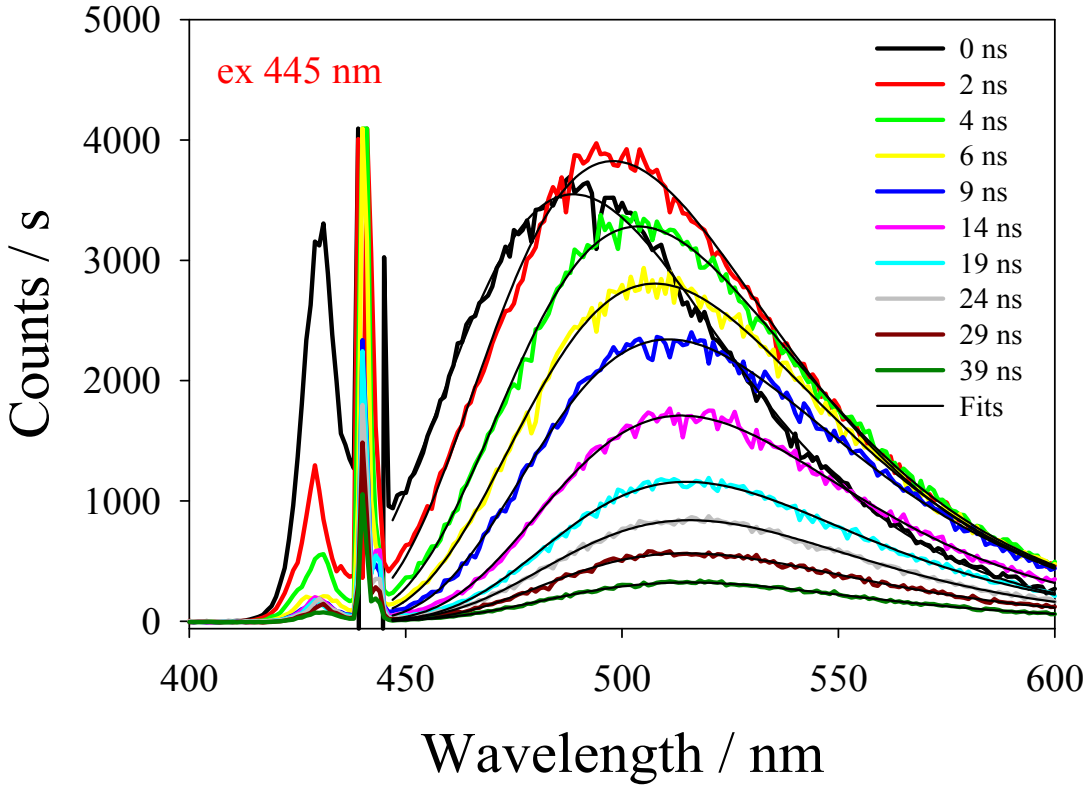

Figure 6-6 Time-resolved spectra of 4-AP in propanol at 183K excited at with excitation wavelength of 445 nm. Colored lines are real data and black lines are fitting curves from a log-normal function. Delay times are shown in the legend corresponding to the spectra with the same color.

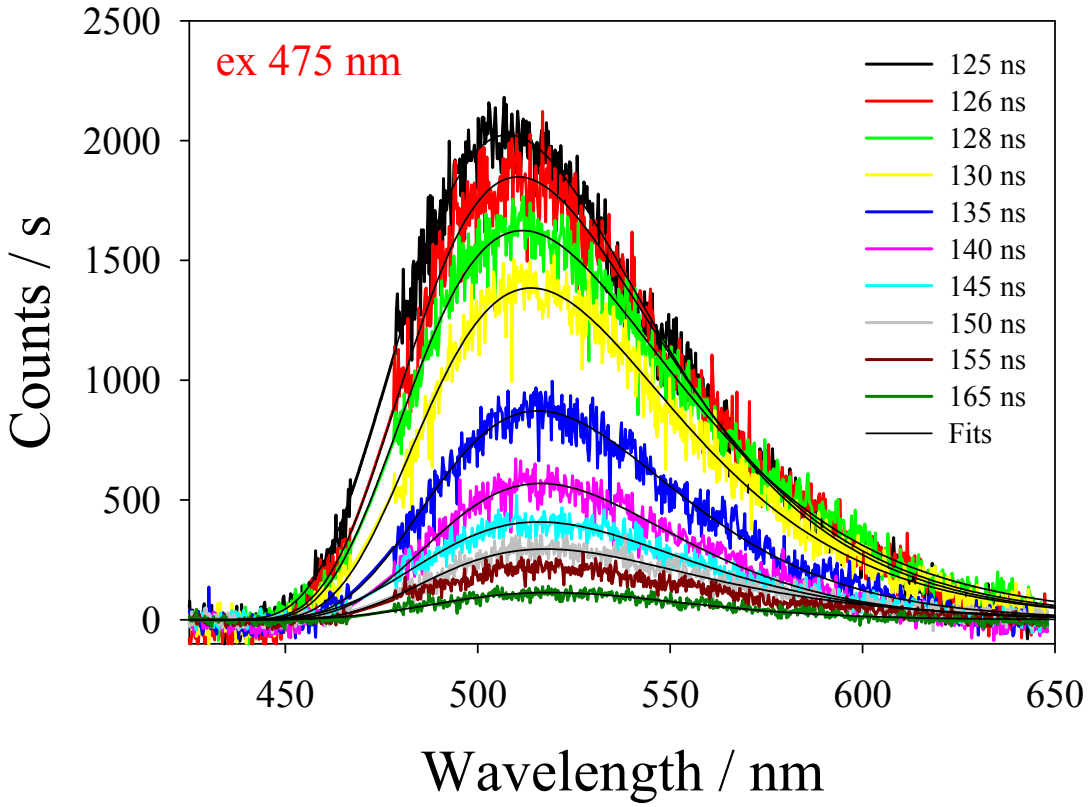

Figure 6-7 Time-resolved spectra of 4-AP in propanol at 183K with excitation wavelength of 475 nm. Colored lines are real data and black lines are fitting curves from a log-normal function. Delay times are shown in the legend corresponding to the spectra with the same color.

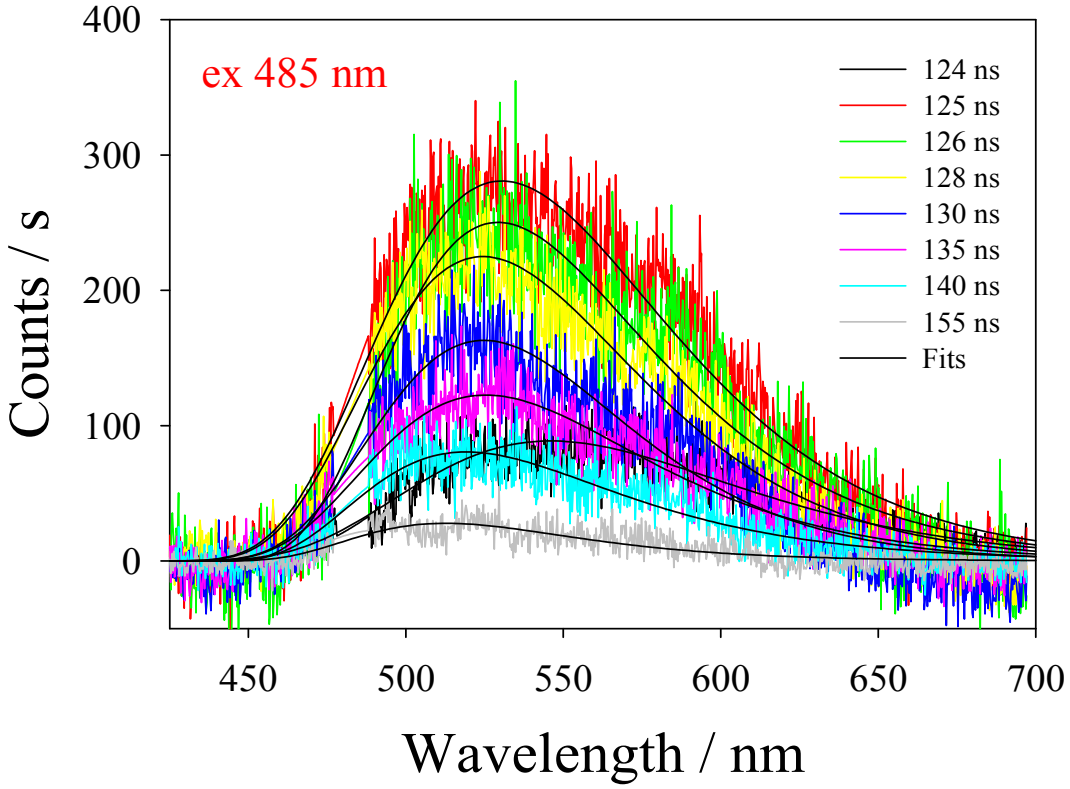

Figure 6-8 Time-resolved spectra of 4-AP in propanol at 183K with excitation wavelength of 485 nm. Colored lines are real data and black lines are fitting curves from a log-normal function. Delay times are shown in the legend corresponding to the spectra with the same color. The black line and fit shows time zero spectrum with less intensity than 1 ns.

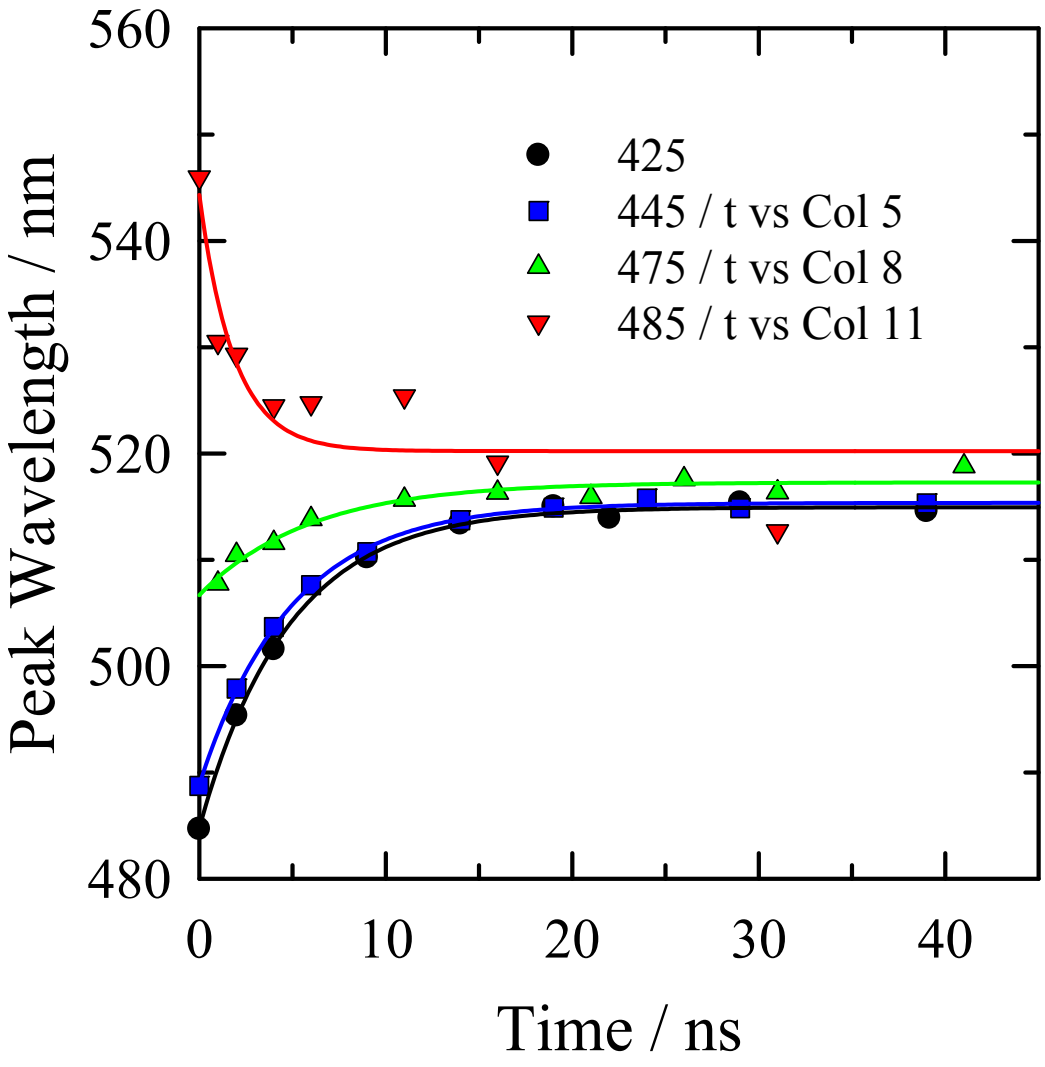

Figure 6-9 Peak wavelength of the fitted time-resolved spectra plot against time. The colored lines are ~~fitting with~~ ~~stretched~~ exponential ~~functions.~~ fits

ν_{exc} /nm	ν_{inf} /nm	$\Delta\nu$ /nm	τ / ns
425	514.9	-30.2	4.8
445	515.3	-26.5	4.9
475	517.3	-10.6	5.9
485	520.2	24.1	1.9

Table 6-1 Summary of ~~fitting parameters of Figure 6-8~~ with exponential function. First column shows the excitation wavelength, second column shows the infinity frequency obtained from fitting, third column is the total Stokes shift ~~from fitting~~ and the last column gives the estimated solvation time ~~from fitting~~.

fits to the data in Fig. 6-8

1.4 Summary and Future Work

As a summary, we are able to reproduce the "up-relaxation" behavior of 4-AP in low-temperature propanol reported by Tomin and coworkers. Our data at 485 nm excitation where uip-relaxation is observed are very noisy. We note that in the original report of this effect only time-resolved spectra excited at 425 nm are shown. These spectra appear to be similar to ours in terms of signal to noise and time resolution. . Since Tomin and coworkers reported that the the same sample was used for all excitation wavelengths, it is likely that their485 nm data are also comparable to those reported here.

In the future, it is very reasonable to use a more concentrated sample for excitation on the far red-edge (475 nm and 485 nm case) to increase the resolution of the spectra. Other choices of probes, such as $Ru(bpy)_2(CN)_2$ which has a lifetime of more than 100 ns can also be considered. Ultimately, we are interested in how the solvation response varies as a function of initial solvation state (δ) selected in ionic liquids.

Reference and Notes

(1) Nemkovich, N. A.; Matseiko, V. I.; Tomin, V. I. Optika I Spektroskopiya 1980, 49, 274.

(2) Rubinov, A. N.; Tomin, V. I. Optics and Spectroscopy-Ussr 1970, 29, 578.

(3) Gardecki, J. A.; Maroncelli, M. Applied Spectroscopy 1998, 52, 1179.

VITA

Xiang Li
104 Chemistry Building, University Park, PA, 16802

Phone: 814-865-5306(o); 814-876-0173(c) Email: xul111@psu.edu

Education:

Ph.D Candidate, Department of Chemistry, Penn State University *2005- now*
Thesis title: **"Ultrafast Charge Transfer and Solvation in Ionic Liquids"**
Advisor: Prof. Mark Maroncelli
B.S. in Chemistry, Fudan University, Shanghai, China *2001-2005*
Advisor: Prof. Dongyuan Zhao

Research Experiences:

Research Assistant, Penn State University *2006-present*
Internship, Food and Drug Administration *05/2009-08/2009*
Teaching Assistant, Penn State University *2005-2008*
Research Assistant, Fudan University, Shanghai, China *2004-2005*

Selected Publications:

your name is on the malononitrile paper

1. **Li, Xiang;** Liang Min; Chakraborty Anjan; Kondo Minako and Maroncelli, Mark. "Solvent-Controlled Intramolecular Electron Transfer in Ionic Liquids," *submitted to Journal of Physical Chemistry B*
2. **Li, Xiang**; Maroncelli, Mark. "Ultrafast Charge transfer of Crystal Violet Lactone" *J. Phys. Chem. A, Article ASAP, Publication Date (Web): September 10, 2010.*
3. **Li, Xiang**; Arzhantsev, Sergey; Kauffman, John; Spencer, John. "Detection of diethylene glycol adulteration in propylene glycol—Method validation through a multi-instrument collaborative study" *Journal of Pharmaceutical and Biomedical Analysis*, ASAP
4. Jin, Hui; **Li, Xiang**; Maroncelli, Mark. "Heterogeneous Solute Dynamics in Room Temperature Ionic Liquids" *Journal of Physical Chemistry B* (2007), 111(48), 13473-13478.

Selected Presentation:

Li, Xiang; Liang, Min; Maroncelli, Mark. **"Ultrafast charge transfer and Solvation in ionic liquids**" *Symposium on the Physical Chemistry of Ionic Liquids*, *239th ACS National Meeting*, San Francisco, United States, March 21-25, 2010

Selected Awards:

2008/9 Student Travel Award
2005 Braddock Homer Scholarship, Penn State University
2005 President Wangdao Scholarship (**top 1%**), Fudan University
2004 Fudan University Creation Foundation Excellent Project